**Proceedings of:**

# *Vibration Assisted Machining Technology*

## *2007 Spring Topical Meeting*

*April 16 and 17, 2007*

*The Carolina Inn*
*Chapel Hill, North Carolina*

*The American Society for Precision Engineering (ASPE) is a multidisciplinary professional and technical society concerned with research and development, design, manufacture and measurement of high accuracy components and systems. ASPE activities encompass relevant aspects of mechanical, electronic, optical and production engineering, physics, chemistry, and computer and materials science. Membership is open to anyone interested in any aspect of precision engineering.*

*Founded in 1986, ASPE provides a new focus for a diverse but important community. Other professional organizations have covered aspects of precision engineering, always as a sideline to their principal goals. ASPE is based on the core of generic concepts necessary to achieve precision in any application; independent of discipline, ASPE intends to be the focus for precision technology, and to represent all facets from research to application.*

*ASPE -- The American Society for Precision Engineering*
*301 Glenwood Avenue, Suite 205, Raleigh, NC 27603*
*P.O. Box 10826, Raleigh, NC 27605*
*Telephone: (919) 839-8444 Fax (919) 839-8039*
*Web site: http://www.aspe.net*

# *Preface*

*This book comprises the proceedings of the 2007 Spring Topical Meeting. The contributions reflect the authors' opinions and are published as presented to ASPE, without change. Their inclusion in this publication does not necessarily constitute endorsement by the ASPE, or its editorial staff.*

*Individual readers of this book and nonprofit libraries acting for them are permitted to make fair use of the material contained in this book to be used in teaching or research; provided they copy said paper in total, as written by the author. Permission is granted to quote excerpts from the scientific or technical works in this book with proper acknowledgment of the source to include: The author's name, the book name, and the ASPE tag line. Reproduction of figures and tables is likewise permitted from the contents of this book, provided that the same acknowledgment of the same source and content is permitted.*

*Any other type reproduction, systematic copying or multiple reproduction of any material in this book is expressly prohibited except with the written permission of the ASPE editorial staff, addressed to the Society's headquarters.*

*ISBN 978-1-887706-42-1*

*2007*

*American Society for Precision Engineering*
*301 Glenwood Avenue, Suite 205*
*Raleigh, NC 27603*

*Printed in the United States of America*

# *2007 Spring Topical Meeting*

## *Contents*


*Preface*... ii

*Contents*... iii

*Program*... iv

*Foreword*... v

*Technical Paper Index*... vi

*Technical Papers*... 3-97

*Author Index*... 99

# *2007 Spring Topical Meeting*

## *Meeting Schedule*

| | ***Monday, April 16*** | ***Tuesday, April 17*** |
|---|---|---|
| *7:30* | *Registration and Continental Breakfast* | |
| *8:30*<br>*10:00* | *TECHNICAL SESSION I* | *TECHNICAL SESSION V* |
| | *Coffee Break* | |
| *10:30*<br>*12:00* | *TECHNICAL SESSION II* | *TECHNICAL SESSION VI* |
| | *Lunch* | |
| *1:30*<br>*3:00* | *TECHNICAL SESSION III* | *TECHNICAL SESSION VII* |
| | *Refreshment Break* | |
| *3:30*<br>*4:30* | *TECHNICAL SESSION IV* | |
| | *Free Time* | |
| *6:30*<br>*8:30* | *DINNER AT THE CAROLINA BREWERY* | |

# *Foreword*

*Normally, engineers try to suppress vibration when designing or implementing manufacturing processes. However, the capability of traditional precision machining methods can be enhanced by application of micrometer-scale high-frequency vibration between tool and workpiece. The intent of the meeting is to discuss the state-of-the-art in vibration assisted technology as applied to manufacturing processes. Presentations of both fundamental and applications-oriented work are encouraged, as are talks with significant tutorial content.*

*Recent developments in vibration-assisted machining present new opportunities and motivate this meeting. For example, elliptical vibration-assisted cutting has been used to diamond-turn optical quality surfaces in high-wear materials such as steel and glass while extending tool life by a factor of twenty or more. Vibration assisted precision grinding minimizes subsurface material damage to ceramics. High aspect-ratio holes and cavities have been created at high material removal rates using micro-EDM with ultrasonic vibration. Controlled high-frequency vibration is suggested as a means of enhancing other processes, such as electron beam machining and micro-extrusion forming.*

*The objective of this meeting is to bring together researchers and practitioners from industry, government and academia to provide a forum for the exchange of ideas. The presentations will cover a broad range of technologies and highlight potential areas for future development. The meeting will emphasize discussions as well as presentations and the participants are encouraged to identify areas needing further research.*


***2007 Spring Topical Meeting Co-Chairmen:***

***Meeting Co-Chairmen:***

*Thomas A. Dow*
*David E. Brehl*
*Precision Engineering Center*
*North Carolina State University*

***Technical Organizing Committee:***

*Y. S. Lee, Samsung Corporation Ltd.*
*Michele H. Miller, Michigan Technological University*
*Scott F. Miller, University of Michigan*
*Gerald L. Overcash, University of North Carolina at Charlotte*
*Eiji Shamoto, Nagoya University*
*Z. W. Zhong, Nanyang Technological University*

# Technical Sessions

## Session I
### Vibration-Assisted Machining (Cutting & Grinding)
*Monday, April 16, 8:30 a.m. – 10:00 a.m.*


1. ***Vibration-Assisted Machining Research at Fraunhofer IPT – Diamond Turning and Precision Grinding (Keynote Paper)*** ..... 3
   *Dambon, O.; Klocke, F.; Heselhaus, M.; Bulla, B.; Weber, A.; Schug, R. (Fraunhofer Institute for Production Technology - IPT); and Bresseler, B. (Aixtooling GmbH)*
2. ***Ultrasonic Vibration-Assisted Cutting of Titanium Alloy*** ..... 11
   *Koshimizu, S. (Shizuoka Institute of Science and Technology)*


## Session II
### Vibration-Assisted EDM /ECM
*Monday, April 16, 10:30 a.m. – 12:00 p.m.*


1. ***Development of 3 DOF Ultrasonic Elliptical Vibration System for Elliptical Vibration Cutting*** ..... 15
   *Suzuki, N.; Hino, R.; Shamoto, E. (Nagoya University)*
2. ***3-D Microstructure Fabrication Using Elliptical Vibration-Assisted Machining*** ..... 21
   *Brehl, D. E.; Dow, T. A. (North Carolina State University)*
3. ***Numerical Simulations of Vibration-Assisted Machining*** ..... 27
   *Patten, J. A.; Williams, A. D. (Western Michigan University)*


## Session III
### Vibration-Assisted Machining (Cutting)
*Monday, April 16, 1:30 p.m. – 3:00 p.m.*


1. ***A Study on the High Aspect Ratio Micro Hole Drilling Using Ultrasonic Assisted Micro-Electro Discharge Machining*** ..... 32
   *Billa, S.; Sundaram, M. M.; Rajurkar, K. P. (University of Nebraska-Lincoln)*
2. ***Influence of Ultrasonic Vibration on Micro-extrusion*** ..... 37
   *Bunget, C.; Ngaile, G. (North Carolina State University)*
3. ***Vibration-Assisted Machining – Application Areas and Barriers to Wider Use***
   *Audience Discussion*


## Session IV
### Vibration-Assisted Machining (Grinding)
*Monday, April 16, 3:30 p.m. –4:30 p.m.*


1. ***Ultrasonic Assisted Grinding of Advanced Ceramics*** ..... 43
   *Uhlmann, E.; Hübert, C. (Technical University Berlin)*
2. ***New Systematic and Time-saving Procedure to Design Complex Shaped Tools for the Application of Ultrasonic Assisted Grinding*** ..... 48
   *Brecher, C.; Schug, R.; Weber, A.; Wenzel, C. (Fraunhofer Institute for Production Technology - IPT)*

## *Session V*
### *Vibration-Assisted Drilling Processes*
*Tuesday, April 17, 8:30 a.m. – 10:00 a.m.*


1. ***Experimental Study on Rotary Ultrasonic Machining of Graphite/Epoxy Panel*** ..... 52
   *Li, Z.C.; Pei, Z.J. (Kansas State University); Sisco, T.; Micale, A. C. (The Boeing Company); and Treadwell, C. (Sonic-Mill Company)*
2. ***Numerical Simulation of Vibration Assisted Electron Beam Machining Process*** ..... 58
   *Wang, Z.G.; Yamazaki, K. (University of California-Davis); Daichi, Y.; Sano, S. (Sodick Co., Ltd.); and Uno, Y. (Okayama University)*
3. ***Vibration-Assisted Machining – Critical Areas for Research and Development***
   *Audience Discussion*


## *Session VI*
### *Vibration-Assisted Machining (Process Analysis)*
*Tuesday, April 17, 10:30 a.m. – 12:00 p.m.*


1. ***Simulation of Elliptical Vibration Cutting Process with Thin Shear Plane Model*** ..... 64
   *Shamoto, E.; Suzuki, N.; Hino, R. (Nagoya University)*
2. ***Material Properties for Modeling Vibration Assisted Machining **** ..... 70
   *Rhorer, R. L. (National Institute of Standards and Technology)*
3. ***Machining Forces for Elliptical Vibration-Assisted Machining*** ..... 71
   *Brehl, D. E.; Cerniway, M. A.; Dow, T. A.; Negishi, N. (North Carolina State University)*


## *Session VII*
### *Vibration-Assisted Machining (Novel Processes & Grinding)*
*Tuesday, April 17, 1:30 p.m. – 3:00 p.m.*


1. ***Wheel Loading Reduction with Vibration Assisted Grinding*** ..... 77
   *Zhang, P.; Miller, M. H. (Michigan Technological University)*
2. ***3D Shape Mirror Surface Grinding of Die Steel with Ultrasonically Oscillated Electroplated Diamond Tools*** ..... 82
   *Hara, K.; Kyusojin, A.; Okada, M. (Nagaoka University of Technology); Isobe, H. (Nagano National College of Technology); and Yoshihara, H. (Niigata Industrial Creation Organization)*
3. ***Micromachining of Brittle Materials Using Ultrasonic Assisted Lapping*** ..... 87
   *Klopfstein, M. J.; Riemer, O.; Brinksmeier, E. (Bremen University)*


*Due to circumstances beyond the author's control, the following paper will not be presented in person:*


***Effect of Ultrasonic Torsional Mode Vibration Cutting on Drilling in CFRP Laminates*** ..... 92
*Yagishita, H. (Numazu National College of Technology)*


* *No extended abstract available at press time*

# Technical Papers

# Vibration-Assisted Machining Research at Fraunhofer IPT – Diamond Turning and Precision Grinding

**Olaf Dambon[1]; Fritz Klocke[1]; Michael Heselhaus[1]; Benjamin Bulla[1]; Andreas Weber[1]; Ralf Schug[2]; Bernd Bresseler[3]**
**[1]Department Process Technology**
**[2]Department Machine Tools**
**Fraunhofer Institute for Production Technology IPT**
**Aachen, Germany**
**[3]Department Production**
**Aixtooling GmbH**
**Aachen, Germany**

## INTRODUCTION

First investigations on ultrasonic assisted grinding were published in 1956 by Colwell [1] and on ultrasonic assisted turning in 1964 by Dohmen [2]. Since then a lot of approaches were made regarding oscillation assisted manufacturing processes. Either the tool or the workpiece were superimposed with an ultrasonic oscillation. All these approaches showed significant advantages regarding reduction of tool wear for ultrasonic assisted turning and achievable surface qualities [3, 4, 8] or reduction of process forces regarding ultrasonic assisted grinding [5, 6, 7].

Nevertheless, most of these results were gathered through experimental setups, which were not capable for batch production. Developments in the past concentrated on the transfer of the gained know-how to industrial applications. In case of ultrasonic assisted grinding robust machine systems for form flexible manufacturing of hard and brittle materials, from Dama Technologies AG, Sauer GmbH, Sonic-Mill® etc., are available since the 90s of last century. These machine tools opened new application areas and markets for ultrasonic assisted grinding. Furthermore, workpieces with complex geometries (e.g. double curved or even free form surfaces) in hard and brittle materials could be machined for the first time. In case of ultrasonic assisted turning Fraunhofer IPT developed within several public funded research projects machine systems for process stable ultrasonic assisted turning. These systems were integrated on precision turning machines. These integrated systems enable process stable ultra-precision machining of glass and ferrous materials by defined cutting edge with mono-crystalline diamond.

## ULTRASONIC ASSISTED GRINDING

For the investigations on ultrasonic assisted grinding Fraunhofer IPT owns the ultrasonic assisted grinding machine DMS50 ultrasonic from the company Sauer GmbH (FIGURE 1). This machine tool is based on a conventional NC-controlled three axes milling machine, with perpendicular axes. The lengths of the guideways are $x = 500$ mm, $y = 400$ mm and $z = 400$ mm. The drives allow a maximum feed rate of $v_f = 5\,000$ mm/min. Furthermore, the machine tool features two manual rotational axes (b and c), which are not NC-controlled and can be used for workpiece alignment.

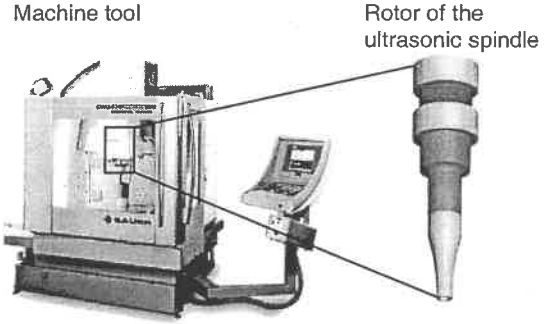


*FIGURE 1. Ultrasonic assisted grinding machine DMS50 ultrasonic from Sauer GmbH.*

The ultrasonic system consists of the oscillation assisted spindle and the generator (FIGURE 2). The generator sends electrical high frequency signals to the piezo crystals, which are part of the rotor of the spindle. The piezoelectric elements transform the electrical energy into mechanical vibration. These are transmitted to the booster and the sonotrode, which clamps the grinding tool. The booster as well as the

sonotrode amplify the mechanical oscillation due to the reason, that the piezo crystal is just able to generate a maximum ultrasonic amplitude of A = 5 $\mu$m (= oscillation width S = 10 $\mu$m), but more than A = 10 $\mu$m are needed at the tip of the grinding tool. The whole rotor oscillates in its longitudinal harmonic oscillation with approximately f = 20 kHz. This means that the active rotating part of the grinding tool can oscillate axially with A = 5 to 25 $\mu$m ultrasonic amplitude and a frequency of f ~ 20 kHz.

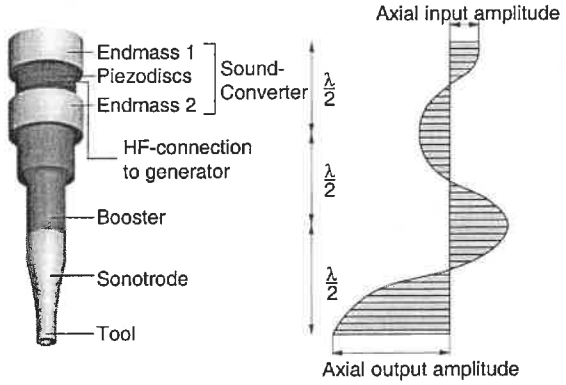


*FIGURE 2. Configuration of the rotor of an ultrasonic assisted grinding spindle.*

The results, which are described in the following, were gained within a public funded research project. This project aims on the economical rough grinding of spherical glass lenses by ultrasonic assisted rotational side grinding (FIGURE 3). The kinematics allows fast and precise machining of spherical shapes through a linear movement of the grinding tool and an angle between the rotational axes of the grinding tool and the rotating workpiece.

To integrate this kinematics in the DMS50 ultrasonic a rotary table was installed. This table is able to overlay the glass lens with a rotational speed up to $n_w = 550\ min^{-1}$. Furthermore, a coordinate transformation was implemented in the NC-control unit to enable an easy feed movement of the grinding tool parallel to the rotational axes of the workpiece. Additional, a force measurement device from Kistler was mounted between the machine table and the rotary table. This allows the measure of process forces acting between the workpiece and the grinding tool. Using a measuring computer the acting process forces could be visualized in real time, to enable fast and direct optimization of the process.

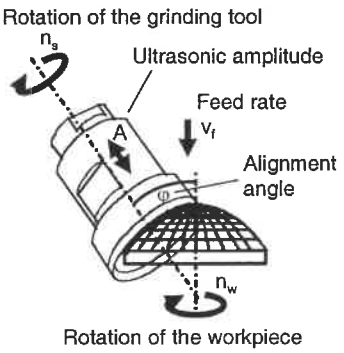


*FIGURE 3. Kinematics of ultrasonic assisted side grinding of spherical glass lenses.*

For the investigations the optical glass N-BK7 was machined. Besides the influence of process parameters feed rate $v_f$, rotational speed of the grinding tool $n_s$ and rotational speed of the workpiece $n_w$ the content of the investigations was focused on the influence of the ultrasonic oscillation and the tool specification on the process force and on the tool wear.

It could be shown that activation of ultrasonic assistance with increased ultrasonic amplitude leads to significant reduction of process forces. In most cases maximum achievable material removal rate (MMR) is limited by a maximum process force ($F_{max}$) to avoid damage of the grinding wheel, machine tool or the workpiece. Therefore, reduction of process forces due to ultrasonic oscillation can be used to increase feed rate $v_f$ respectively material removal rate (FIGURE 4).

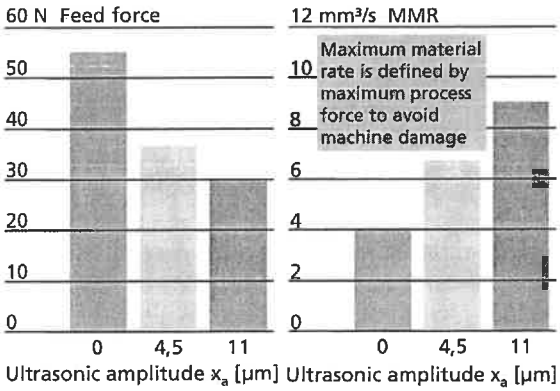


*FIGURE 4. Influence of ultrasonic amplitude on feed force and on achievable MMR.*

The reduction of mean process forces can be explained by effects on both the workpiece and

the grinding tool. On the one hand due to the oscillation micro cracks are generated into the subsurface region of the workpiece. Investigations on subsurface damage showed that the SSD-value of a conventional ground lens is ~ 20 $\mu$m (feed rate $v_f$ = 4 mm/min, cutting speed $v_c$ = 14 m/s, rotational speed of the workpiece $n_w$ = 500 $min^{-1}$, average diamond size D = 46 $\mu$m). By activation of ultrasonic oscillation to an amplitude of A ~ 5 $\mu$m a SSD-value of ~ 26 $\mu$m and to amplitude of A ~ 12 $\mu$m a SSD-value of ~ 31 $\mu$m could be observed. These micro cracks weaken the workpiece material and reduce its resistance to be removed by the rotation of the grinding tool. On the other hand ultrasonic oscillation leads to slivering at the diamonds of the grinding tool. SEM-pictures of used grinding wheels showed clearly diamond grains with slivered areas. This behavior leads to a sharp tool and therefore lower process forces. Furthermore, it is easier to achieve self-sharpening mode in comparison to a conventional process. Nevertheless, ultrasonic oscillation increases significantly tool wear.

Reduction of process forces and increase of tool wear due to ultrasonic oscillation can be decisively influenced by grinding tool specifications. As stated above ultrasonic oscillation leads predominantly to brittle wear mechanisms at the diamond grains. The overall impulsive load by virtue of ultrasonic oscillation is spread on all active diamond grains. By increasing the number of active grains through raised diamond grain concentration the load on each grain is decreased. Furthermore, a reduction of bonding hardness usually leads to a higher elasticity. Therefore, the whole tool can be deformed stronger due to ultrasonic oscillation and the overall load is decreased. Both variations of grinding tool specifications lead to less load on the diamond grains and therefore less appearance of brittle wear of the diamonds. This results in a lower cutting ability and consequently in higher process forces, because the probability of brittle wear mechanism at the diamond grains as well as self-sharpening mode is reduced. Nevertheless, tool wear is much lower (TABLE 1). Thus, grinding tools with low grain concentration and high bonding hardness should be used for roughing and grinding tools with high grain concentration and low bonding hardness for finishing.

| | Process force | Tool wear |
|---|---|---|
| Increase of bonding hardness | ↘ | ↗ |
| Reduction of diamond grain concentration | ↘ | ↗ |

*TABLE 1. Influence of bonding hardness and of diamond grain concentration on process force and on tool wear*

Ultrasonic assisted grinding offers a wide range of advantages like reduced process forces or increased maximum material removal rate. Nevertheless, increased subsurface damage as well as increased tool wear have to be taken into consideration. But adapted process strategies can take advantage of increased productivity without suffering the disadvantages.

## ULTRASONIC ASSISTED TURNING

Compared to the described vibrational assisted rotating grinding tools the ultrasonic assisted turning technology works with a fixed transducer. On top of the mounted sonotrode and booster system a mono-crystalline diamond tool tip is clamped. As written before the aim is to utilize mono-crystalline diamond tools for the manufacture of ultra-precise hardened steel parts, which can be applied for injection molding of plastics or precision molding of glass optics. Usually the diamond tip underlies excessive tool wear while machining ferrous materials due to the affinity of carbon (tool) and iron (workpiece).

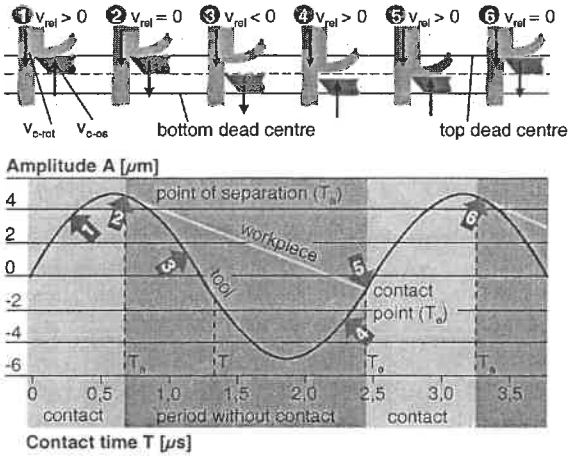


*FIGURE 5. Kinematics of US assisted process.*

In several publications it was shown that the diamond tool wear can be reduced by the superimposed vibration. This was applied for the first time by Moriwaki for ultra-precision machining purposes [2, 3].
Two different principles of tool vibrations are known, whereas one works with elliptical [3] and the other one with unidirectional [4, 8] tool movement. In this paper the results are shown for the unidirectional tool movement. The vibration acts here in cutting direction as shown in FIGURE 5.

It is essential for the transition from the conventional to the vibration-assisted process, that the maximum oscillation speed reached in the zero-crossing, is bigger than the constant workpiece speed (FIGURE 5). Only when this condition is met the tool does detach itself from the chip during the downward motion (Point 2, relative speed $v_{rel} = 0$). The contact occurs again during the upward motion after the vibrational direction has changed at the lower dead center (Point 5).

Accordingly, the effective contact time between the part and the cutting edge is reduced by the high frequency excitation of the tool. As previously demonstrated, this modification in the kinematics of the turning process has a considerable impact on the efficiency of ultra-precision operations conducted on critical materials such as steel or glass [8]. The positive characteristics of this technology are

- reduction of effective contact duration between tool and workpiece,
- decrease of average process forces
- better inflow of coolant for a decreased cutting temperature and
- reduced friction.

This all leads to a reduction of tool wear as well as an improved ductile cut.

The relationships shown, permit mathematical interrelationships to be derived for the exact calculation of time, position and speed of the workpiece ($s_{rot}$, $v_{c\text{-}rot}$) and of the tool ($s_{os}$, $v_{c\text{-}os}$) as well as of the associated relative values ($v_{rel}$). The derivation of the mathematical relationships illustrates the complex kinematics correlations involved in vibration-assisted machining. It is evident that the variables of vibration amplitude and vibration frequency, used to describe the tool movement, are closely related to the parameters rotational speed n, and workpiece radius r, which determine the cutting speed in conventional turning operations.
In accordance with the description of the operating cycle, the cutting speed in the machining zone $v_{c\text{-}rel}$, is dependent not only on the workpiece motion caused by the spindle rotation, but also on the oscillation of the tool (see FIGURE 5):

$$v_{c\text{-}rel}(t) = v_c = v_{c\text{-}rot} + v_{c\text{-}os} \qquad (1)$$

Rübenach tried to determine the exact times regarding the contact Te and separation Ta of workpiece and tool. His calculations showed that a complete analytical solution is not possible due to occurring transcendent equations [8]. However he could derive the parameters which have the greatest influence on the process:

- entrance duration ED: relative contact time between workpiece and tool within one vibrational cycle and
- entrance speed $v_{in}$: relative velocity between workpiece and tool in the moment of contact $v_{c,rel}(t=Te)$.

However, these parameters have to be transformed into set-up parameters for the workpiece speed $v_{c,rot}$ and amplitude A of the ultrasonic transducer. The relationship between parameters was derived numerically and its results are illustrated in FIGURE 6.

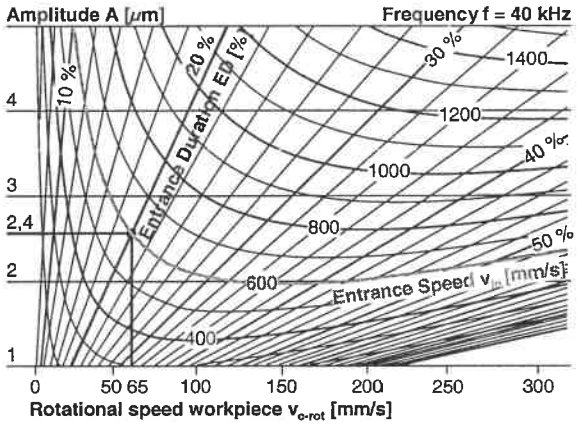


*FIGURE 6. Field of parameters for f = 40 kHz for the ultrasonic assisted turning process.*

Exemplarily a point is shown with an entrance duration of ED = 20% and a entrance speed $v_{in}$ = 600 mm/s which leads to a rotational speed

$v_{c,rot}$ of 65 mm/s and tool amplitude A = 2,5 $\mu$m. This parameter set was chosen as a starting point for the test series.

Beside the theoretical derivation of appropriate parameters several successful machining tests were conducted on different glass materials by Rübenach [8].

The results shown here are related to the ultrasonic turning of plane hardened steel cylinders with a diameter of D = 22 mm. The ultrasonic tool system was mount on an ultra-precision lathe from the company Rank Pneumo. The applied steel material is the commonly known mold and die steel 1.2083 (STAVAX® ESU, X42Cr13) which was hardened and annealed in four discrete configurations (35, 40, 45, 53 HRC).

The conducted machining tests focused on the variation of classical machining parameters like depth of cut $a_p$ and feed rate f. Furthermore, an investigation of the influence of the derived kinematical parameters entrance duration ED and entrance speed $v_{in}$ is mandatory to characterize the process in detail.

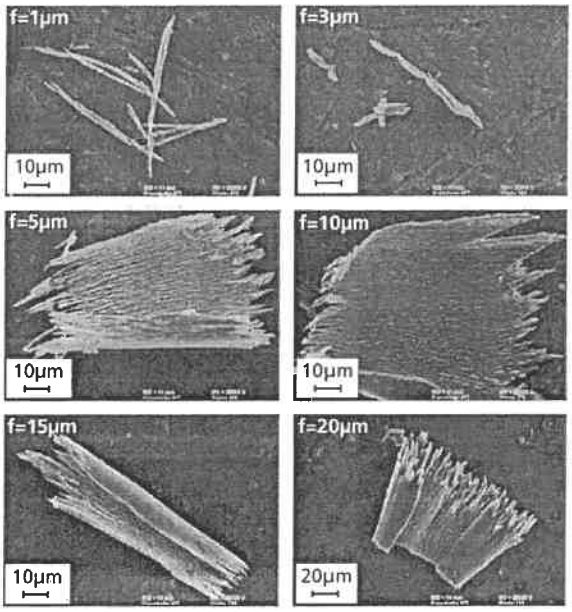


*FIGURE 7. Chip formation at varying feed rates (workpiece hardness: 45 HRC).*

The discrete variation of the depth of cut $a_p$ = 1, 3, 5, 10 $\mu$m (f = 5 $\mu$m) and feed rate f = 1, 3, 5, 10, 15, 20 $\mu$m ($a_p$ = 5 $\mu$m) could show that the results are comparable to classical ultra-precision machining of non ferrous materials. In detail, the depth of cut and the various material hardness have no significant influence on the reachable surface roughness Ra, which is in a range of Ra = 6 - 10 nm. In opposite to these results the variation of the feed rate f has considerable influence on the surface roughness which was for all material configurations at Ra < 10 nm at feed rates between f = 5 - 10 $\mu$m. Below and above these feed rates classical effects like the »size effect« respectively the kinematical roughness $R_{t,theo}$ affected the roughness negatively. Additionally, the achievable surface roughness tends to decrease in quality at higher material hardness.

The chips which were collected during the test series (FIGURE 7) show classical sawtooth geometry for a feed rate greater than f = 3 $\mu$m which are commonly known from the high precision hard turning process with cubic boron nitride (cBN) tools. Usually this chip form is generated for a material hardness above 50 HRC and is caused by the low material deformation capability – at lower material hardness a continuous chip is generated. Due to the intermitting cut of the ultrasonic tool vibration the sawtooth chip is generated at lower material hardness. The backside of the chips look smooth which indicates the ductile cut. Furthermore, it can be clearly seen that the chip segments coil up at higher feed rates due to the higher energy input. At low feed rates f < 5 $\mu$m the generated needle chips experience a lower energy input and thus a typical welded zone between the chip segments can not be generated which is characteristic for saw tooth chips.

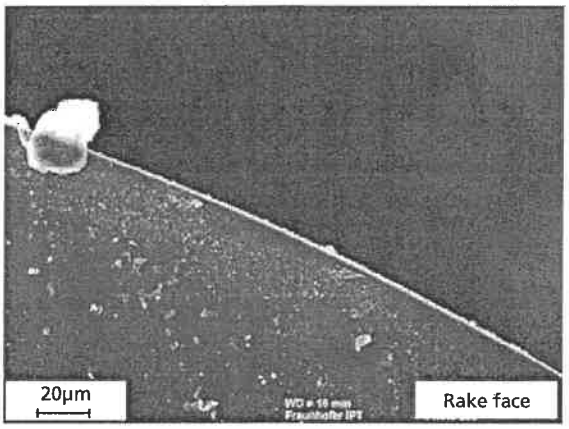


*FIGURE 8. Cutting edge after 400 m length of turning (f = 1 µm, material hardness 45 HRC).*

Considering the diamond tool wear it can be stated that the tool wear after a turning length of l = 400 m (f = 1 $\mu$m at D = 22 mm) was not detectable with a scanning electron microscope (SEM). Except some adhering workpiece particles could be found on the rake face (FIGURE 8).

The following results show the variation of the ultrasonic specific parameters entrance duration ED and entrance speed $v_{in}$. The discrete variation of the entrance duration ED = 20, 30, 50 % ($v_{in}$ = 600 mm/s, f = 5 $\mu$m, $a_p$ = 5 $\mu$m) show a significant influence.

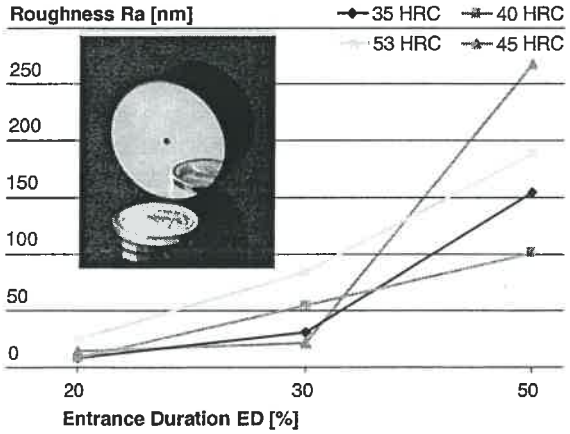


*FIGURE 9. Influence of ED on Ra.*

At higher entrance durations the quality of the achieved surface roughness decreases (FIGURE 9). One reason for this effect can be seen in the kinematics of the process. A higher entrance duration ED can be adjusted by higher rotational speed $v_{c,rot}$ with a minor decrease of the amplitude (FIGURE 6). This implies a faster transit of one workpiece point through the vibration zone of the tool. Thus, at lower entrance durations a workpiece point can be machined twice or three times per workpiece revolution. In contrast at higher entrance durations a workpiece point is machined once per revolution. Combined with the effect of radial vibrations of the tool, caused by the axial contraction and expansion of the sonotrode, the workpiece surface quality will decrease. In contrast, if a workpiece point is machined twice or three times the generated kinematical roughness will be smoothed. Additionally, a second effect occurs. The tool wear, which is at low entrance durations justifiable by diffusion and oxidation (no chipping or abrasion) is at higher entrance durations justifiable by abrasion and chipping. The discrete variation of the entrance speed $v_{in}$ = 400, 600, 700, 800 mm/s had no significant influence on the achieved surface roughness. A ductile cut with a roughness of Ra = 5 - 15 nm occurred for all speeds. However, a further increase (test have to be conducted) presumably will show a higher surface roughness and a non ductile cutting behavior.

One of the most neglected parameters for the ultrasonic assisted turning technology is the tool frequency. All in the literature known investigations have been performed with 20 or 40 kHz. Higher frequencies have not been considered yet. The Fraunhofer IPT developed in co-operation with industrial partners a new ultrasonic tool device, which can work at f = 60 kHz in the unidirectional mode. The advantages are discussed here theoretically and will be verified in future machining tests. As explained above the unidirectional excitation of the tool causes vibrations which are orthogonal to the axis of the sonotrode. These undesirable vibrations work directly in passive direction of the tool and thus into the surface of the workpiece which leads to lower surface qualities. The reason for this behavior can be seen in the assumed volume constancy of the sonotrode during the vibration, which leads also to a contraction and expansion of the sonotrode in radial direction. The new 60 kHz transducer was developed with the aim to minimize the radial sonotrode vibrations.

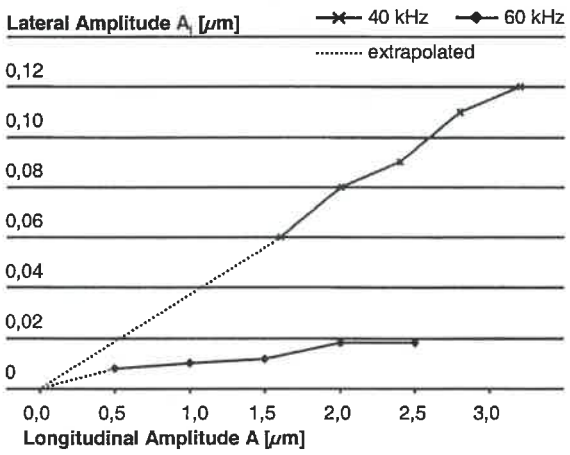


*FIGURE 10. Comparison of lateral vibrations between new developed 60 kHz and current 40 kHz transducer.*

A comparison of the radial sonotrode vibration of the current (40 kHz) and new System (60 kHz) is shown in FIGURE 10.

The vibrations were measured with a non tactile capacitive Sensor. Obviously the radial sonotrode vibrations are significant (factor 4) lower for the 60 kHz system which should have a positive influence on the workpiece roughness.

However, beside the dynamical considerations an increase of frequency leads to new kinematical boundary conditions.

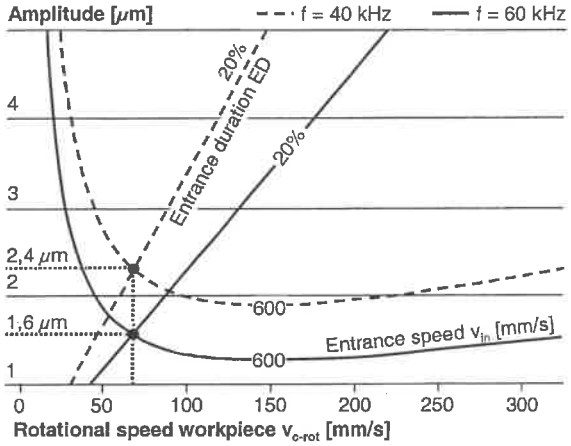


*FIGURE 11. Comparison of 40 kHz and 60 kHz parameter field for equal working points.*

Figure 11 illustrates the influence on the parameter field for an increased frequency. Considering equal working points for 40 kHz and 60 kHz (ED = 20%, $v_{in}$ = 600 mm/s) leads to a decrease of 33% in amplitude for the higher frequency of 60 kHz. Thus, this effect will also lead to an additional decrease of radial sonotrode vibrations.

Finally it can be stated that the superposition of the general lower radial amplitude of the 60 kHz transducer and the decreased working amplitude will presumably lead to better surface qualities.

## SUMMARY AND CONCLUSION

The potential for ultrasonic assisted tools with undefined and defined cutting edges is shown for grinding and turning, whereas the cutting mechanisms are different.

Ultrasonic assistance for grinding tools is applied to exceed the fracture toughness and thus to induce cracks in the workpiece material. This effect can be used to increase maximum material removal rate or to lower process forces compared to a conventional grinding process at comparable process parameters. Beside the advantages unfortunately the SSD is higher for the ultrasonic assistance which has to be taken into consideration of the process strategy's design.

Ultrasonic assistance for ultra-precision turning is applied to decrease the excessive diamond tool wear for ductile machining of hardened steel. The kinematical consideration is the key to achieve appropriate surface conditions as well as reduced tool wear. The investigations show that the conventional parameters like depth of cut $a_p$ and feed rate f lead to similar results compared to conventional ultra-precision machining. However, a consideration of the kinematical parameters entrance duration ED and entrance speed $v_{in}$ is likewise mandatory and show the massive influence of the entrance duration ED regarding the surface roughness.

Theoretical investigations show also the potential of higher frequencies for the ultrasonic assisted turning process.

## REFERENCES


[1] Colwell, L.: The Effects of High-Frequency Vibrations in Grinding, Transactions of American Society of Mechanical Engineers, May 1956, Page 124-131

[2] Dohmen, H.G.: Zerspanungsuntersuchungen beim Drehen mit periodisch bewegtem Schneidwerkzeug, PhD Thesis University of Aachen, 1964

[3] Moriwaki, T.; Shamoto, E.: Ultraprecision Diamond Turning of Stainless Steel by Applying Ultrasonic Vibration, Annals of the CIRP Volume 40/1/1991, Page 559-562

[4] Klocke, F.; Heselhaus, M.; Puellen, J.: Vibration Assisted Diamond Tools for Ultra-precision Turning of Hardened Steel Alloys, Euspen Conference Proceedings, 2005

[5] Pei, Z. J.: Ferreira, P.M.: An Experimental Investigation of Rotary Ultrasonic Face Milling, International Journal of Machine Tools & Manufacture 39, 1999, Page 1327-1344

[6] Spur, G.; Uhlmann, E.; Holl, S.-E.; Daus, N.-A: Influences on Surface and Subsurface during Ultrasonic Assisted Grinding of Advanced Ceramics, Proceedings of the Fourteenth Annual Meeting of the American Society for Precision Engineering, 1999, Page 481-484
[7] Suzuki, K.; Makizaki, T.; Uematsu, T.: Ultrasonic Grinding Utilizing Traveling Wave Vibration, Euspen Conference Proceedings, 1999, Page 286-289
[8] Rübenach, R.: Schwingungsunterstützte Ultrapräzisionsbearbeitung optischer Gläser mit monokristallinen Diamant-werkzeugen, PhD Thesis, RWTH Aachen, 2001, Page 42-54

# Ultrasonic Vibration-Assisted Cutting of Titanium Alloy

**Shigeomi Koshimizu**[1]
[1]**Department of Mechanical Engineering**
**Shizuoka Institute of Science and Technology**
**2200-2 Toyosawa, Fukuroi, Shizuoka, Japan**

## INTRODUCTION

Titanium alloy has superior characteristics such as lightness, high strength and high corrosion resistance. These characteristics make titanium alloy highly suited for aircraft parts and medical implants. Although titanium is a very useful material and becoming more in demand, we are faced with difficulties in working the material to manufacture products. Especially, in the case of turning, titanium alloy is chemically active, therefore causing chips to adhere to the tool tip. Accordingly, when the adhesive chips separate from the tool tip, they take with them part of the tool material, causing severe wear. Another issue is that chips can become entangled between tool and workpiece. This results in damage to the surface of the workpiece and the surface roughness increases.

In this research, we have proposed the use of ultrasonic vibration-assisted cutting of titanium alloy in order to overcome these problems. By applying ultrasonic vibration to the tool tip, interrupted cutting, rather than continuous cutting, can be applied. This technology may enable us to prevent the adhesion and entanglement of chips, improving tool wear and surface roughness of the workpiece.

## EXPERIMENTAL SETUP AND PROCEDURE

Fig. 1 shows the external view of the ultrasonic vibration cutting machine (Taga Electric, SB-50) used in this study. Fig. 2 shows a cross-sectional view of the same ultrasonic vibration unit. Ultrasonic vibrations generated by a bolted Langevin's element are transmitted to the cutting tool tip via the cone and horn. The frequency of the ultrasonic vibration is 19 kHz and the amplitude is 0.03 mm. The direction of the vibration is parallel to the cutting direction. A triangular tip (KENNAMETAL:TPGT110204K) is used as the cutting tool.

The face cutting of a titanium alloy (Ti-6Al-4V) was carried out by means of the ultrasonic vibration unit attached to the turret of a CNC lathe as shown in Fig. 3.

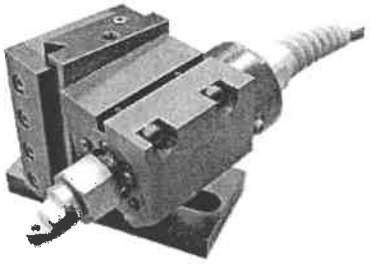

*FIGURE 1. Ultrasonic vibration cutting machine*

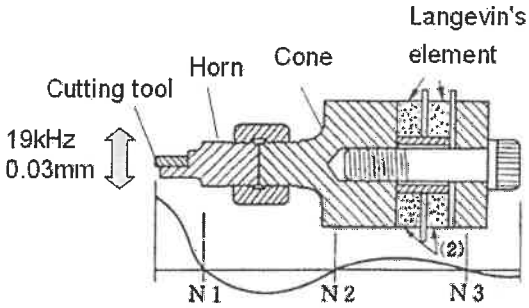


*FIGURE 2. Cross-sectional view of ultrasonic vibration unit*

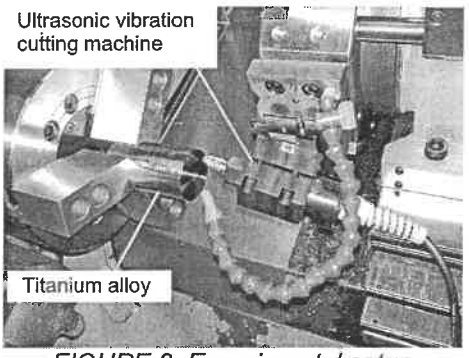


*FIGURE 3. Experimental setup*

## EXPERIMENTAL RESULTS

### Cutting Resistance

Fig. 4 shows the results of the measurements of the cutting resistance made using a force sensor (KISTLER:9257B). The results indicate that the cutting resistance in the ultrasonic vibration-assisted cutting process is between one-half to

one-third of that in the conventional cutting process without ultrasonic vibrations. Whereas the coefficient of friction, being defined by principal force Fz divided by thrust force Fy, in the case of conventional cutting gives a result of 0.84, in the case of ultrasonic vibration-assisted cutting this result is almost halved, to 0.44.

In the case of conventional cutting, chip adhesion was observed and tool wear became more apparent as shown in Fig.5(b). It is supposed that this is due to high cutting temperature. On the other hand, there was less tool wear and chip adhesion in the case of ultrasonic vibration-assisted cutting as shown in Fig.5(a).

*TABLE 1. Cutting conditions*

| | |
|---|---|
| Workpiece | Ti-6Al-4V , φ50 |
| Cutting tool | KENNAMETAL TPGT110208K |
| Depth of cut | 0.1mm |
| Feed rate | 0.15mm/rev |
| Cutting speed | 30m/min |
| Ultrasonic Vibration | 19kHz , 0.03mm |
| Coolant | Dry |

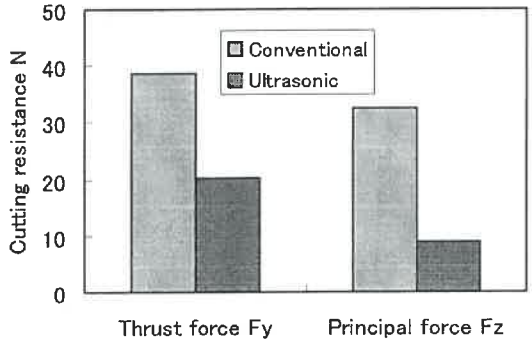


*FIGURE 4. Cutting resistance*

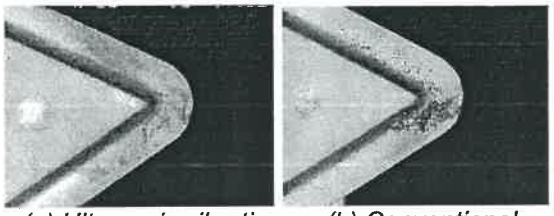

*(a) Ultrasonic vibration (b) Conventional*
*FIGURE 5. Cutting tool tip images*

**Properties of Cutting Surface**

Another issue of the conventional cutting of titanium alloy is that chips can become entangled between tool and workpiece. This results in damage to the surface of the workpiece and the surface roughness increases. Ultrasonic vibration-assisted cutting of Titanium alloy shows more effective chip discharge in comparison to conventional cutting. Flow type chips were discharged and no entanglement was observed as shown in Fig.6.

Fig. 7 shows the difference in the properties of the cut surface with and without ultrasonic vibrations. In the ultrasonic vibration-assisted cutting process, the material is removed little by little, producing "fish scale-like" marks.

The surface roughness Ra was 1.37 μm in the conventional cutting process, and was improved to 0.55 μm in the ultrasonic vibration-assisted cutting process. In the ultrasonic vibration-assisted cutting process, the surface roughness is very close to the theoretical roughness.

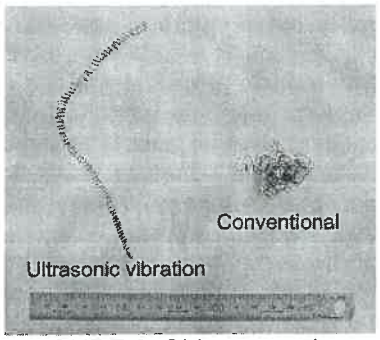


*FIGURE 6. Chip comparison*
*(Cutting conditions: Depth of cut=0.2mm, Feed=0.1mm/rev, Cutting speed=20m/min)*

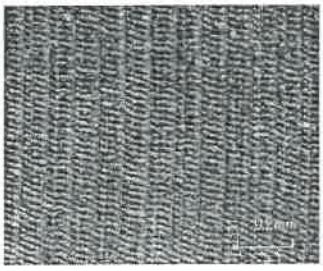

*(a) Ultrasonic vibration cutting : Ra=0.55 μm*

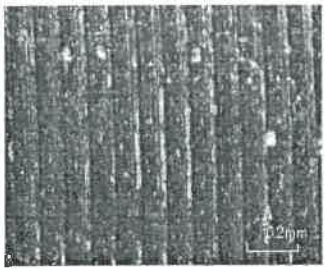

*(b) Conventional cutting : Ra=1.37 μm*

*FIGURE 7. Cutting surface*
*(Cutting conditions: Depth of cut=0.1mm, Feed=0.1mm/rev, Cutting speed=30m/min)*

## Comparison of Cutting Fluid Supply Methods

In the ultrasonic vibration-assisted cutting of the titanium alloy, cutting experiments were carried out using three cutting fluid supply methods - dry, semi-dry and wet - to investigate the surface roughness and the tool wear under these conditions.

In the dry cutting process, no cutting fluid was used. In the semi-dry cutting process, a vegetable oil was supplied at a rate of 4 mℓ/h in the mist form. In the wet cutting process, a water-soluble cutting fluid was supplied at a rate of 10 ℓ/min.

Fig. 8 shows the effects of the cutting fluid supply method on the surface roughness. The semi-dry method consistently resulted in low surface roughness. Fig. 9 shows the effects of the cutting fluid supply method on the flank wear of the tool. The tool wear was the smallest in the semi-dry cutting process. In the ultrasonic vibration-assisted cutting process, the lubricating ability of the semi-dry method was effective in reducing the surface roughness and the tool wear.

Fig. 10 shows images of the cutting face of the tool. The wear of the cutting edge of the tool was significant in the wet cutting process. In the ultrasonic vibration-assisted cutting process, the vibrating cutting edge of the tool intermittently cuts the workpiece. The temperature of the materials peaks when the cutting edge cuts into the workpiece, and drops down sharply when it is pulled back. In the wet cutting process, a large temperature difference occurs at the cutting edge repeatedly, causing a large thermal shock to the edge. Consequently, microchipping occurs at the cutting edge. Based on these results, in the ultrasonic vibration-assisted cutting of the titanium alloy, the semi-dry cutting process was the most suitable, surpassing the wet cutting process and dry cutting process. The semi-dry cutting process also has the advantage of being environmentally friendly.

*TABLE 2. Cutting conditions*

| | |
|---|---|
| Workpiece | Ti-6Al-4V , φ50 |
| Cutting tool | KENNAMETAL TPGT110208K |
| Depth of cut | 0.1mm |
| Feed rate | 0.1mm/rev |
| Cutting speed | 20m/min |
| Ultrasonic Vibration | 19kHz , 0.03mm |
| Coolant | Dry, Semi-dry, wet |

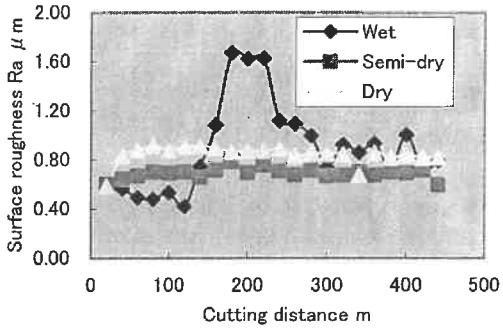


*FIGURE 8. Surface roughness*

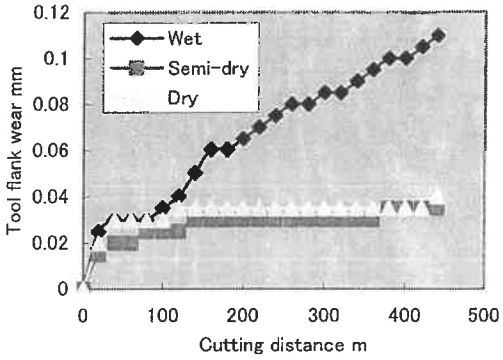


*FIGURE 9. Tool wear*

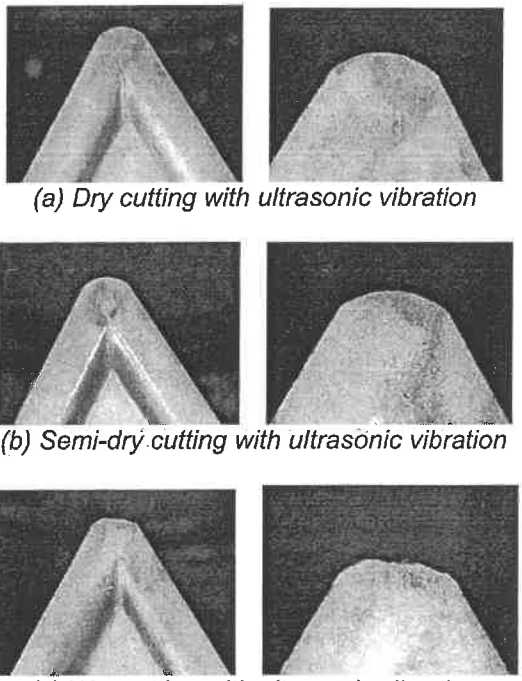

*(a) Dry cutting with ultrasonic vibration*

*(b) Semi-dry cutting with ultrasonic vibration*

*(c) Wet cutting with ultrasonic vibration*

*FIGURE 10. Cutting tool tip images*

**Effect of Cutting Speed**

Experiments with different speeds were tried to examine the effects of the cutting speed on the surface roughness of the workpiece and the flank wear of the tool, which are shown in Fig. 11. Both the surface roughness and the tool wear sharply increased at around a cutting speed of 30 m/min. The cutting speed of 30 m/min is about 30% of the maximum speed of the ultrasonic vibrating tool. Based on this, in order to achieve satisfactory cutting and a long tool life in the ultrasonic vibration-assisted cutting process, the cutting speed needs to be set at below 30% of the maximum speed of the ultrasonic vibrating tool.

*TABLE 3. Cutting conditions*

| | |
|---|---|
| Workpiece | Ti-6Al-4V , φ50 |
| Cutting tool | KENNAMETAL TPGT110208K |
| Depth of cut | 0.1mm |
| Feed rate | 0.1mm/rev |
| Cutting speed | 10 – 80 m/min |
| Ultrasonic Vibration | 19kHz , 0.03mm |
| Coolant | Semi-dry |

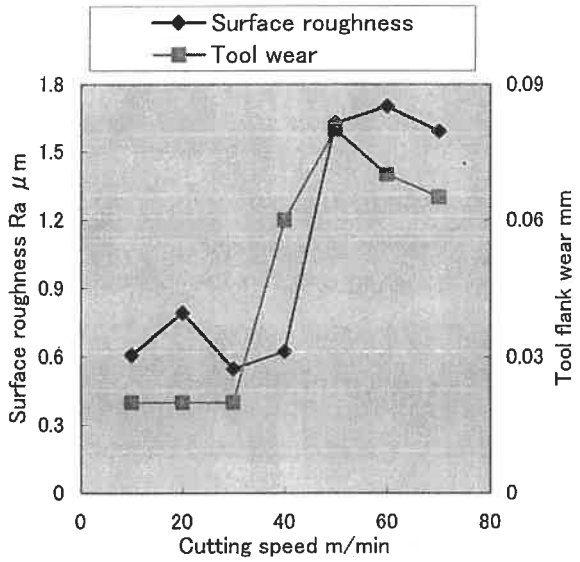


*FIGURE 11. Effect of cutting speed*

**CONCLUSIONS**

The effects of ultrasonic vibration-assisted cutting of titanium alloy were experimentally investigated. The results obtained are summarized as follows:

1. Using ultrasonic vibration-assisted cutting of titanium alloy, we succeeded in reducing the cutting resistance between one-half to one-third of that in conventional cutting.
2. Compared to conventional cutting, an improvement in surface roughness is observed in the case of ultrasonic vibration-assisted cutting of titanium alloy.
3. In regards to cutting fluid supply methods, comparisons were made of wet cutting, semi-dry cutting and dry cutting. We found that semi-dry cutting was the most suitable for ultrasonic vibration-assisted cutting of titanium alloy.
4. On investigating the effect of cutting speed in ultrasonic vibration-assisted cutting, we discovered that a cutting speed of 30 m/min showed the best performance. This speed is approximately 30 % of the maximum speed of the ultrasonic vibration at the tool tip.

**REFERENCES**


[1] Rahman M, Wong Y S, Zareena A R. Machinability of Titanium alloy. JSME Int Journal. Ser C. Vol.46, No.1,1993; 107-115.

[2] Klocke F, Schulz A, Gerschwiler K, Rehse M. Clean Manufacturing Technology – The competitive Edge of Tomorrow. Int. Journal for Manufacturing Science & Production. Vol.1, No.2, 1998; 77-86.

[3] Moriwaki T, Shamoto E. Ultraprecision Diamond Turning of Stainless Steel by Applying Ultrasonic Vibration. CIRP Ann, Vol.40, No.1, 1991; 559-562.


**ACKNOWLEDGEMENTS**


This study was conducted with financial assistance from the Ministry of Education, Culture, Science and Technology. We wish to acknowledge their kind support.

# Development of 3 DOF Ultrasonic Elliptical Vibration System for Elliptical Vibration Cutting

**Norikazu Suzuki[1], Rei Hino[1], and Eiji Shamoto[1]**
**[1]Department of Mechanical Science and Engineering**
**Nagoya University**
**Nagoya, Aichi, Japan**

## INTRODUCTION

Hardened steel for dies and molds is generally machined by ball endmilling. However, it is difficult to obtain mirror surfaces by the conventional method because cutting edges, made of cemented carbide or cubic boron nitride, cannot be finished to be smooth like single crystal diamond. Thus, mechanical polishing is applied subsequently when mirror surfaces are required.

Meanwhile, the authors have proposed a novel efficient machining method to machine sculptured mirror surfaces without polishing by combining elliptical vibration cutting and 4-axis control machining [1,2]. In order to realize proposal machining, three degrees of freedom (3 DOF) elliptical vibration system is required. A 3 DOF ultrasonic elliptical vibrator, which can generate a longitudinal and two directional bending vibrations, is designed. A method to adjust resonant frequencies and nodal positions of the vibration modes is developed and examined so that the vibrator can generate desirable ultrasonic elliptical vibration in the three dimensional (3D) space. A vibration controller and a cross talk remover to control the developed 3 DOF vibrator are also elaborated. The developed 3 DOF ultrasonic elliptical vibration system is applied to machining experiments of hardened steel.

## ELLIPTICAL VIBRATION CUTTING OF SCULPTURED SURFACES

Figure 1 shows the proposed machining method. In the elliptical vibration cutting, the tool is vibrated elliptically and fed in the nominal cutting direction relatively to the workpiece at the same time, so that the chip is formed intermittently and pulled out in each vibration cycle. Since the friction between the chip and the tool rake face is drastically reduced or reversed, the shear angle is increased and consequently the cutting force and the cutting energy are reduced significantly [3]. The intermittent cutting process at an ultrasonic frequency is also effective in preventing the tool wear and the adhesion, and diamond cutting of hardened steel can be realized as reported in the previous paper [4].

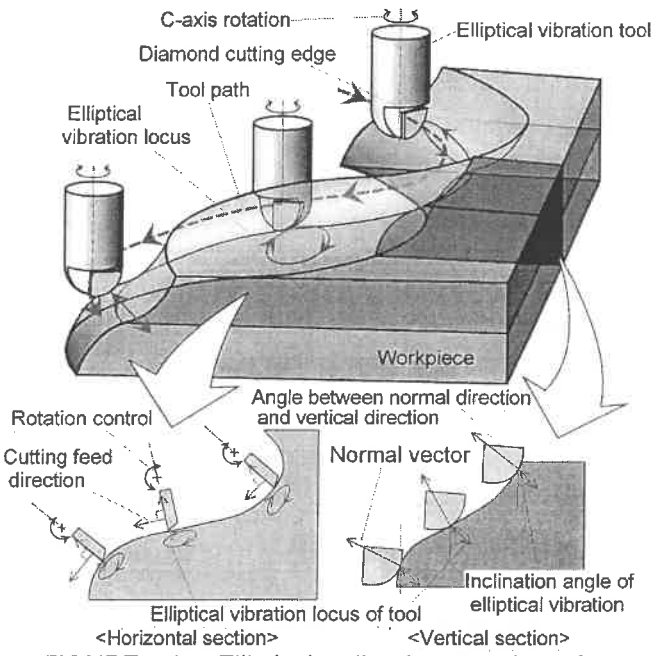


*FIGURE 1. Elliptical vibration cutting for sculptured surfaces.*

In the proposed machining method, the tool is vibrated elliptically in the desirable plane, and it is fed along the sculptured surface while the relative rotational position between the tool and the workpiece is precisely controlled in accordance with the sculptured surface orientation as shown in the figure.

Both the elliptical vibration cutting and the endmilling processes are intermittent, but the vibration frequency is much higher in the ultrasonic elliptical vibration cutting. This enables efficient machining at higher cutting feed speed with smaller theoretical roughness as compared with the endmilling [2].

In the proposed machining, a slender tool like an end mill needs to be vibrated elliptically at ultrasonic frequency in an inclined plane as shown in the figure. Additionally the ultrasonic

vibration has to be kept ultra-precisely in the set elliptical locus in the inclined plane while cutting in order to guarantee machining accuracy.

## DEVELOPMENT OF 3 DOF VIBRATION TOOL

In order to attain the desirable vibration, the 3 DOF vibrator shown in Fig. 2 was designed. The insert tool is attached at the end of the vibrator. The vibrator is excited in the 2nd longitudinal mode and the 5th bending modes by piezoelectric actuators. The longitudinal and the bending modes correspond to the vibrations in the axial and two perpendicular radial directions. By combining the three directional vibrations at the same frequency, elliptical vibration with an arbitrary locus in an arbitrary plane in the 3D space can be generated at the tool tip.

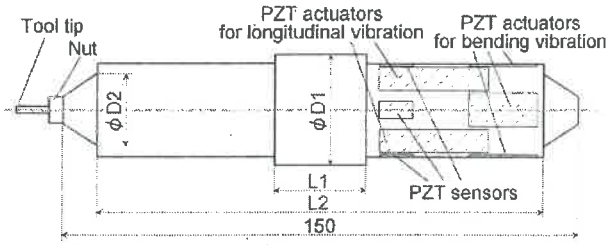


*FIGURE 2. Designed elliptical vibration tool.*

In order to gain enough vibration amplitude at the exciting frequency, the resonant frequencies of the three vibration modes should be as close as possible. The nodal positions of the three vibration modes should also be close in order not to prevent the vibrations at the clamps, which support the vibrator rigidly near the nodes. It is easy to obtain the same resonant characteristics between the two directional bending modes because the vibrator can be axisymmetric. However, it is difficult between the longitudinal and bending modes.

Thus, the 3 DOF vibrator is designed to have a stepped portion and tapered portions, as shown in the figure. Its resonant frequencies and nodal positions are adjusted by changing sizes of the portions, D1, D2, L1 and L2. The Finite Element Method (FEM) is employed to calculate the relationship between the sizes and the resonant characteristics, i.e. the resonant frequencies and the nodal positions, as shown in Fig. 3 and Fig. 4. As shown in the figures, the resonant characteristics are expected to change significantly as each size changes. The sizes D1 and L1 affect differences of the resonant frequencies and the nodal positions in the same way, as well as D2 and L2. Therefore, the frequencies and the nodal positions cannot be adjusted independently by changing D1 and L1, or D2 and L2. On the other hand, they can be adjusted independently by changing the sizes of D1 (or L1) and D2 (or L2), i.e. shapes of the stepped and tapered portions, at the same time.

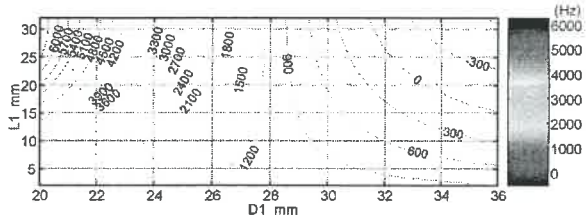


*(a) Difference between resonant frequencies of longitudinal and bending modes*

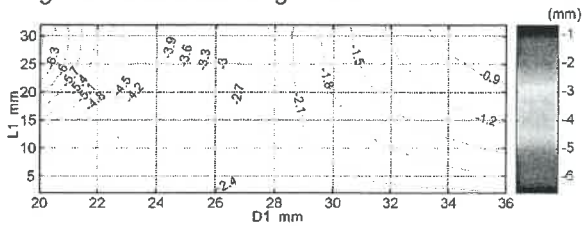


*(b) Difference between nodal positions of longitudinal and bending modes*

*FIGURE 3. Relationship between sizes of stepped portion and vibration modes.*

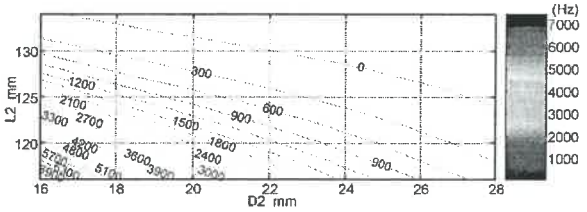


*(a) Difference between resonant frequencies of longitudinal and bending modes*

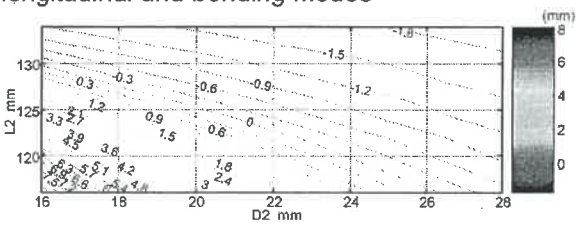


*(b) Difference between nodal positions of longitudinal and bending modes*

*FIGURE 4. Relationship between sizes of tapered portions and vibration modes.*

The sizes are optimized analytically according to the calculated relationships between the sizes and the resonant characteristics. Figure 5 shows each vibration mode calculated with the optimized values. Their differences of the resonant frequencies and nodal positions are

negligible, and the adjusted resonant frequency is 34.4 kHz.

Based on the analytical results, the vibrator was produced as shown in Fig. 6. The vibrator is clamped at eight points at two nodal positions with sharpened bolts. A diamond tool tip is fixed at the left end of the vibrator.

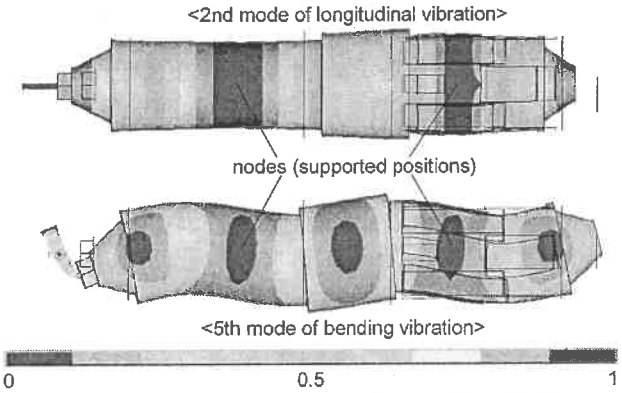


*FIGURE 5. Resonant modes simulated by FEM. D1=32 mm, L1=26 mm, D2=23 mm, L2=131.5 mm*

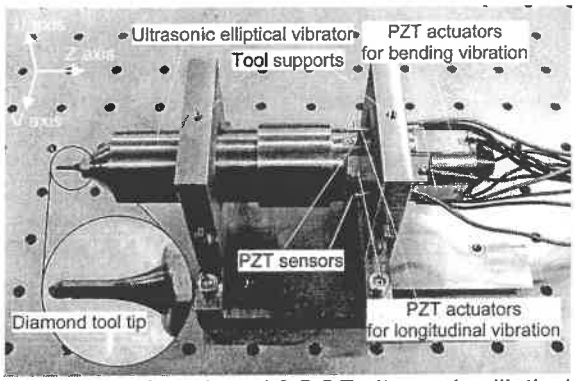


*FIGURE 6. Developed 3 DOF ultrasonic elliptical vibration tool.*

Figure 7 shows the three directional vibrations measured by laser Doppler vibrometers. It is confirmed that it can generate an arbitrary ultrasonic elliptical vibration in the 3D space by combining the three directional vibrations.

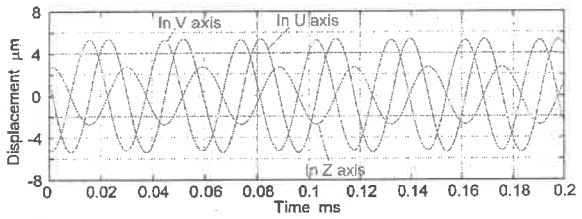


*FIGURE 7. Measured vibrations.*

Figure 8 shows frequency responses of the vibration modes measured at the end of the tool tip. The differences between the resonant frequencies are less than 23 Hz and small enough. Thus, large elliptical vibration can be obtained effectively by exciting the three vibration modes at an intermediate frequency among the three resonant frequencies.

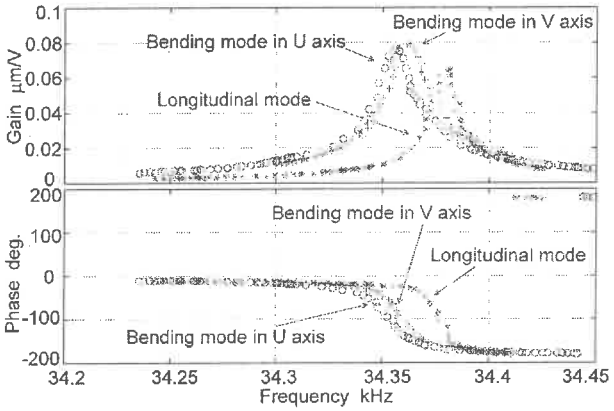


*FIGURE 8. Measured frequency responses of vibration modes.*

The tool tip is screwed and fixed with a nut as shown in Fig. 6, and thus its projection length can be changed slightly. Figure 9 shows effects of the projection length on the resonant frequencies. The effect on the longitudinal mode is small, but those on the bending modes are relatively large. Thus the resonant frequencies can be adjusted slightly by changing the projection length of the tool tip.

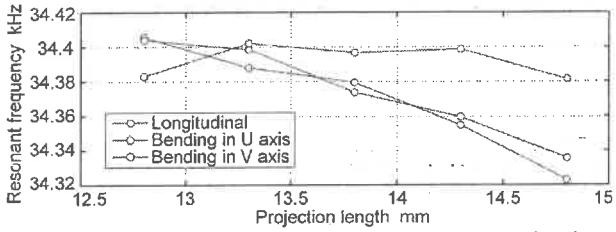


*FIGURE 9. Relationship between projection length of tool tip and resonant frequencies.*

## DEVELOPMENT OF 3 DOF VIBRATION CONTROLLER

The cross talks between the longitudinal mode and the two directional bending modes should be small enough in order to control each vibration mode independently. However, each vibration mode interferes considerably in practice with the other modes. Thus, a cross talk remover for the 3 DOF vibrator is developed here by extending the conventional cross talk remover for the 2 DOF elliptical vibrators [5]

The cross talks are assumed to be caused by cross factors in mass, damping, stiffness and exciting force, and the practical vibration system can be expressed as Eq. (1):

$$\begin{bmatrix} m_{11} & m_{12} & m_{13} \\ m_{21} & m_{22} & m_{23} \\ m_{31} & m_{32} & m_{33} \end{bmatrix} \begin{Bmatrix} \ddot{x}_1 \\ \ddot{x}_2 \\ \ddot{x}_3 \end{Bmatrix} + \begin{bmatrix} c_{11} & c_{12} & c_{13} \\ c_{21} & c_{22} & c_{23} \\ c_{31} & c_{32} & c_{33} \end{bmatrix} \begin{Bmatrix} \dot{x}_1 \\ \dot{x}_2 \\ \dot{x}_3 \end{Bmatrix} + \begin{bmatrix} k_{11} & k_{12} & k_{13} \\ k_{21} & k_{22} & k_{23} \\ k_{31} & k_{32} & k_{33} \end{bmatrix} \begin{Bmatrix} x_1 \\ x_2 \\ x_3 \end{Bmatrix} = \begin{bmatrix} f_{11} & f_{12} & f_{13} \\ f_{21} & f_{22} & f_{23} \\ f_{31} & f_{32} & f_{33} \end{bmatrix} \begin{Bmatrix} F_1 \\ F_2 \\ F_3 \end{Bmatrix}, \quad (1)$$

where $x$ and $F$ are displacements and exciting forces. $m$, $c$, $k$ and $f$ denote coefficients for the mass, the damping, the stiffness and the exciting force. Subscripts 1, 2 and 3 indicate the longitudinal and two bending modes.

In order to remove the cross components the matrixes underlined in Eq. (2), i.e. local cross feedback gains, are inserted,

$$\begin{bmatrix} m_{11} & m_{12} & m_{13} \\ m_{21} & m_{22} & m_{23} \\ m_{31} & m_{32} & m_{33} \end{bmatrix} \begin{Bmatrix} \ddot{x}_1 \\ \ddot{x}_2 \\ \ddot{x}_3 \end{Bmatrix} + \begin{bmatrix} c_{11} & c_{12} & c_{13} \\ c_{21} & c_{22} & c_{23} \\ c_{31} & c_{32} & c_{33} \end{bmatrix} \begin{Bmatrix} \dot{x}_1 \\ \dot{x}_2 \\ \dot{x}_3 \end{Bmatrix} + \begin{bmatrix} k_{11} & k_{12} & k_{13} \\ k_{21} & k_{22} & k_{23} \\ k_{31} & k_{32} & k_{33} \end{bmatrix} \begin{Bmatrix} x_1 \\ x_2 \\ x_3 \end{Bmatrix}$$
$$= \begin{bmatrix} f_{11} & f_{12} & f_{13} \\ f_{21} & f_{22} & f_{23} \\ f_{31} & f_{32} & f_{33} \end{bmatrix} \begin{bmatrix} f_{11} & f_{12} & f_{13} \\ f_{21} & f_{22} & f_{23} \\ f_{31} & f_{32} & f_{33} \end{bmatrix}^{-1} \left( \begin{Bmatrix} F_1 \\ F_2 \\ F_3 \end{Bmatrix} + \begin{bmatrix} 0 & k_{12} & k_{13} \\ k_{21} & 0 & k_{23} \\ k_{31} & k_{32} & 0 \end{bmatrix} \right.$$
$$\left. - \omega^2 \begin{bmatrix} 0 & m_{12} & m_{13} \\ m_{21} & 0 & m_{23} \\ m_{31} & m_{32} & 0 \end{bmatrix} \begin{Bmatrix} x_1 \\ x_2 \\ x_3 \end{Bmatrix} + \begin{bmatrix} 0 & c_{12} & c_{13} \\ c_{21} & 0 & c_{23} \\ c_{31} & c_{32} & 0 \end{bmatrix} \begin{Bmatrix} \dot{x}_1 \\ \dot{x}_2 \\ \dot{x}_3 \end{Bmatrix} \right), \quad (2)$$

where exciting angular frequency is $\omega$, which is assumed to be constant.

The inserted matrixes add some forces, which are proportional to the displacements or their derivatives, to the exciting forces. A block diagram of the developed cross talk remover is shown in Fig. 10, whose signal gains correspond to elements of the inserted matrixes.

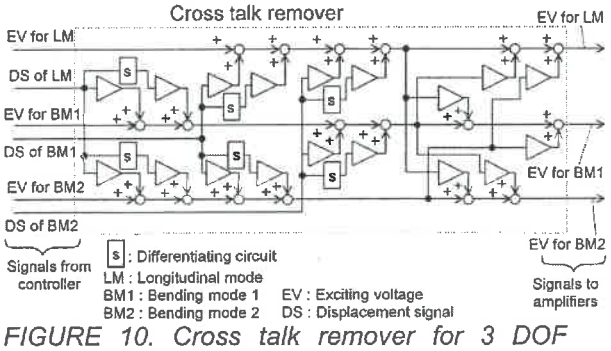


*FIGURE 10. Cross talk remover for 3 DOF vibrator.*

Figure 11 shows measured frequency responses of the three directional vibrations. As shown in Fig. 11(a), there were large cross talks, especially in the bending modes when the longitudinal mode was excited. On the other hand, the cross talks were reduced considerably by applying the developed cross talk remover.

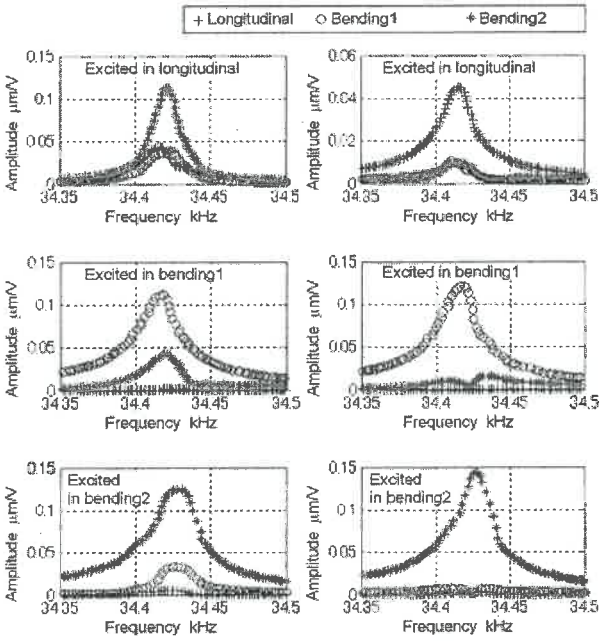


*(a) Without remover (b) With remover*

*FIGURE 11. Measured frequency responses with and without developed cross talk remover.*

A new 3 DOF ultrasonic vibration controller, including the cross talk remover, was also elaborated to keep a desirable ultrasonic elliptical vibration ultra-precisely in the 3D space. Figure 12 shows the developed vibration control system.

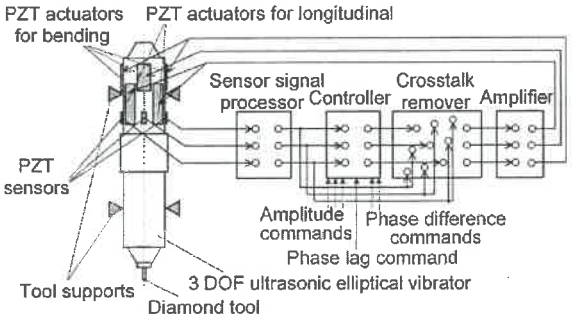


*FIGURE 12. 3 DOF ultrasonic elliptical vibration control system.*

Each displacement is detected by using small PZT sensors, which are attached on the vibrator. The longitudinal displacement can be detected by addition of signals of the front and back sensors. On the other hand, the bending

displacement can be detected by subtraction of those signals.

The detected displacement signals are compared with commands, and the errors are inputted to PI controllers. The PI controllers output exciting voltages to the cross talk remover, and the remover modifies the exciting voltages and applies them to PZT actuators. The developed feedback control system keeps the amplitudes of the three directional vibrations and their phase differences to be the commands, and locks the vibration frequency to an average value of the resonant frequencies.

Figure 13 shows step responses of the controlled parameters. As shown in the figure, all settling times are less than 5 ms. Especially the amplitude responses are quick and stable, and thus high machining accuracy can be achieved.

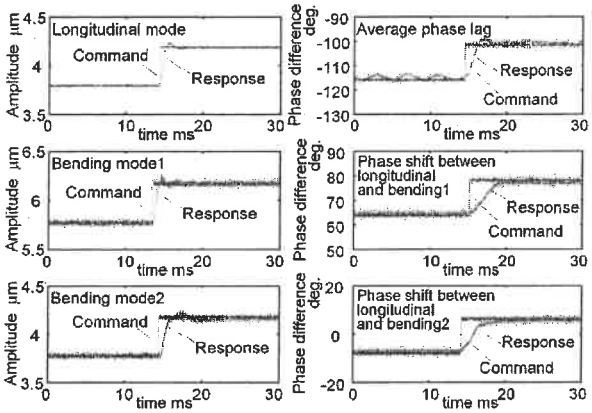


*FIGURE 13.. Step responses of controlled parameters.*

## MACHINING EXPERIMENTS

Machining experiments were carried out to examine performance of the developed 3 DOF vibration system. First, the developed vibrator with the vibration controller was attached to an ultraprecision planing machine, NIC-300 made by Nagase Integrex Co., Ltd., and they were applied to ultraprecision planing of hardened steel with a single crystal diamond tool to clarify the basic performance. Then, the developed vibration system was attached to a 4 axis precision machine tool, MU-400VA-DD made by OKUMA Corp., as shown in Fig. 14. They were applied to the proposed 4-axis machining of spherical hardened steel. The machining conditions are summarized in Table 1.

Figure 15 shows the flat mirror surface machined in the planing experiment. Figure 16 shows surface profiles measured by a stylus surface profiler. High quality mirror surfaces with maximum roughness of less than 0.09 μm Rz were obtained. Theoretical roughness in the feed direction is 0.05 μm, which is close to the measured one. This shows that the elliptical vibration locus was controlled successfully while cutting.

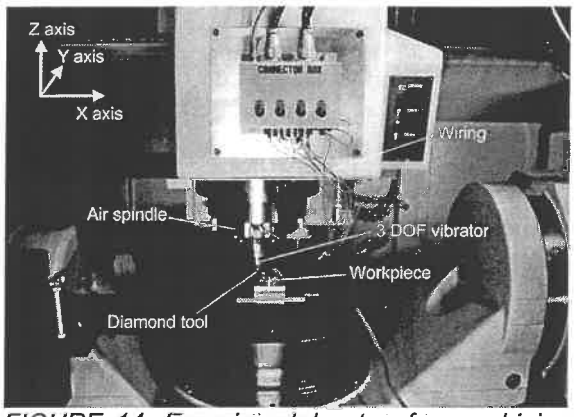


*FIGURE 14. Experimental setup for machining spherical workpiece.*

*Table 1. Machining conditions.*

| Machined shape | | Flat | Spherical |
|---|---|---|---|
| Vibration conditions | Frequency kHz | 34.4 | 34.4 |
| | Amplitude in U-V-Z direction μm | 4-4-4 | 8-8-4 |
| | Phase differences U-V, U-Z deg. | -90, 90 | -90, 90 |
| Cutting conditions | Pick feed μm | 20 | 15 |
| | Depth of cut μm | 5 | 3 |
| | Feed speed m/min | 0.2 | less than 1.34 |
| | Cutting fluid | Oil mist | Oil mist |
| Tool | Material | Diamond | Diamond |
| | Rake angle deg. | 0 | 0 |
| | Nose radius mm | 1 | 1 |
| Workpiece | Material | Hardened steel | Hardened steel |
| | JIS | SUS420J2 | NAK80 |
| | Hardness | HRC54 | HRC40 |
| | Shape | ϕ6-27 | R30, ϕ56 |
| Machine tool | | NIC-300 | Mu-400VA-DD |

Figure 17 shows the spherical surface finished in the 4-axis machining experiment. Figure 18 shows surface profiles measured at a radius of 5.3 mm. The spherical mirror surface with a maximum roughness of less than 0.16 μm Rz is attained by the sculptured surface machining.

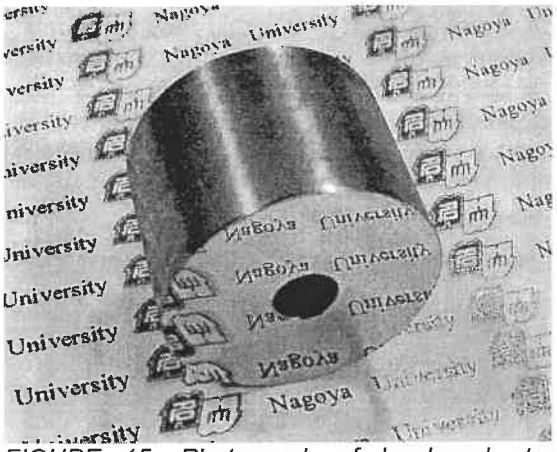


*FIGURE 15. Photograph of hardened steel machined in planing experiment.*

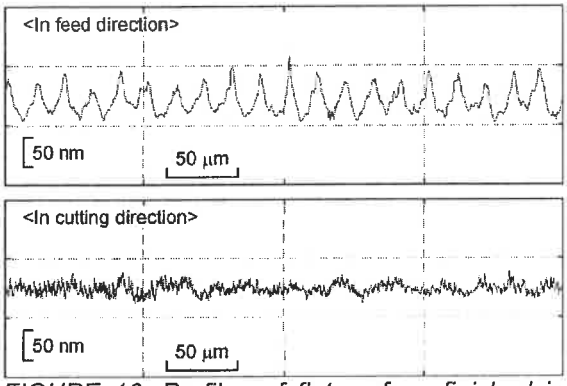


*FIGURE 16. Profiles of flat surface finished in planing experiment.*

## CONCLUSION

The new ultrasonic elliptical vibration system was developed in the present research to realize the sculptured surface machining of die steel by applying the elliptical vibration cutting. The 3 DOF vibrator was produced, and it was confirmed that an arbitrary ultrasonic elliptical vibration in the 3D space can be generated at 34.4 kHz by combining the three directional vibrations. The new ultrasonic vibration controller, including the cross talk remover, was also developed for the 3 DOF ultrasonic vibrator. The developed vibration control system was attached to the two precision machine tools, and they were applied to the machining experiments of hardened steel with single crystal diamond tools. The flat mirror surface of the die steel with a maximum roughness of less than 0.09 μm Rz was obtained by the fundamental planing experiment. The spherical mirror surface with a maximum roughness of less than 0.16 μm Rz was also attained by the proposed sculptured surface machining method.

*FIGURE 17. Photograph of hardened steel finished by sculptured surface machining method.*

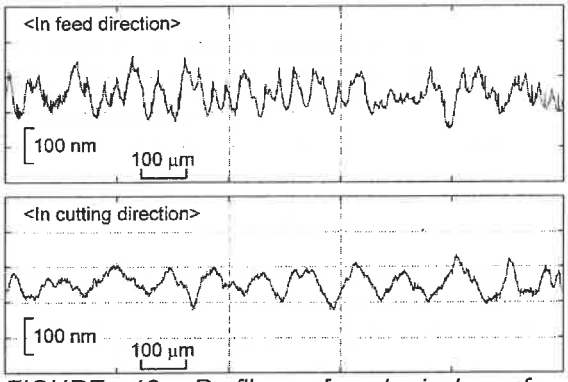


*FIGURE 18. Profiles of spherical surface finished by sculptured surface machining method.*

## REFERENCES

[1] Shamoto E, Suzuki N, et al. Development of 3 DOF Ultrasonic Vibration Tool for Elliptical Vibration Cutting of Sculptured Surfaces. Ann. CIRP: 2005; 54: 321-324.

[2] Shamoto E, Suzuki N, et al. Sculptured Surface Machining of Die Steel by Applying Elliptical Vibration Cutting (in Japanese). J. JSPE: 2006; 72/9: 1139-1145.

[3] Shamoto E, Moriwaki T. Study on Elliptical Vibration Cutting. Ann. CIRP: 1994; 43: 35-38

[4] Shamoto E, Moriwaki T. Ultraprecision Diamond Cutting of Hardened Steel by Applying Elliptical Vibration Cutting. Ann. CIRP: 1999; 48: 441-444.

[5] Shamoto E, Suzuki N, et al. Development of Ultrasonic Elliptical Vibration Controller for Elliptical Vibration Cutting. Ann. CIRP: 2002; 51: 327-330.

# 3-D MICROSTRUCTURE CREATION USING ELLIPTICAL VIBRATION-ASSISTED MACHINING[1]

**D. E. Brehl, T.A. Dow**
**Precision Engineering Center**
**North Carolina State University**
**Raleigh, North Carolina, USA**

## INTRODUCTION

"Elliptical vibration-assisted machining" (EVAM) is a diamond-tool machining process that can be used to create 3-dimensional micro-structures. In EVAM, the tool tip is driven very rapidly through a small (tens of micrometers) ellipse at multi-kHz frequencies. This elliptical motion is superimposed on the normal tool feed motion. EVAM shows potential for fabrication of micro-scale devices with true 3-D geometry, with greater material and shape flexibility than lithography methods derived from the semiconductor industry. When feature tolerances of ~200 nm suffice, it is more economical than methods such as micro-electro-discharge machining, focused ion beam, or laser ablation. EVAM also avoids problems of tool deflection, chatter, runout, and vibration associated with chip-making processes like micro-milling [1]. Because the tool is cutting in the workpiece for only part of each elliptical cycle, average cutting forces, and tool wear from mechanical and chemical effects, are reduced compared to conventional machining [2].

To date, EVAM has mostly been used in turning or facing operations to create precision macro-scale parts such as optical quality flats and molds with complex but low-aspect ratio geometries. For example, Negishi [3] made an annular flat in silicon carbide with a surface roughness of < 7 nm RMS. Shamoto *et al* have used an ultrasonic EVAM system to create steel micromolds for high-sag and Fresnel lenses [4], flat and hemispherical steel mirrors [5], and groove structures in several brittle materials [6].

The Precision Engineering Center's EVAM tool, the Ultramill, has been used to machine binary microstructures. These have feature heights of 500 nm to 1 $\mu$m above the background. The Angstrom symbols in Figure 1 are machined in hard-plated copper. The large feature is 1 mm x 1 mm and was made with a 1 mm nose radius tool. The small Angstrom symbol (inset in Figure 1) is shown to the same scale, and is 200 $\mu$m x 200 $\mu$m. It was made using a tool with a 50 $\mu$m nose radius. Its smallest feature (vertical bar on the topknot symbol) is only 15 $\mu$m across. The Angstrom symbols have RMS surface roughness of 15-25 nm and are seen to be burr-free when imaged by SEM. The thunderbird logo in Figure 2 was machined in 17-4 stainless steel using a 1 mm nose radius tool. It is approximately 1.08 mm x 1.08 mm, with surface roughness of 20 nm RMS with burr-free edges.

The goal of the current research is to use EVAM to create complex microstructures with features representative of micromolds and MEMS devices. Objectives to be achieved are a minimum feature resolution of 1 $\mu$m, 1:1 vertical aspect ratio, and an ability to create structures with both sculpted 3-D geometry and straight, steep sidewalls. If microstructures meeting these criteria can successfully be machined in previously intractable materials such as steel, glass, or brittle optical materials, then EVAM will provide an important addition to existing MEMS fabrication methods based on lithography, LIGA, or soft polymer molding techniques.

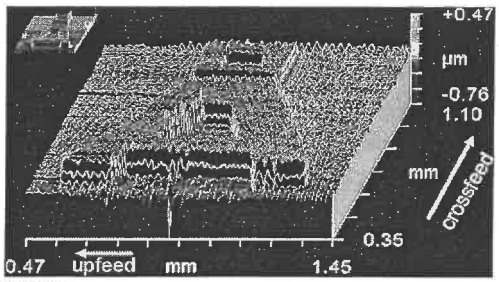


*FIGURE 1. Interferograms of 1 mm x 1 mm (main image) and 200 µm x 200 µm (inset) Angstrom symbols machined by EVAM. Hard plated copper material [7].*

[1] Research sponsored by NSF grant DMI-0423315, monitored by G. Hazelrigg.

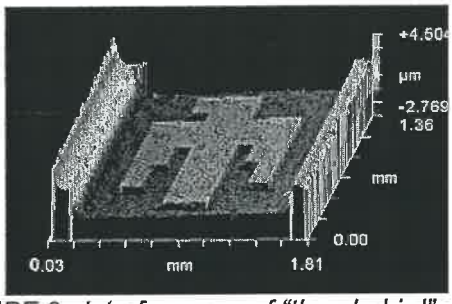


*FIGURE 2. Interferogram of "thunderbird" machined in 17-4 stainless steel using EVAM.*

## PROCESS

Figure 3 shows how EVAM can be achieved using two parallel piezoelectric actuators to drive a diamond tool. Applying cyclic voltages to the stacks causes them to change length in a cyclical manner. The toolholder acts as a linkage to convert the linear stack motion into an elliptical path. By changing the voltage amplitude and/or phase difference between the stacks, the ellipse geometry (aspect ratio, tilt, and dimensions) can be varied through a wide range.

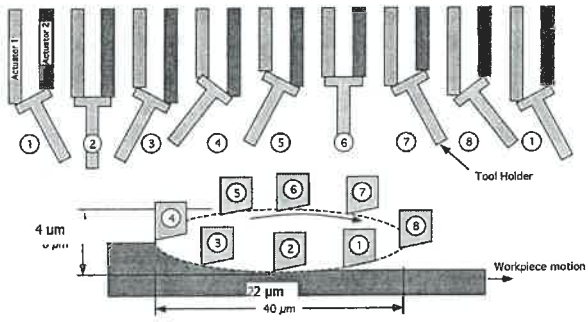


*FIGURE 3. Ultramill EVAM concept*

Figure 4 shows the tool motion in EVAM for two consecutive cutting cycles. During each cutting cycle, the work advances relative to the elliptical tool path. The overlapping toolpaths produce thin chips, resulting in greatly reduced tool forces compared to conventional cutting.

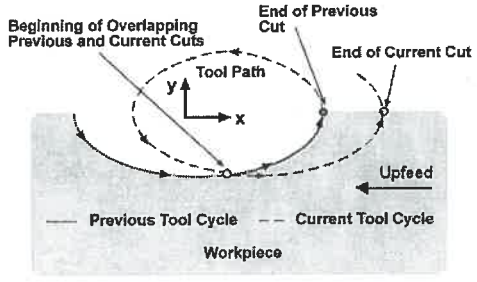


*FIGURE 4. EVAM process cycle*

Chip geometry is affected by the ratio between depth of cut and the ellipse vertical amplitude. When the depth of cut is equal to or smaller than the ellipse vertical amplitude, the tool exits the workpiece before completing its elliptical pass and small discontinuous chips are produced. When the depth of cut is greater than the ellipse vertical amplitude, the chip remains attached to the workpiece. A long discontinuous chip is produced with evenly spaced attached segments corresponding to the discontinuous chips in the preceding case. To create features that have a significant dimension in the depth direction, roughing passes can be made at a DOC larger than the semi-minor axis of the tool path ellipse. This economically achieves most of the required material removal. A finish pass is then made with DOC smaller than the ellipse semi-minor axis, to complete the part with excellent surface finish and sub-micrometer feature tolerance.

In EVAM the theoretical surface roughness in the upfeed direction is a function of the ellipse size and the upfeed increment, $F_{UP} = V/f$, where $V$ is the workpiece velocity and $f$ is the vibration frequency. The smaller the value of $F_{UP}$, the smaller is the theoretical feature height caused by the geometry of overlapping elliptical tool passes. When raster machining microstructures, axis moves are typically only a few tens to a few hundreds of micrometers in length. In this situation, the maximum upfeed velocity attained during a move is limited by the axis acceleration. Peak velocity is generally less than 1 mm / sec, which means that a theoretical upfeed surface roughness of 1 nm PV can be achieved with a vibration frequency in the KHz range. EVAM at such a relatively low frequency means that vibratory forces generated by the Ultramill are well below the natural frequency of the DTM's axes. The input power and cooling requirement for the piezoelectric actuators are also reduced.

## EQUIPMENT

Figure 5 shows a cutaway view of the Ultramill. The two piezoelectric actuators are cooled by a dielectric fluid circulating continuously through the steel chamber. The hollow lightweight ceramic toolholder rests on alumina pins on the tops of the piezo stacks. A diamond tool is cemented to the toolholder. The titanium diaphragm exerts preload force on the piezo stacks and seals the coolant chamber. The Ultramill operates at frequencies up to 4 kHz.

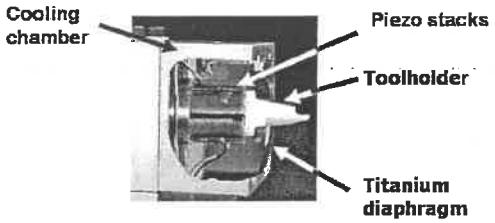


*FIGURE 5. Ultramill EVAM tool*

Figure 6 shows the Ultramill installed on a 3-axis diamond turning machine (DTM), which provides X-Y-Z motion for raster machining (the spindle is locked when using the Ultramill). The DTM's three axes are supported by hydrostatic oil bearings with nanometer-scale encoder resolution. The workpiece is held in place for machining by a vacuum chuck attached to the spindle. To facilitate touchoff, a video-microscope camera provides a view of the tool rake face and the work surface.

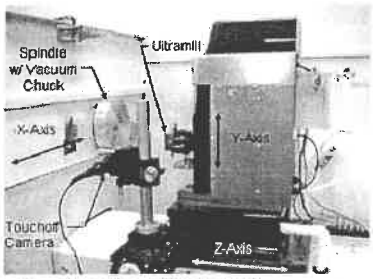


*FIGURE 6. 3-axis diamond turning machine (DTM). Spindle is currently locked when using the Ultramill.*

## 3-D MICROSTRUCTURES MADE USING ROUND-NOSED TOOLS

Several microstructures have been made with sculpted 3-D geometry, using round-nosed diamond tools.[2] Two representative parts are described here. In both cases the Ultramill was operated at a frequency of 1000 Hz with an elliptical toolpath of 22 $\mu$m x 4 $\mu$m (long axis parallel to the work surface).

### Convex Cylinder Section

Figure 7(a) shows an SEM image of a feature consisting of a convex cylindrical surface, oriented with its longitudinal axis parallel to the upfeed direction. The design cylinder radius is 1000 $\mu$m, with a chordal width of approximately 400 $\mu$m and a length of 1 mm. From the flat background to the top of the cylindrical feature is 20 $\mu$m. The part was machined with 3 sets of crossfeed passes at an increment of 5 $\mu$m. The first two sets of passes were for material removal with depth of cut 10 $\mu$m and 9 $\mu$m respectively, followed by a 1 $\mu$m deep finishing pass. The part took 58 minutes to complete. Figure 7(b) is a white-light interferogram of the cylinder feature. A cross section was extracted from the interferometer data and a least-squares best-fit circle applied to estimate the radius of the convex portion of the machined feature. The residuals between the measured surface and the best fit radius approximately represent the outward normal surface profile of the part. These residuals give a crossfeed surface roughness of approximately 100 nm PV. This compares with a crossfeed surface roughness of 30 nm PV in the flat portion of the part background. The theoretical crossfeed roughness derived from the tool radius and crossfeed increment is 3.1 nm. The surface roughness in the upfeed direction is 80 nm PV along the crown of the convex segment and 42 nm PV for the flat background,. The theoretical upfeed surface roughness is 2.1 nm based on the ellipse dimensions, upfeed velocity, and vibration frequency.

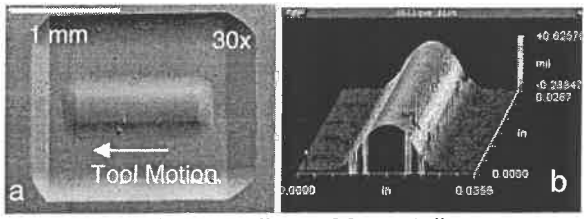


*FIGURE 7. 1 mm radius x 20 µm tall convex cylinder segment made with 1 mm nose radius tool. (a) SEM image (b) Interferogram*

### Sculpted 3-D Groove Microstructure

Figure 8 shows the design of a microstructure consisting of parallel grooves with sculpted 3-D geometry. The grooves have a sinusoidal section in the crossfeed direction, which is superimposed on a cosine profile in the upfeed direction. The width (or wavelength) of each groove is 320 $\mu$m and their maximum depth is 5 $\mu$m, giving an aspect ratio of 0.016. The length (or upfeed wavelength) of the part is 1.28 mm while the amplitude of the sinusoidal section s 4.5 $\mu$m. The part was machined with a crossfeed spacing between raster passes of 5 $\mu$m. The part was made with a single set of crossfeed passes and took 51 minutes to cut.

[2] Diamond tools provided by Chardon Tool.

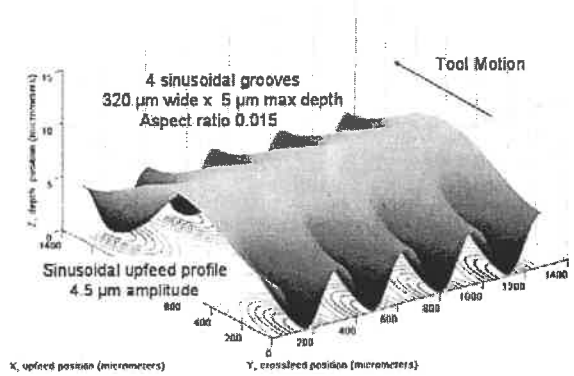


*FIGURE 8. Design rendering of 3-D sculpted geometry microstructure made using 1 mm nose radius tool. Grooves have sinusoidal cross section and sinusoidal profile in upfeed direction.*

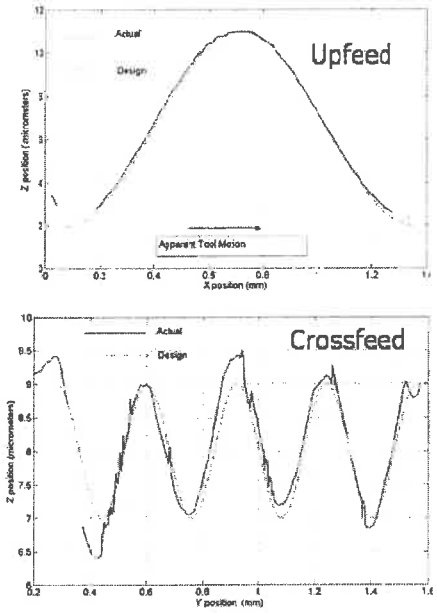


*FIGURE 9. Profiles of part in Figure 11 from white-light interferometry data. (top) Upfeed profile (bottom) Crossfeed profile showing form error apparently caused by system thermal instability.*

White-light interferometery was used to measure the sinusoidal groove part. The tilt of the surfaces was sufficiently shallow so that data could be obtained over almost the entire part. Figure 9 shows upfeed and crossfeed profiles made from the interferometry data. The upfeed profile was taken along the bottom of one of the grooves. In the upfeed direction the machined profile closely matched the intended profile. In the crossfeed direction, there is form error with one groove bottom and one ridge top being displaced vertically by 500 nm. This form error resulted from slow thermal expansion and contraction of the Ultramill during the machining run, in the depth of cut direction. Corrective measures have been identified and the part will be recut.

## SHARP-NOSE TOOLS

Round nose tools are limited to making low-aspect ratio features with shallow curved sidewalls. The minimum possible groove width for a round tool grows significantly with increasing depth of cut due to the rapid increase in chord width of the tool cross section. For example, a tool of 50 $\mu$m nose radius will cut a groove 20 $\mu$m wide at a 1 $\mu$m depth of cut, but for a 5 $\mu$m deep cut the groove width increases to 44 $\mu$m. The groove width defines the minimum crossfeed spacing of positive features.

Figure 10 shows an SEM image of a sharp nose tool with a 40° included nose angle. The cutting edges are on the sides of the tool. With such a tool, straight side walls can be made which are within 20° of vertical. For a 5 $\mu$m depth of cut, such a tool will produce a groove only 3.6 $\mu$m wide at its top. The tool in Figure 10 is "dead-sharp" with a nose radius less than 100 nm. For a crossfeed increment of 1 $\mu$m such a tool will produce a theoretical crossfeed surface roughness of 1373 nm PV. Most applications require much smoother finishes on horizontal or sculpted surfaces. Therefore a "hybrid" sharp-nose tool with a 1-2 $\mu$m nose radius may be more suitable. For example, a sharp-nose a tool with 2 $\mu$m nose radius produces a theoretical crossfeed surface roughness of 62 nm at a crossfeed increment of 1 $\mu$m.

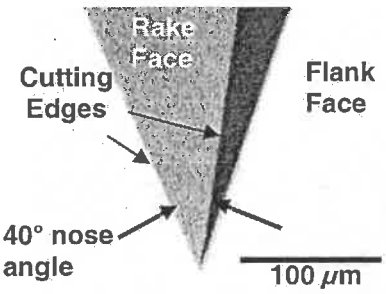


*FIGURE 10. SEM image of a "dead sharp" diamond tool with 40° nose angle.*

An important difference between round-nose and sharp-nose tools is the relative velocity between the cutting edge and the work material. For a round-nose tool, the angle between the

# NUMERICAL SIMULATIONS OF VIBRATION ASSISTED MACHINING

**John A. Patten, Andre Williams**
**Manufacturing Research Center**
**Western Michigan University**
**Kalamazoo, Michigan**

**Keywords:** Finite Element Model (FEM), Force Analysis, Temperature Analysis, SPDT

## ABSTRACT

A two-dimensional (2-D) finite element model (FEM) has been developed to perform numerical simulations of vibration assisted machining (VAM). The model is based on an updated Lagrangian formulation, with adaptive remeshing. The model is capable of simulating the amplitude and frequency independently of the tool in the cutting (x) and thrust (y) force directions over a wide range of values. The resultant vibrations include linear, circular, and elliptical paths. Results of the finite element analysis include: chip formation, work piece deformation, cutting and thrust forces, pressures, temperatures, stress, strain, and strain rate. Materials modeled include: aluminum, steel and silicon carbide. These materials represent a comprehensive array of material properties and demonstrate the general utility of the modeling method. Other variables in the model include: cutting edge radius, rake angle, clearance angle, feed, cutting speed, depth of cut, length of cut, work piece dimensions, friction coefficient, and ambient conditions. The simulation results allow for a detailed study of the materials behavior in response to the VAM process variables. The work reported in this paper includes nano to micro meter feeds and depth of cut. VAM results are compared to base line simulations without vibrating conditions. The results reported are for diamond cutting tool material, i.e. single point diamond turning (SPDT) operation. The VAM results show a significant reduction in cutting ($F_c$) and thrust ($F_t$) forces as the degree of vibration (amplitude) and frequency are increased. Other parameters determined directly from the simulation results of interest include: Force ration ($F_c/F_t$), maximum temperatures and maximum pressures in the work piece. The results and analyses for the VAM process demonstrate the model's general utility over a wide range of process conditions (work piece materials), machining parameters (speeds, feeds and depth of cut) and VAM variables (amplitude and frequency of vibration). Comparisons to experimental results are included. Future work will attempt to reduce the scale of the vibration, to nanometers, and provide enhancements to the tool wear model to directly incorporate the effect of VAM to improve the machining process. This latter work will concentrate on further reductions in tool forces and temperatures, and research on the beneficial results of cutting fluids to the machining process in general the VAM process in particular. It is expected that improved tool designs will directly result from this work.

## INTRODUCTION

Vibration assisted machining (VAM) has proved beneficial at machining metals and ceramics, with special applications being applied to steels and SiC [1-3]. This paper presents complementary work on numerical simulations of the VAM process using a commercial FEM software package AdvantEdge, from Third Wave Systems Inc. One of the authors (Patten) worked with TWS on the development and implementation of the VAM module, which is now incorporated into their commercial software product. The software has been tested and evaluated for a limited set up materials and process conditions. The work reported on in this paper concerns diamond turning of steels, as practiced by Overcash [2]. Of particular interest is the evaluation of the forces (cutting and thrust) and resultant temperatures. It is often assumed that the primary benefit of the VAM process to do reduce tool wear, when cutting (particularly diamond machining) difficult to machine materials (such as steels and ceramics). Reduced tool wear is assumed to result from decreased machining forces and/or decreased temperatures during machining. Tool wear is not explicated considered in this paper, nor is the application of a cutting fluid or coolant addressed. These conditions will be explored further in future work.

## EXPERIMENTS-SIMULATIONS

A 2-D Lagrangian Finite Element Model (FEM), utilizing adaptive remeshing is utilized [5] for the simulations. Process parameters of interest include, which are explicated simulated include: feed, speed, amplitude and frequency of vibration. The work reported in this paper is for machining steel with single crystal diamond tooling. The work piece material is a 12L14 Steel [2] and the diamond tool used is a zero degree rake angle of varying cutting edge radius (0.002 to 0.001 mm). A constant frequency of vibration of 10,000 Hz is utilized in all of the results reported on herein [2], however the simulation model is capable of a wide range of vibration frequencies. The feed, or uncut chip thickness, used for these simulations is 20 micrometers ($\mu$m, or 0.020 mm) and the amplitude of vibration ranges include: 0, 2, 4 and 8 micrometers (0, 0.002, 0.004, and 0.008 mm respectively). Three different cutting speeds are reported on in this paper, these are: 1 m/s, 0.5 m/s and 0.25 m/s. The simulated conditions are summarized in Table 1. Only circular vibrations are considered in this paper, i.e. the x and y vibrations are identical (amplitude and frequency); however the software can simulate linear and elliptical vibrations as well. For reference, at the intermediate cutting speed, 0.5 m/s, the tool and work piece partially separate (lose contact) at the highest vibration amplitude (8 $\mu$m, in accordance with [1]).

*TABLE 1. Simulated Process Variables*

| Amplitude ($\mu$m) | 0 | 2 | 4 | 8 |
|---|---|---|---|---|
| | | | | |
| Speeds (m/s) | 1.0 and 0.5 | 1.0 and 0.5 | 1.0 and 0.5 | 1, 0.5 and 0.25 |
| Thermal on/off | On/off | On/off | On/off | On/off |

## RESULTS

The VAM simulation results are included for the effects of vibration amplitude and cutting speed on the resultant cutting forces and temperatures (tool and work piece).

### Cutting Forces

The force values reflect the time varying periodic nature of the forced vibrations of the VAM process. These characteristic force signals are similar to the actual VAM processes as shown by Brehl and Dow [1]. The periodic nature of the time varying cutting force values are shown in figure 1, for the case of a 4 $\mu$m amplitude at a cutting speed of 1.0 m/s, these conditions are just below the threshold where the tool and work piece separate during the VAM machining process; i.e. there is no actual separation of the tool and work piece due to the VAM action.

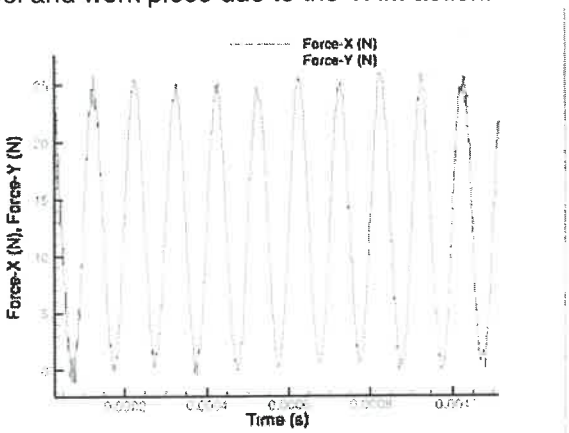


*FIGURE 1. Cutting Forces (not filtered)*

The average of the maximum or peak force values, at steady state, as a function of vibration amplitude are shown in figure 2. These values were determined by averaging the peak forces, as seen in the force plots (such as figure 1), to establish a force for comparison with thermal conditions not included, i.e. no thermal effect. The observed effects are due to the mechanical oscillations alone and do not include a thermal component, this is useful for separating out the influence of the mechanical induced vibrations from any resultant thermal effects due to the relative change in apparent cutting velocity (due to the vibration oscillations being superimposed on the cutting velocity).

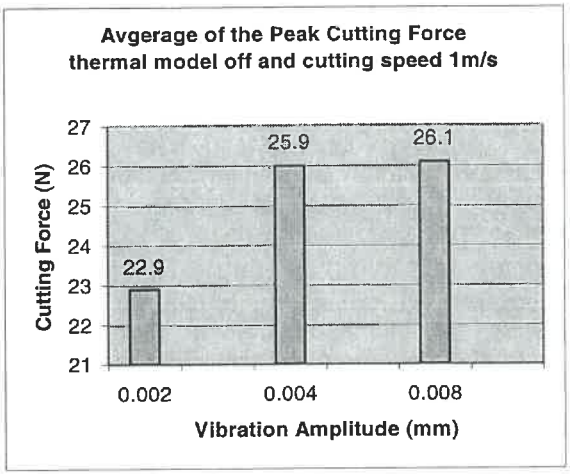


*FIGURE 2. Cutting Forces (average of peak forces) as a function of vibration amplitude*

The filtered force data results are presented in figure 3, where these values are representative of what a dynamometer would measure during an actual cutting test (the oscillations associated with the vibrations are filtered and smoothed). The reduction in cutting force with increasing vibration amplitude is expected, and is considered one of the primary benefits of the VAM process.

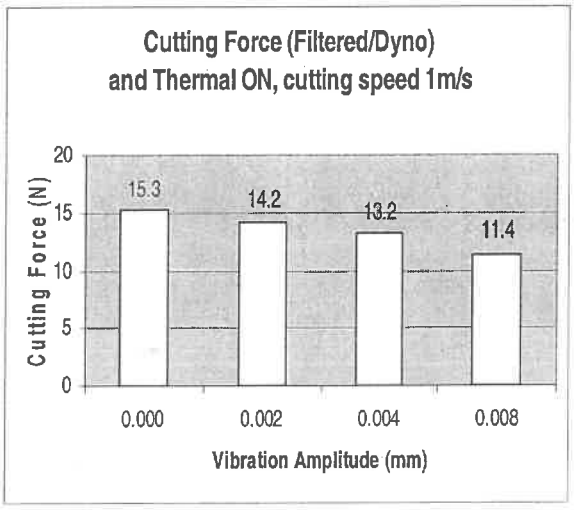


*FIGURE 3. Cutting force for Various Vibration Amplitudes*

## Temperatures: Tool and Work piece

Two sets of simulations were conducted to evaluate the effect of the VAM process on the resultant temperatures associated with the machining operation. Initially, simulations were conducted without any thermal conditions or calculations being employed, i.e. thermal effects are ignored (as shown in figure 2). These simulations provide a base line to study the influence of the VAM process on the resultant forces, without a thermal component or influence. Next, the software's thermal model was implemented and the resultant temperature effects were determined (as shown in figure 3). However, the difference between the resultant forces, for the same simulated conditions (cutting speed and vibration amplitude) with thermal conditions on and off, were not significant (< 2% change), and are not specifically included in this paper. These results are also consistent with the small change in resultant temperatures (< 5 C) due to the affects of vibration amplitude. These latter results are also not included in this paper as they were determined to be insignificant.

## Speed Effects:

The effect of the cutting speed relative to the resultant cutting forces and temperatures are shown in figures 4-6. Generally, in traditional machining processes, cutting forces are not sensitive to cutting speed. An exception to this general rule is when strain rate or thermal softening effects develop as a result of high speed machining. For the machining conditions reported in this paper, these effects are assumed to be negligible at the low cutting speeds evaluated. Figure 4 shows a reduction in cutting force with a decrease in cutting speed for the largest amplitude evaluated (8 $\mu$m). This result is consistent with the anticipated enhancement from the VAM process, i.e. as the cutting speed decreases, the relative influence and benefit of the vibrations increase.

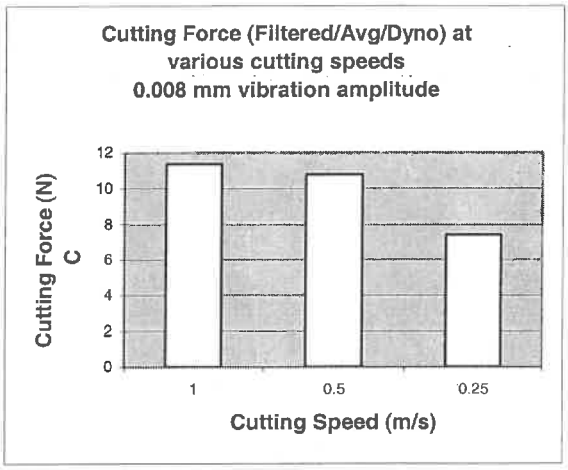


*Figure 4. Cutting Force at various cutting speeds*

Figures 5 and 6 show a reduction in peak (maximum) tool and work piece temperatures respectively as the cutting speed decreases; for the largest vibration amplitude evaluated (8 $\mu$m). A decrease in maximum or peak tool and work piece temperatures is expected as the cutting speed (velocity) decreases.

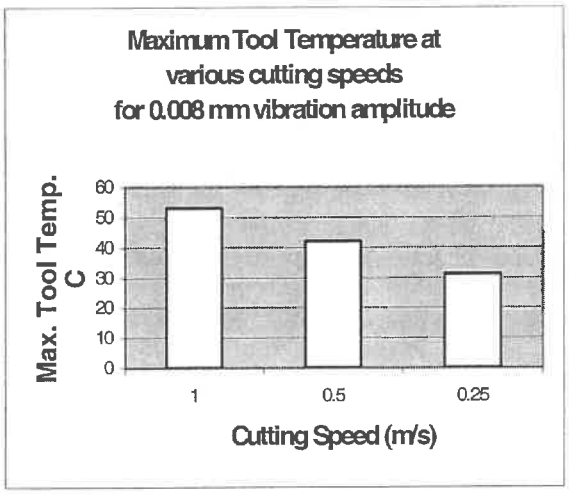


*Figure 5. Peak Tool Temperatures at Various Cutting Speeds*

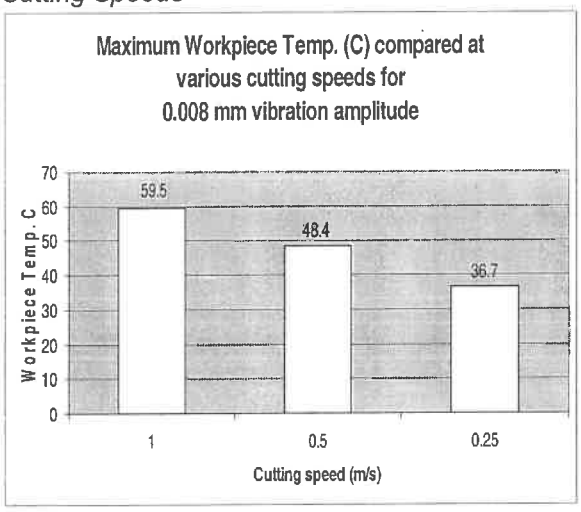


*Figure 6.* Peak Work piece Temperatures at Various Cutting Speeds

## DISCUSSION

The peak force, associated with the peak in vibration amplitude, increased with an increase in the amplitude of vibration (as shown in figure 2). The filtered forces, cutting and thrust, (equivalent to a measured dynamometer force during an actual cutting experiment) decreased with an increase in the amplitude of vibration (cutting forces are shown in figure 3). These latter results are as expected, and is considered to be and consistent with one of the fundamental benefits of the VAM process, i.e. to reduce the resultant forces, which is expected to lead to reduced tool wear.

The variations in the tool and work piece temperature change, as a function of vibration amplitude, were minimal (about 5 C or less, showing a slight decreasing trend as the amplitude of the vibration increased) at the same cutting speed. Cutting speed had a much greater effect relative to the resultant temperatures produced, i.e. as the cutting speed is reduced, the temperatures are reduced significantly (20 to 40%, or 15 C to over 30 C), for the range of conditions simulated. This suggests that a cooling affect, for dry cutting conditions (the simulated conditions did not include a cutting fluid model), does not contribute significantly to the machining process, i.e. the change in vibration amplitude alone only had a small effect on the resultant temperatures. However, a cutting fluid or coolant may prove beneficial if the fluid can enter the chip-work piece-tool contact zone at higher vibration amplitudes. But, based upon the conditions evaluated in this research and presented in this paper, it does not appear that the potential contribution for additional cooling (and reduced temperatures) is significant.

No specific consideration was given as to the effects of strain rate on the material behavior and deformation. It is possible that the increase in "apparent" cutting velocity, due to the VAM action being superimposed on the process cutting velocity, that strain rate effects might be manifested as a result of the change in strain rate during the chip formation process.

## CONCLUSIONS

The FEM is an excellent tool for studying the VAM process. The simulation results indicate that the cutting forces are directly and significantly affected by the vibration amplitude and the cutting speed (as shown in figures 3 and 4), while the resultant temperatures are mostly affected by the cutting speed (as shown in figures 5 and 6) and not significantly affected by the vibration amplitude. Also, there does not appear to be any significant thermal effects associated with the vibration amplitude alone that would contribute to a change in cutting force. All of the VAM process parameters are readily implemented in the commercially available machining simulation software package (AdvantEdge from TWS Inc.) used in this research project. While the focus of this paper is on SPDT of steel, ongoing work involves VAM of SiC and AlTic materials to evaluate the potential valuable effects associated with the VAM process on these hard and brittle (and nominally diamond turnable) materials. In addition to the work reported on in

this paper (effects of vibration amplitude and thermal effects on the resultant forces), the software is capable of simulating the effects of cutting fluids (on friction and forces) and tool wear. Future work will be directed at evaluating these additional process parameters; in particular the influence on of a cutting fluid on tool and work piece temperatures as a function of vibration amplitude is of interest.

**ACKNOWLEDGEMENTS**

The authors wish to thank Third Wave Systems Inc. for providing the software used in these simulations, and to Jerald Overcash at the UNC Charlotte's Center or Precision Metrology for inspiring this work. The contribution of Jerry Jacob from WMU is also gratefully acknowledged.

**REFERENCES**

[1] Brehl, D.D., Dow, T.A.., Review of Vibration Assisted Machining for Precision Fabrication Proceedings ASPE Annual Meeting, 2006.

[2] Overcash, J.L., Cuttino, J.F., Tunable Ultrasonic Vibration Assisted Diamond Turning, Proceedings ASPE Annual Meeting, 2006.

[3] Wang, X., Zhou, M., Gan, J.G-K., Ngoi, B., Theoretical and Experimental Studies of Ultraprecision machining go Brittle Materials and Ultrasonic vibration, Int. J. Advance manufacturing Technology. 2002,; 20: 99-102.

[4] Third Wave Systems, Inc., AdvantEdge Machining Simulation Software, http://www.thirdwavesys.com

[5] Marusich, T.D., Askari, E., Modeling Residual Stress and Wrokpiece Quality in Machining Surfaces online reference. 2001

# A STUDY ON THE HIGH ASPECT RATIO MICRO HOLE DRILLING USING ULTRASONIC ASSISTED MICRO- ELECTRO DISCHARGE MACHINING

**Sridevi Billa, Murali M. Sundaram and Kamlakar P. Rajurkar**
**Center for Nontraditional Manufacturing Research, University of Nebraska-Lincoln, Lincoln, Nebraska, USA**

## ABSTRACT

Unique features of micro electro discharge machining (micro EDM) include its ability to machine hard and brittle materials and absence of mechanical contact force for the machining of fragile components. Therefore, micro EDM has emerged as one of the predominant complementary micro machining technology with applications in diverse industries such as biotechnology, aeronautical, automotive. However, to achieve high aspect ratio (>10) micro hole drilling, micro EDM needs to overcome inherent problems associated with debris removal as accumulated debris causes arcing and hence hinders the machining process. This paper presents the experimental results of ultrasonic vibration assisted micro EDM. Using this method, drilling of high aspect ratio (micro holes in austenitic stainless steel with an aspect ratio of 20) has been achieved in this study. Another benefit of ultrasonic vibration is that the savings in machining time. It is also noticed that the ultrasonic vibration causes some shape distortion and produces rougher machined surface.

Keywords: deep hole drilling, micro EDM, ultrasonic vibration

## 1. INTRODUCTION

Microengineering technologies have been extensively developed in recent years. There has been a considerable development in micro manufacturing technologies to attain the different mold features. Micro EDM in particular is an important micro manufacturing process because it is unconstrained by the hardness or material strength of the material being machined. One major reason for its wide implementation is that there is no direct contact of the electrode and the machined component; hence no contact forces are induced during the machining process.

The demand for high aspect ratio micromachining is ever increasing. Specific examples include micro-chemical-reactors and micro-heat-exchangers, made of metals and ceramics [1]. Deep hole drilling with an aspect ratio above 10 is a formidable task for any micromachining process. In micro EDM this is due to the problems associated with debris removal. Accumulated debris cause arcing and hence hinders the machining process. To overcome this difficulty in achieving high aspect ratio holes, debris has to be effectively removed from the inter-electrode gap. However traditional methods such as pressure flushing and suction flushing are not applicable to micro EDM due to the dimensional constraints.

The work in this paper aims at drilling of high aspect ratio micro holes in austenitic stainless steel using ultrasonic assisted Micro EDM. Introduction of ultrasonic vibration causes phenomena such as acoustic streaming and results in better debris removal [2]. The effect of process parameters, especially that of vibration and discharge energy and feed rate under these conditions on the depth of machining and machining time were studied. Quality of the machined feature namely the shape of the machined hole and the roughness of the machined surface were also studied.

Following section presents the literature review on the ultrasonic assisted micro EDM. The experimental details, results and discussion about the effects of the machining parameters and conclusions are presented in the subsequent sections respectively.

## 2. LITERATURE REVIEW

The beneficial effects of tool/workpiece vibration in EDM are known for over a decade. Masuzawa et al. introduced tool withdrawal and 2D vibration (sinusoidal motion of tool) to an EDM process for machining deep holes to increase the flushing effect [3, 4]. Ghoreishi and Atkinson have reported that a combination of rotary and vibratory movements (vibro-rotary) of electrode produces higher material removal [5]. Kremer et al applied ultrasonic vibrations (20 KHz) to the tool to achieve process improvements [6, 7]. They have reported that the process stability improved due to better slurry circulation caused by the pumping action of the electrode. Moreover, the pressure variation in the gap, caused by the ultrasonic vibration, improved the MRR as larger pressure drop causes lesser resolidification of molten metal. Kozak et al have reported that the MRR in ultrasonic assisted macro EDM is maximum when ultrasonic frequency was matched with the EDM pulse frequency [8]. Murti and Philip have identified cavitation (nucleation, growth and burst of gaseous bubbles), ultrasonic field forces (radiation force, Stoke's force, Bernoulli's attraction) and acoustic streaming as the factors having pronounced effects in ultrasonic assisted EDM. Their finding is that the debris formed in ultrasonic assisted EDM is solid (rather than hollow) with higher spherodicity. It is reported that there is evidence of collision of particles in the form of dents, splats, attached satellites and cracks [9]. Zhang et al utilized the combined effect of EDM and ultrasonic machining to machine conductive ceramics by replacing the pulse generator in EDM by a constant DC source and ultrasonic tool vibration [10,11]. Guo et al reported an increase in cutting efficiency, decrease in surface residual stress and reduced probability of rupture of wire with an application of ultrasonic vibration in wire EDM [12,13]. Similarly the introduction of ultrasonic vibration in micro EDM has been reported to improve the process performance [2,14-16].

## 3. EXPERIMENTAL WORK

The experiments were conducted using the commercial Panasonic MG-ED72W micro EDM. An ultrasonic vibration system having a peak power of 45 W was used in the experiments.

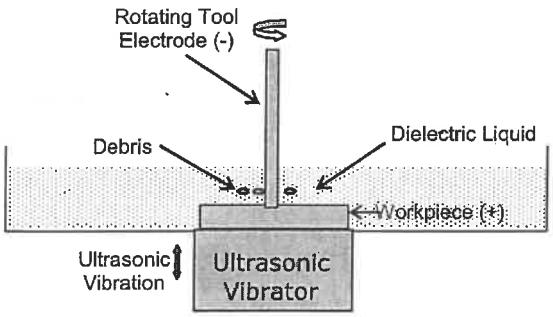


*FIGURE 1. Schematic Experimental Setup.*

The work piece was ultrasonically vibrated as shown schematically in the figure 1. The amplitude of the vibration was found to be approximately 6 µm. The experimental conditions used are given in Table 1.

*TABLE 1. Experimental Conditions*

| | |
|---|---|
| Work material | Stainless steel (2 mm in thickness) |
| Tool material | Tungsten-carbide |
| Tool diameter | 90 µm |
| Capacitance | 1000, 3300 (pF) |
| Voltage | 80, 110 (V) |
| Programmed feed rate | 5, 10,15 (µm/sec) |
| Ultrasonic frequency | 41.616 (KHz) |
| Amplitude of vibration | 0, 6 (µm) |

All experiments were conducted with programmed hole depth of 3000 µm. The actual feed of the tool electrode was noted for every 5 minutes starting from the point of the first spark. The readings were noted until a through hole is drilled or in some cases where the tool electrode stops penetrating further because of the accumulation of the debris. Time taken to drill particular length were also recorded with uniform interval which will help in knowing the machining time for desired hole diameter and depth. It was noticed that drilling 2 mm deep through hole was possible with ultrasonic vibration of the workpiece. The geometry of the machined holes were studied using an optical microscope. The surface roughness was measured by contact method using XP - 2 stylus profilometer.

## 4. RESULTS AND DISCUSSION

The effects of different process parameters on the performance of ultrasonic vibration assisted micro EDM are discussed in this section.

## 4.1 Effect of Ultrasonic Vibration

Since the measurement of actual depth machined in a high aspect ratio micro hole is an extremely difficult task, feed (an indicator of machining depth) is compared in Table 2. The overall feed achieved with the assistance of ultrasonic vibration was higher than that without vibration for all process parameters used in this study.

*TABLE 2: Feed Achieved*

| Process Parameters (Capacitance, Voltage, Feed rate) | Overall Feed Obtained Without Ultrasonic Vibrations | Overall Feed obtained With Ultrasonic Vibrations |
|---|---|---|
| 3300 PF, 110 V, 15 µm | 2724.8 µm | 3000 µm |
| 3300 PF, 110 V,10µm | 2719.2 µm | 3000 µm |
| 3300 PF, 110V, 5 µm | 2412.3 µm | 3000 µm |
| 1000 PF, 80 V, 15 µm | 1784.1 µm | 2678.9 µm |
| 1000PF, 80V, 10 µm | 1542.8 µm | 2600 µm |
| 1000 PF, 80 V, 5 µm | 919.9 µm | 3000 µm |

Another benefit of using ultrasonic vibration is the reduced machining time as shown in fig 2.

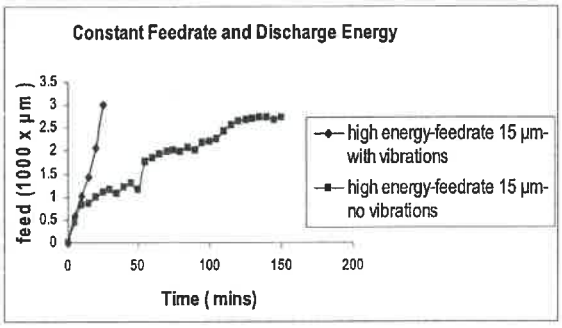
Constant Feedrate and Discharge Energy
feed (1000 x µm)
Time ( mins)
high energy-feedrate 15 µm-with vibrations
high energy-feedrate 15 µm-no vibrations

*FIGURE 2. Effect of vibrations : Feed Vs Machining Time*

## 4.2 Effect of discharge energy

The effect of discharge energy is shown in fig 3. The depths reached using the high discharge energy with and without vibration are always greater when compared to the low discharge energy. With 3300 PF capacitance and 110 volts drill through holes could be drilled with all the three feed rates provided the work piece was subjected to vibration.

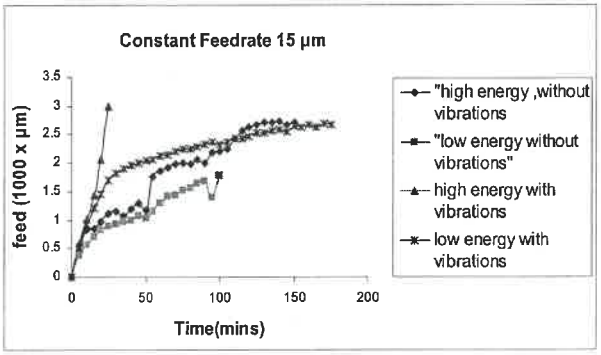


*FIGURE 3. Effect of discharge energy on the depth reached*

## 4.3 Hole geometry

Shapes of the top and bottom of a through hole machined with ultrasonic vibration are shown in fig 4. It can be observed in fig 4(a) that the hole geometry on the upper side of the work piece is a little distorted compared to the one on the lower side of the work piece. This suggests that vibration causes some wandering of initial drill location. However this is restrained with further drilling probably by dielectric oil in the confined space in the inter electrode gap of the hole. Fig 4 (b) shows improved geometry at the hole exit.

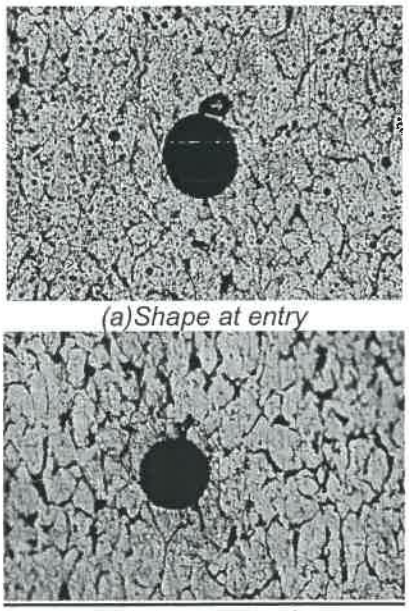

*(a)Shape at entry*

*(b) Shape at exit*

*FIGURE 4 Hole geometry*

### 4.4 Surface Roughness

The surface roughness values of the spark eroded surfaces with the different machining conditions were measured using XP - 2 stylus profilometer and are listed in Table 3.

*TABLE 3.Surface roughness values*

| Process Parameters (Capacitance, Voltage, Feed rate) | Roughness values Without vibrations ($R_a$) µm | Roughness values With vibrations ($R_a$) µm |
|---|---|---|
| 3300 PF, 110 V, 15 µm | 0.03 | 0.17 |
| 3300 PF, 110 V, 10 µm | 0.06 | 0.08 |
| 3300 PF, 110 V, 5 µm | 0.08 | 0.09 |
| 1000 PF, 80 V, 15 µm | 0.06 | 0.07 |
| 1000 PF, 80 V, 10 µm | 0.13 | 0.14 |
| 1000 PF, 80 V, 5 µm | 0.06 | 0.11 |

Since the ultrasonic vibration facilitates better dielectric liquid circulation at the inter electrode gap, the amount of resolidifying material will be lesser than that without vibration. Hence the craters produced are deeper and as a result the surface is rougher. This is confirmed by the observation that the peak to valley surface roughness measurement ($R_t$) is 3.7 µm and 2.09 µm respectively for the surfaces machined with and without vibration.

## 5. CONCLUSIONS

The performance of ultrasonic vibration assisted micro electro discharge machining of austenitic stainless steel is presented in this paper. It is clear from the experimental results that ultrasonic assisted micro EDM has the potential for deep hole drilling. An aspect ratio of 20 has been achieved in the machining of micro holes in austenitic stainless steel in this study. Another benefit of ultrasonic vibration is that the savings in machining time. It is also noticed that the ultrasonic vibration causes some shape distortion and produces rougher machined surface.

## 6. ACKNOWLEDGEMENT

The financial support from the NSF under grant number DMI-0355380 is acknowledged.

## 7. REFERENCES

[1] Cao, D.M., Jiang, J., Yang, R., Meng, W.J., Fabrication of high-aspect-ratio microscale mold inserts by parallel mEDM, Microsystems Technology 2006; 12:839-845

[2] Yeo S H, Tan L K. Effects of ultrasonicvibrations in micro electro-discharge machining of microholes. Journal of Micromech. Microeng. 1999; 9: 345-352

[3] Masuzawa, T. and Heuvelman, C. J., Self flushing method with spark-erosion machining. CIRP Annals - Manufacturing Technology.1983; 32: 109-111.

[4] Masuzawa, T., Cui, X. X. and Fujino, M. A New Flushing Method for Edm Diesinking - Effect of 2d Small Vibration of the Electrode. Bulletin of the Japan Society of Precision Engineering.1990; 24: 223-224.

[5] Ghoreishi, M. and Atkinson, J. A comparative experimental study of machining characteristics in vibratory, rotary and vibro-rotary electro-discharge machining. Journal of Materials Processing Technology.2002;120: 374-384.

[6] Kremer, D. Effects of ultrasonic vibrations on the performances in EDM. Annals of the CIRP; 1989; 38: 199-202.

[7] Kremer, D., Lhiaubet, C. and Moisan, A. Study of the effect of synchronizing ultrasonic vibrations with pulses in EDM.CIRP Annals-Manufacturing Technology.1991; 40: 211-214.

[8] Kozak J. Rajurkar K.P Venkataprakash P., Electrical Discharge Machining with Ultrasonic Assistance. JSME/ASME International Conference On Materials and Processing.2002;10.2:416-421

[9] Murti, V. S. R. and Philip, P. K., An analysis of the debris in ultrasonic-assisted electrical discharge machining, Wear, 1987;117:. 241-250.

[10] Jia, Z. X., Zhang, J. H., Ai, X. and Ai, Z. L. Combined Machining of USM and EDM for Advanced Ceramics. Journal of Advanced Materials.1995; 26: 16-20.

[11] Zhang, J. H., Lee, T. C., Lau, W. S. and Ai, X., Spark erosion with ultrasonic frequency.

Journal of Materials Processing Technology, 1997; 68: 83-88.
[12] Guo, Z. N., Lee, T. C., Yue, T. M., and Lau, W.S., Ultrasonic-aided wire electrical discharge machining," Journal of Materials Processing Technology.1997; 63: 823-828.
[13] Guo, Z. N., Lee, T. C., Yue, T. M. and Lau, W. S. Study on the machining mechanism of WEDM with ultrasonic vibration of the wire. Journal of Materials Processing Technology.1997; 69:212-221.
[14] Yeo, S. H. and Goh, K. M. The effect of ultrasound in micro electro discharge machining on surface roughness. Proceedings of the Institution of Mechanical Engineers Part B-Journal of Engineering Manufacture.2001; 215: 271-276.
[15] Huang, H., Zhang, H., Zhou, L. and Zheng, H. Y. Ultrasonic vibration assisted electro-discharge machining of microholes in Nitinol. Journal of Micromechanics and Microengineering.2003; 13: 693-700.
[16] Murali, M. and Yeo, S. H. Rapid biocompatible micro device fabrication by micro electro-discharge machining. Biomedical Microdevices.2004; 6: 41-45.

# INFLUENCE OF ULTRASONIC VIBRATION ON MICRO-EXTRUSION

**Cristina Bunget[1] and Gracious Ngaile[1]**
**[1]Department of Mechanical and Aerospace Engineering**
**North Carolina State University**
**Raleigh, NC, USA**

## INTRODUCTION

The production of micro-parts has become more important in fields such as electronics, computers, communication, biotechnology, medicine, optics and environmental monitoring. Typical example for such parts are pins for IC-carriers, fasteners, micro-screws, lead frames, sockets, and any kind of connecting element (Figure 1). Traditionally these precision mechanical parts are fabricated by machining. The net shape or near net shape processes, such as metal forming processes, are best suited for miniaturization because of the higher productivity and accuracy.

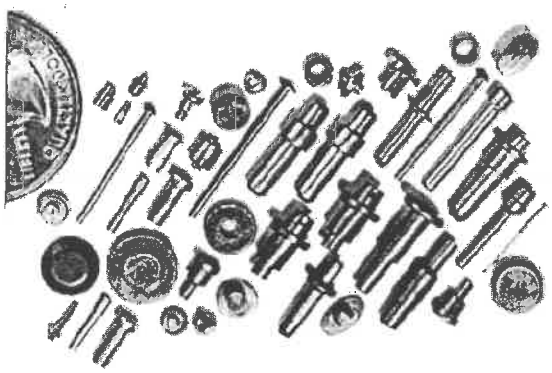

*FIGURE 1. Extruded micro-parts [1].*

Despite the advantages of micro-forming, full utilization of this process has not been realized. Besides the problems that appear in conventional forming processes, like tool design and wear, there are also specific problems related with the miniaturization itself, such as material behavior, higher friction and tools fabrication. When the process is scaled down, the microstructure and the surface topography remain unchanged resulting in different material flow as compared to conventional process. A series of tests in sheet micro-forming has shown that flow stress of material decreases with miniaturization and also tribological conditions are more severe at micro-scale level. The influence of size on flow stress has thoroughly been investigated and well understood [2, 3]. The tribological effects are, however, not well understood. The double cup extrusion test was used to study lubrication conditions for different specimen sizes ranging from 4 to 0.5 mm diameter. The results showed an increase in apparent friction factor by a factor of 20 when the specimen size decreased to 0.5 mm diameter [4]. An analytical model to explain this behavior was proposed, but there is no any means yet to overcome this effect. The investigations have also shown an increase in scattering with miniaturization [3], and therefore difficulty in achieving desired tolerances. Other problems that appear in micro-forming are the fabrication of the tools, which need to be very small with very close tolerances and a good surface quality. The fact that micro-forming tools are also subjected to forces that may exceed the capacity of available die materials presents a great challenge as these tools are prone to short tool life. New manufacturing methods have been developed, such as micro-electrical discharging machining: micro-wire EDM, micro die sinking, electrical discharge drilling, micro-electrical discharge milling and grinding, but the problem of the high forces exerted on the tools still needs to be resolved [5].

There is a great potential to overcome some of the drawbacks of the miniaturization by applying the ultrasonic vibration during micro-forming process. The application of ultrasonic vibration in metal forming at macro-scale has been discussed for many years and some benefits were observed, such as a reduction in the flow stress and a considerable reduction of the external friction between tool and workpiece. The flow stress was observed experimentally to be considerably lowered by the ultrasonic oscillations superimposed on the compressive forming process [6]. This phenomenon was attributed to dynamical effects of stress, velocity and acceleration due to vibration, and also thermal effects due to heat generation, which was directly related with the amplitude of the vibration. Studies of the effects of the longitudinal oscillations imposed on the wire drawing found two possible effects of the ultrasonic oscillations superimposed on the

forming process: volume effects and surface effects [7, 8]. The volume effects are related with a decrease in the flow stress. The surface effects are related with the changing of the frictional conditions at the die/specimen interface. Longitudinal, radial and torsional oscillations were applied during the rolling process, and the results indicated changes in the apparent friction coefficient, as a result of the pumping of the lubricant, softening or melting the asperities, separation of the surfaces, allowing a re-distribution of the lubricant [9]. Investigations done by superimposing ultrasonic oscillations on the tube drawing are reported in [10]. Their experiments showed a reduction in the flow stress, a greater reduction in the diameters and a surface finish superior to that obtained without ultrasonic, particularly on the inside surface. Other investigations were done to study the effect of the shape and length of the concentrator, or the tool attachment, an important part in the ultrasonic system [11]. The shapes found to be appropriate were conical, stepped and exponential, and the optimal length was found to be equal to a multiple of half of the wavelength. All the studies and experiments reached the same conclusions regarding the effect of the ultrasonic oscillations on the metal forming process: reduction of the forming forces, reduction of the flow stress, reduction of the friction between die and workpiece and production of better surface qualities and higher precision.

The objectives of this study are to investigate the possibility of applying the ultrasonic vibrations in the micro-forming process and to investigate their influence on material flow, forming load and tribological characteristics. It is anticipated that ultrasonic technology can overcome some of the difficulties brought by miniaturization.

## METHODOLOGY

Three micro-extrusion processes are investigated in this study. These processes are: double cup extrusion (DCE), forward extrusion (FE) and forward-backward cup extrusion (FBCE). These processes were selected as being representative for forging micro-parts.

### Physics of the Process

The superimposing of the ultrasonic oscillations on the forming process and the creation of the openings is illustrated in Figure 2 for Forward extrusion (FE) process. The punch has the velocity $v_0$. The material will enter with velocity $v_0$, but will exit with a different velocity, $v_e$. The die will vibrate with an oscillatory velocity $v_D$. This velocity is larger than the velocity of the material to be deformed. Because of the relative velocity between the die and material, the opening between die and material is created and closed at every cycle of oscillation. The pressure applied on the asperities when the die touches the material will contribute to elastic-plastic deformation of the asperities. Because of the deformation and the friction at the tool – workpiece interface heat will be generated. The increase in the temperature at the die-specimen interface will influence the behavior of the lubricant. It can be observed that under ultrasonic oscillations the direction of the friction force reverses for every period of oscillation, thus changing the friction characteristic at the tool-workpiece interface. Therefore, with proper design of an ultrasonic micro-forming system, tribological performance can be enhanced.

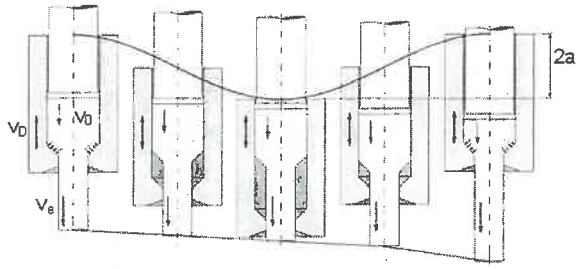


*FIGURE 2. Superimposing ultrasonic oscillations on the forward extrusion process.*

### Design of the Tooling

A set of tooling capable to superimpose the ultrasonic vibrations on the micro-extrusion process was designed. The concentrator is the most important part for the design. This part will be connected to the transducer, and for this purpose had to be designed to resonate at the same frequency. The concentrator also holds the tools for the micro-extrusion process (dies and punches). The objective of the design is to obtain a tooling with the natural frequency of the system as close as possible to the imposed frequency; otherwise the energy will be lost and the vibration will be transmitted to the rest of the structure, limiting the efficiency and causing damage. For this purpose, the design of the concentrator and the holding system must respect some constructive principles given by the equation of the standing wave transmitted through concentrator (Eq.1) [9]:

$$u = a \cdot \cos\frac{2\pi x}{\lambda} \cdot \sin 2\pi ft \qquad (1)$$

Where $u$ is the displacement, $a$ the amplitude of vibration (given peak-to-peak), $x$ the position, $\lambda$ the wavelength, $f$ the frequency of the vibration and $t$ the time. From this equation, it can be concluded that the displacement is maximum when $x$ is $0$ or $\lambda/2$, and $0$ for $\lambda/4$.

Figure 3 illustrates the two waves transmitted into the concentrator system: (a) a longitudinal wave that comes directly from the piezoelectric transducer and (b) a wave transmitted into the disc that holds the concentrator. The length of the concentrator is half of the wavelength of the transmitted wave, with a maximum at the transducer/concentrator interface and another maximum at the other end, were the micro-forming tooling and the deformation zone will be. At the middle, there is a zero amplitude node, used for holding the concentrator. Even if the disc is in the zero amplitude zone, there is still the possibility that the wave will be transmitted into the disc, and from the disc to the entire tooling. In order to obtain zero amplitude in the clamping zone the diameter of the disc needs to be equal with the wavelength.

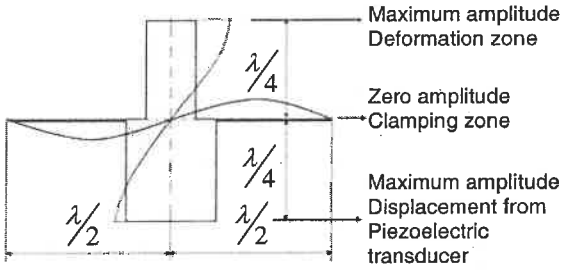


*FIGURE 3. Design considerations.*

These constructive principles were verified through harmonic response analysis. A varying load is applied and the amplitude of vibration at a point corresponding to the deformation zone are obtained. The amplitude response in radial and longitudinal (vertical) directions is shown in Figure 4. The finite element analysis was carried out assuming an ultrasonic generator of 2 kW and a piezoelectric transducer which provides maximum amplitude of 20 microns. The longitudinal displacement received from the imposed vibration is amplified five times for the frequency of 20 kHz.

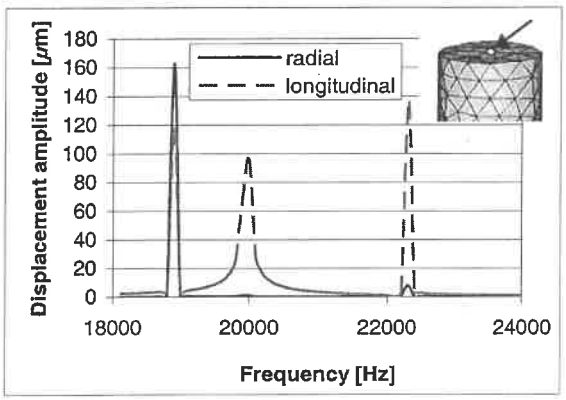


*FIGURE 4. The radial and longitudinal displacement amplitude response.*

Assisted by finite element analysis, the tooling was designed and optimized. Figure 5 presents the components of the concentrator system. The deformation zone is in the upper part of the concentrator, where the die and punch are placed. There are two possibilities to tune the frequency of the system by modifying the dimensions, after this has been manufactured: the tuning cone and the disc.

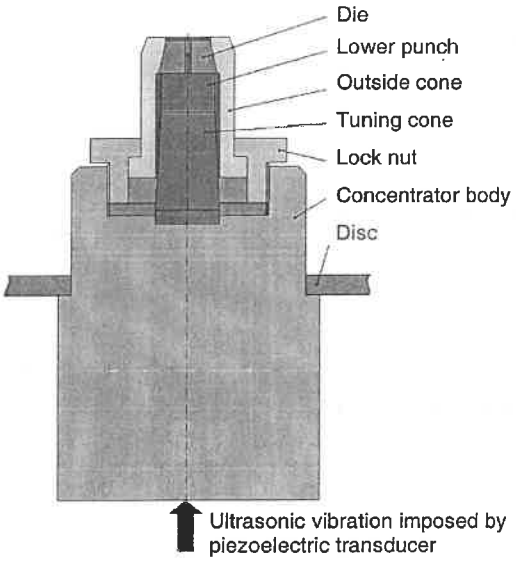


*FIGURE 5. The concentrator system.*

**Test Set-up**

The set-up used for conducting the ultrasonic microforming tests is shown in Figure 6. The assembly consists of common parts for both microforming and ultrasonic microforming. The first category includes the lower punch and die assembly, upper punch assembly and a lever. A

scale is attached to the lever for recording the forming load. The ultrasonic system includes three parts: ultrasonic generator which gives an electric signal of 20 kHz frequency at amplitude of 22-23 $\mu$m, with the possibility of variation between 50 % and 100% of this value, the ultrasonic piezoelectric transducer used to transmit the ultrasonic oscillations to the lower punch assembly, and the ultrasonic concentrator. The dies and the punches are presented in Figure 7 for forward extrusion (FE) and for double cup extrusion (DCE). Note that for forward-backward cup extrusion test, the tools are a combination of those used in the other two tests.

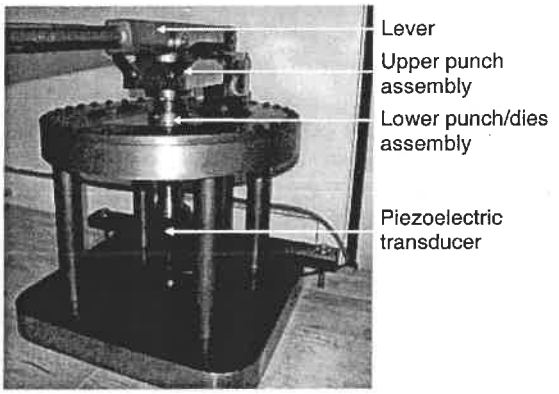


*FIGURE 6. Microforming and ultrasonic tooling.*

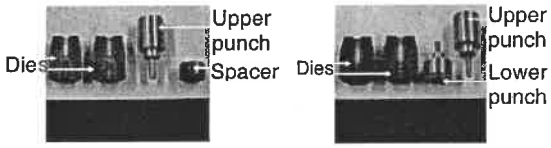


*FIGURE 7: Dies and punches for (a) FE and (b) DCE.*

**Test Procedures**

The tooling presented in Figure 6 was used to test the influence of the ultrasonic vibration on micro-extrusion. The material used for the specimen is aluminum (1100), obtained from wire of 2 mm diameter, and cut to the length of 3 mm for DCE, 4 mm for FE and 5 mm for FBCE. Figure 8 presents the micro-parts obtained through our experiments.

Micro-extrusion tests with and without ultrasonic vibration were conducted. Three different lubricants were tested: a polymeric based lubricant (Lub 1), an oil based lubricant (Lub 2) and a water based lubricant (Lub 3). The forming load, the surface finish and the lubricant distribution after deformation were some of the aspects investigated. The forming load was recorded for all tests. Scanning electron microscopy (HITACHI S 3200 NSEM) was used in studying the influence of the ultrasonic oscillations on the surface quality.

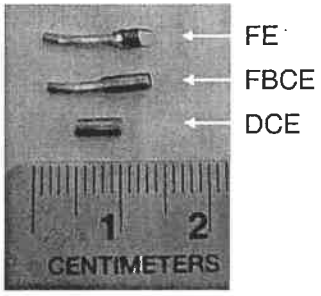


*FIGURE 8. Micro-extruded parts obtained.*

## RESULTS AND DISCUSSION

**Influence of the Ultrasonic Vibration on the Forming Load**

During the experiment the load was recorded for each sample. Figure 9 shows the forming load for each type of extrusion process and each lubricant, with and without ultrasonic vibration.

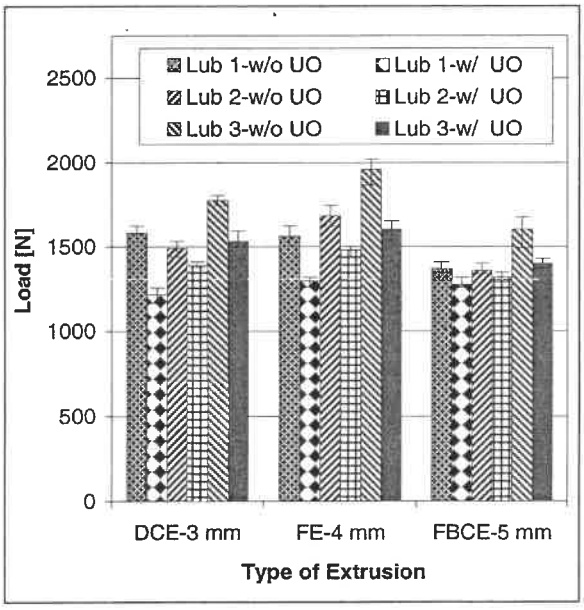


*FIGURE 9. Influence of the ultrasonic vibration on the forming load.*

The reduction in the forming load as compared to non-ultrasonic process was 12-18% for

forward extrusion, 7-23% for double cup extrusion, and 3-13% for forward-backward cup extrusion, the forming load was also reduced, by 3%-13%. The percent of load reduction depends on the process and on the type of lubricant used. Among the three lubricants tested, lubricant 1 had a smaller forming load, and lubricant 2, an oil based lubricant, was found to be the most effective under ultrasonic vibrations.

**Influence of the Ultrasonic Vibration on the Surface Finish**

The surface obtained after the tests with and without ultrasonic oscillations was analyzed, this being a key in understanding the lubrication mechanism. Micrographs were taken for all types of tests and all lubricants, and compared. The surface quality was observed to be improved in all ultrasonic tests, more significantly for lubricant 3.

The differences between the surface finish obtained after classic double cup micro-extrusion test and the ultrasonic test are presented in Figure 10. Micrographs were taken in different zones: the lower cup zone (1), the middle zone (2), characterized by high pressure at the interface, and the upper cup zone (3). The surfaces obtained in non-ultrasonic conditions presents scaring, indicating sticking conditions, and localized smearing indicating lubrication breakdown and metal-to-metal contact with subsequent shearing and smearing of the junctions, especially in zone 3. The surfaces obtained when ultrasonic oscillations were used show a significant improvement in the lubrication conditions. There are some isolated scaring in zones 1 and 2, indicating boundary lubrication. In zone 3, the absence of scaring and presence of roughening and formation of pits (lubricating pockets) indicates mixed-film lubrication, therefore a much more favorable lubrication regime.

The differences in the surface quality are attributed to various factors, some of which can be understood by studying the possible lubrication mechanisms in non-ultrasonic and ultrasonic test. Ultrasonic oscillation results in high instantaneous relative velocities at the tool-workpiece interface. This leads to reduction of adhesive bond formation and hence better lubrication condition.

At the same time, because of the change in the direction of the relative movement, there will be a change in the direction of the friction force that will help the material to flow downward easier than in the classic case. Also because of the relative velocity, the pockets formed by the surface roughness will trap the lubricant and will keep it in the deformation zone. The lubricant will be better distributed at the interface. Therefore the lubricant is helped to keep up with the expansion of the surface and the generation of the new surface due to deformation. Due to these changes, the lubrication regime will be improved and the effective friction coefficient will decrease.

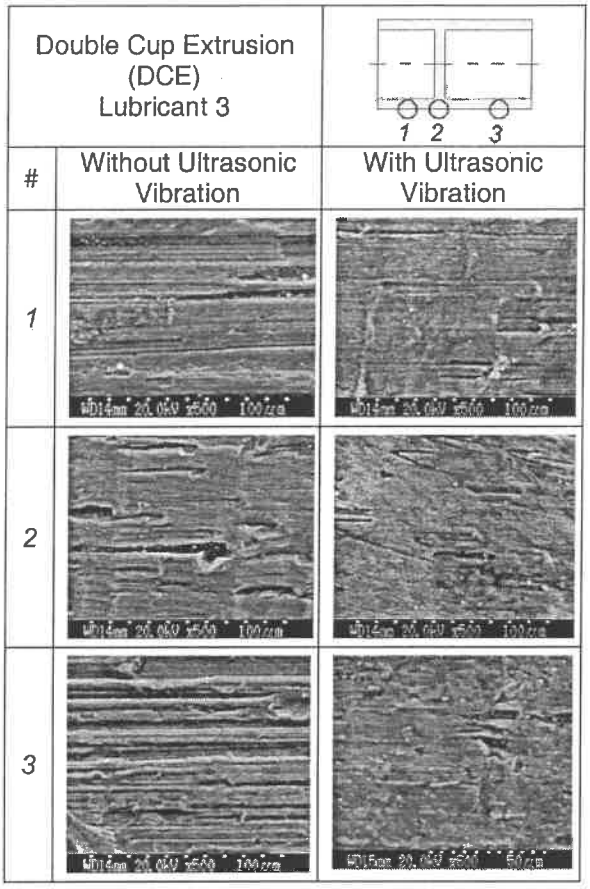


*FIGURE 10. Micrographs taken in different location for DCE test. Lubricant used: Lub 3.*

## CONCLUSIONS

In this paper the influence of ultrasonic vibration on micro-extrusion processes is investigated. An ultrasonic micro-forming tooling was developed and micro-extrusion experiments were conducted. The forming load and the surface finish were some of the aspects studied. Based on results of the tests, the following conclusions were reached:

- Ultrasonic oscillations influence significantly the friction and lubrication mechanism at the die/workpiece interface. Higher instantaneous sliding velocities help to shift a boundary lubrication regime to a mixed-film regime and sticking conditions to a boundary regime.
- Better lubrication conditions and better surface finish with ultrasonic oscillations suggest that ultrasonic micro-forming is a viable process for difficult-to-lubricate materials.
- The magnitude of the ultrasonic oscillations effects depends on the type of the extrusion process, but is also influenced by the lubricant composition.
- The reduction in friction will result in a reduction in load, thus in less energy consumption.

In conclusion, the study has demonstrated that there is high potential for using ultrasonic vibration as a way to overcome the difficulties brought by the miniaturization.

**ACKNOWLEDGEMENTS**
The authors would like to express their sincere gratitude to Mr. Florian Scherer who participated in the early stage of tooling design.

**REFERENCES**
[1] F. Vollertsen, Z. Hu, H. Schulze Niehoff, C. Theiler. State of the art in micro forming and investigations into micro deep drawing. Journal of Materials Processing Technology. 2004; 151: 70-79.
[2] M. Geiger, F. Vollertsen, R. Kals. Fundamentals on the manufacturing of sheet metal microparts. Annals of the CIRP. 1996; 45/1: 277-282.
[3] A. Messner, U. Engel, R. Kals, F. Vollertsen. Size effect in the FE-simulation of micro-forming processes. Journal of Materials Processing Technology. 1994; 45: 371-376.
[4] U. Engel. Tribology in microforming. Wear. 2006; 260: 265-273.
[5] E. Uhlmann, S. Piltz, U. Doll. Machining of micro/miniature dies and moulds by electrical discharge machining – Recent development. Journal of Materials Processing Technology. 2005; 167: 488-493.
[6] O. Izumi, K. Oyama, Y. Suzuki. Effects of superimposed ultrasonic vibration on compressive deformation of metals. Transactions of the Japan Institute of Metals. 1966; 7: 162-167.
[7] C.E. Winsper, D.H. Sansome. Fundamentals of 'ultrasonic' wire drawing. Journal of the Institute of Metals. 1969; 97: 274-280.
[8] C.E. Winsper, G.R. Dawson, D.H. Sansome. An introduction to the mechanics of oscillatory metalworking. Metals and Materials. 1970; 4: 158-162.
[9] V.P. Severdenko, V.V. Klubovich, A.V. Stepanenko. Ultrasonic Rolling and Drawing of Metals. New York: 1972.
[10] C.E. Winsper, D.H. Sansome. Application of ultrasonic vibrations to the plug drawing of tube. Metal Forming. 1971; 3: 71-75.
[11] M.J.R. Young, C.E. Winsper, D.H. Sansome. The effect of tool attachment on the resonant characteristics of ultrasonic waveguides. Applied Acoustics. 1970; 3: 217-224.
[12] A.E. Eaves, A.W.Smith, W.J. Waterhouse, D.H. Sansome. Review of the application of ultrasonic vibrations to deforming metals. Ultrasonics. 1975; 7: 162-170.

# Ultrasonic Assisted Grinding of Advanced Ceramics

**Eckart Uhlmann[1], Christoph Hübert[1]**
**[1]Institute for Machine Tools and Factory Management**
**Technische Universität Berlin**
**Berlin, Germany**

## INSTRUCTIONS

Among all manufacturing technologies cutting with geometrically undefined cutting edges is considered a serious challenge in terms of process understanding and optimization. The main reasons for this situation are the high complexity of interaction between setting parameters and work results, the stochastic nature of the cutting edges, the occurrence of the cutting action on a microscopic level and a permanent flushing of the active zone with cooling lubricant preventing a visual inspection.
Based on experiences in the field of turning and milling the use of simulation tools for grinding applications is a major research focus at the IWF Berlin and elsewhere for many years. The overall aim of the modeling activities is to generate a simulation tool which allows a comparative characterization of different grinding processes, a reduction in experimental work and an optimized selection of machine parameters and tool specifications. Due to the increased number of setting parameters, today's limited base of process understanding and its unique kinematical system Ultrasonic Assisted Grinding is particularly suited for a new simulation approach.

## TECHNOLOGY OF ULTRASONIC ASSISTED GRINDING

Ultrasonic Assisted Grinding is a comparatively novel grinding technology which is characterized by the superposition of a conventional grinding operation with an ultrasonic vibration. This new hybrid manufacturing technology was developed from the idea of combining the impact-like material removal of ultrasonic assisted lapping and the high efficiency of grinding with bound abrasive grains. The vibration is usually generated with components based on the piezo-electric principle and can be introduced into the process through the workpiece or the tool. The most common form in today's industrial application is the face grinding operation for the manufacture of through-holes or grooves as depicted in Figure 1 where the grinding tool is excited with a frequency above 18 kHz [1, 2].

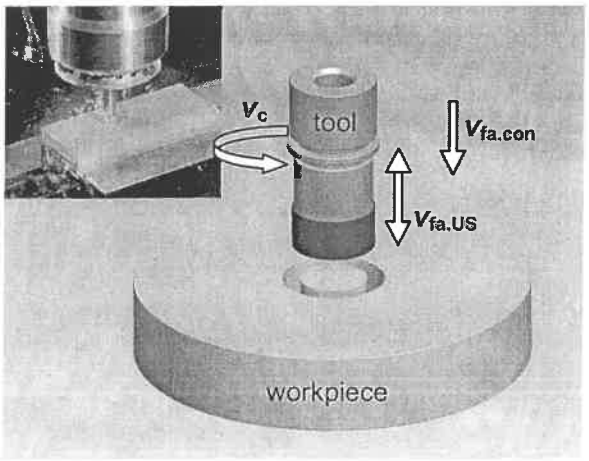


*FIGURE 1. Schematic illustration of Ultrasonic Assisted Grinding.*

In every form of Ultrasonic Assisted Grinding the cutting conditions of the abrasive grains change drastically. Depending on the setting of the ultrasonic parameters amplitude ($A_{US}$) and frequency ($f_{us}$) the scratching contact between grain and workpiece changes into a sinusoidal and impact-like penetration into the material. On the macroscopic level a considerable reduction in cutting forces is measured as shown in Figure 2.

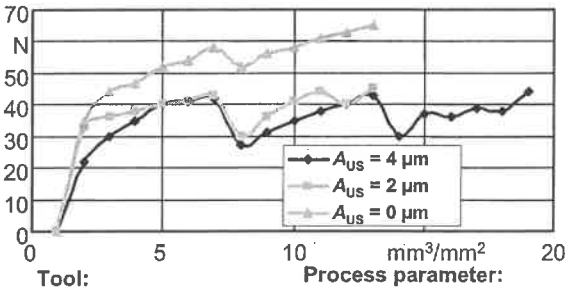


**Tool:**
D64, D=4mm
electroplated

**Workpiece material:**
$Al_2O_3$

**Process parameter:**
$v_c$ = 1,13 m/s
$v_{fa}$ = 3 mm/min
$f_{us}$ = 28 kHz
$A_{us}$ = variable
**Coolant:**
Solution, 4 %

*FIGURE 2. Process forces during face grinding with and without ultrasonic assistance.*

The influence of the amplitude of the vibration with respect to the axial process force is depicted in Figure 2 proving the potential of this technology to increase the productivity of a grinding operation tremendously within a given allowable process force range.

The extent of the reduction of process forces is directly linked to the brittle-hard behavior of the ground material, thus making the grinding of advanced ceramics and glass the predominant field of this manufacturing technology. Interestingly there is no deterioration in surface quality or subsurface integrity in comparison to conventional process observable [1, 2, 3]. The major reason for the benefits mentioned above is a shift in the wear behavior of the active grains away from the flattening and blunting of the grain tips toward an increased micro-splintering. The increased grain related normal forces and the highly dynamic process forces promote a self-sharpening of the active grain providing a permanent supply of sharp cutting edges. The change in the microscopic wear behavior can be proven through the analysis of the characteristic topography properties such as the reduced peak height $R_{pk}$ or the peak area $A_1$ shown in Figure 3. After an identical initial state of the tool topography via dressing a significant reduction in the overall grain protrusion during the conventional process ($A_{US}$ = 0 µm) can be observed in comparison with an ultrasonic assisted operation ($A_{US}$ = 4 µm).

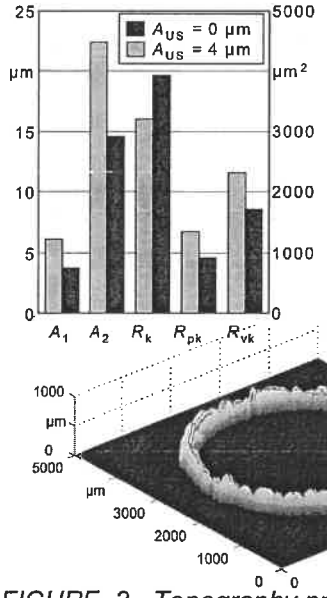


**Tool:**
D64, D= 4 mm,
electroplated
**Workpiece material:**
$ZrO_2$
**Process parameter:**
$v_c$ = 1,7 m/s
$v_{fa}$ = 1 mm/min
$f_{us}$ = 28 kHz
$A_{us}$ = variable
$V'_w$= 18 mm³/mm
**Coolant:**
Solution, 4 %

*FIGURE 3. Topography properties of grinding tools after machining with and without ultrasonic assistance.*

Moreover the change in the cutting conditions due to the superposition of a high-frequency secondary movement in a face grinding operation can be retraced in terms of the produced cutting particles. Figure 4 illustrates the generation of slightly larger particles during Ultrasonic Assisted Grinding which corresponds well in its general trend with the simulation results presented below.

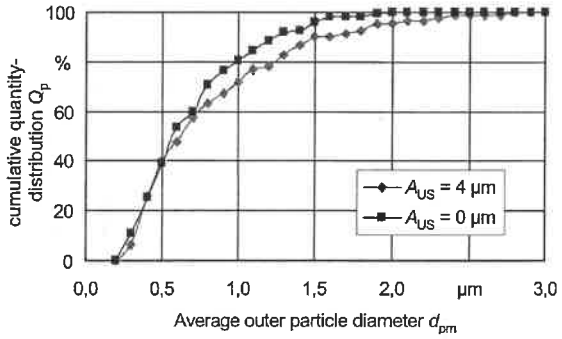


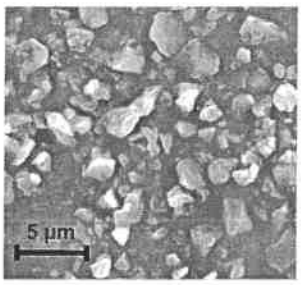


**Tool:**
D64, D=4mm
electroplated
**Workpiece material:**
$Al_2O_3$
**Process parameter:**
$v_c$ = 1,13 m/s
$v_{fa}$ = 3 mm/min
$f_{us}$ = 28 kHz
$A_{us}$ = variable
**Coolant:**
Solution, 4 %

*FIGURE 4. Distribution of cutting particles after grinding with and without ultrasonic assistance.*

## VOXEL-BASED KINEMATICAL SIMULATION OF ULTRASONIC ASSISTED GRINDING

A profound knowledge of the cutting conditions in the active zone is a prerequisite for a general understanding of grinding processes [4, 5]. This includes the assessment of the mechanical and thermal load of the active cutting edges which determines the material removal mechanisms and the tool wear. Due to the problems of acquiring them on a microscopic level directly a number of approaches for the analytic description through characteristic chip parameters like undeformed chip thickness or engagement angle have been introduced. The basic goal for these efforts is the analysis of the microscopic cutting events under ideal boundary conditions with a selective variation of grinding parameters and tool specifications. This offers an opportunity to compare different settings

within a certain operation or with other grinding operations [4, 5].
The macroscopic description of the movement of the abrasive grains in relation to the workpiece has been derived by several authors in detail and can be put into the following equation for the case of straight face grinding in z-direction (see Figure 1 [1, 2]:

$$\vec{l}_e(t) = \begin{Bmatrix} l_{ex}(t) \\ l_{ey}(t) \\ l_{ez}(t) \end{Bmatrix} = \begin{Bmatrix} r_s \cdot \sin(2 \cdot \pi \cdot n_s \cdot t) \\ r_s \cdot \cos(2 \cdot \pi \cdot n_s \cdot t) \\ v_{fa,con} \cdot t - A_{US} \cdot \sin(2 \cdot \pi \cdot f_{US} \cdot t) \end{Bmatrix},$$

wherein $n_s$ the rotational speed of the tool and $v_{fa.con}$ the permanent feed rate are.
For the description of the micro-kinematical processes a new modeling concept was developed. Based on past research activities at the IWF Berlin a voxel-based approach was introduced - which applies a 3-dimensional penetration of discrete volume elements, frequently called "voxel" [6]. This represents a major improvement with respect to the previous approaches which used exclusively a 2-D envelope of a virtual tool which sweeps through a workpiece surface. Due to the high engagement angles in Ultrasonic Assisted Grinding this concept is not feasible, hence a real penetration of 3-D bodies was necessary to be developed. A Boolean operation between the now 3-dimensional tool and workpiece generates a chip geometry, which is used to derive the characteristic chip parameters. Presently the simulation assumes ideal cutting meaning a total removal of volume elements of the workpiece which intersect with elements from the tool during the cutting process. Obviously this does not fully represent the interaction of the material removal mechanisms that have been observed in reality especially in the case of brittle-hard materials. But there is a broad knowledge about the correlation between characteristic chip parameters and the observable material removal behavior for conventional grinding operations which becomes now available for the new kinematical system of Ultrasonic Assisted Grinding [1, 2, 3].
The structure of the simulation tool was based on an approach being summarized as follows

- Generation of a statistical grain model,
- Generation of a statistical tool model,
- Calculation of the Boolean operation and
- Analysis of the chip geometry and surface topography.

Due to the statistical nature of the size and shape of the abrasive grains a large number of actual grains was analyzed using SEM-pictures from different view angles. In order to determine the distribution of grains on the surface of typical tools a SEM-based visual inspection as well as a laser topography measurement was conducted.

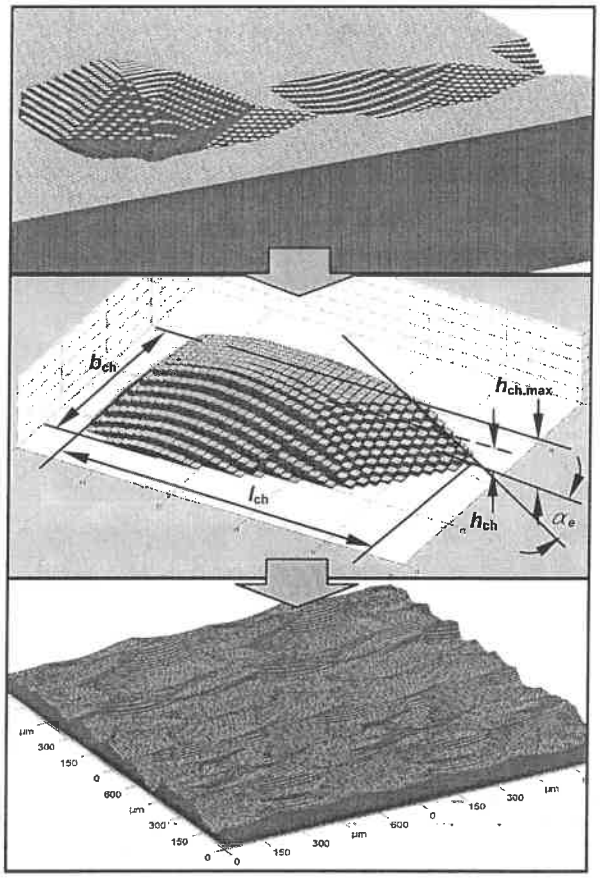


*FIGURE 5. Schematic illustration the voxel-based simulation of Ultrasonic Assisted Grinding*

The general procedure behind the newly developed simulation tool is depicted in Figure 5. Beside the opportunity of a visual inspection of the generated virtual surfaces the geometry of each virtual chip can be analyzed and statistically edited. The results of a set of simulated operation under the variation of the ultrasonic amplitude are presented in Figure 6. The introduction of the ultrasonic - secondary movement of the grinding tool significantly alters the chip parameters. In contrast a further increase of the ultrasonic amplitude has only a minor effect on the shape of the virtual chips. Hence the observed process improvement of the grinding operation by increasing the ultrasonic amplitude, which is reported by several authors

[1, 2 ,3] must be connected with other phenomena such as the change in the fluid flow conditions through the active grinding zone. In order to acquire basic knowledge about this situation another numerical simulation method is presented below.

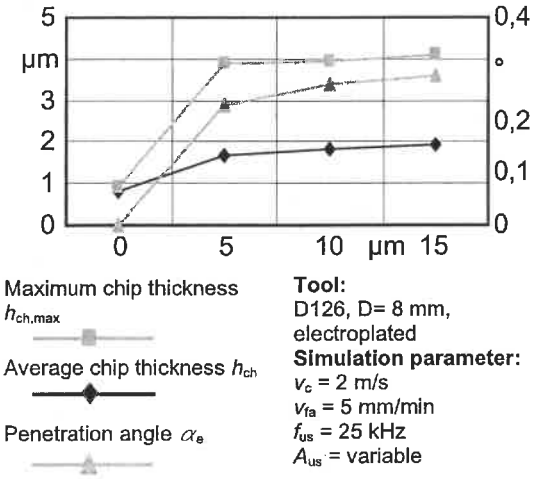


*FIGURE 6. Results of the simulation for different ultrasonic amplitudes $A_{US}$.*

## CFD-SIMULATION OF FLUID FLOW IN ULTRASONIC ASSITED GRINDING

A discontinuous contact between the tool and the workpiece with a frequency above 18 kHz is a distinct characteristic for Ultrasonic Assisted Grinding. As mentioned above it changes the contact conditions of the cutting edges but also the fluid flow conditions in the active zone. Many authors attributed at least to some extend the advantageous process behavior to the improved flushing of the active zone in particular at high aspect ratio of the ground holes. In contrast to peripheral grinding operations it is nearly impossible to analyze visually the fluid flow through the active zone during face grinding [1, 3].

The usage of Computational Fluid Dynamic (CFD) tools appears to be a promising method to reassess the flow conditions and develop strategies to improve the coolant supply system. The first step toward an optimized process control is the modeling of the actual state for a given set of representative parameters. At the IWF Berlin a simplified model was set up using the pre-processor GAMBIT of Fluent Inc. Subsequently a number of different simulations have been carried out applying the CFD-software FLUENT of Fluent Inc. First results of those calculations have been displayed in Figure 4 where the total pressure for the conventional process ($A_{US}$ = 0 µm) as well as for different points in time within a vibration cycle can be seen.

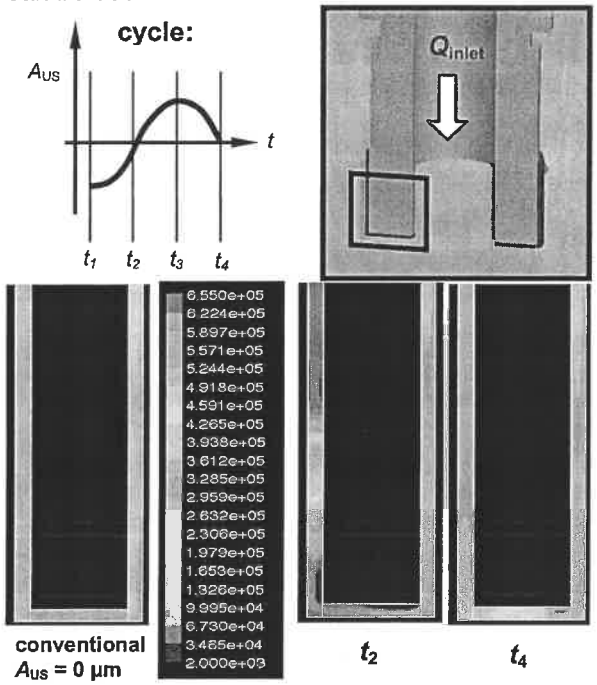


**Simulation parameter:**

| | |
|---|---|
| Rotational speed: | $n$ = 1000 1/min |
| Ultrasonic frequency: | $f_{US}$ = 11 kHz |
| Ultrasonic amplitude: | $A_{US}$ = 15 µm |
| Inlet pressure: | $p_{KSS,zu}$ = 5 bar |
| Ambient pressure: | $p_a$ = 1 bar |
| Width grinding gap: | $b_{Spalt}$ = 90 µm |
| Depth of drill hole: | $t_W$ = 5 mm |
| Tool diameter: | $d_a$ = 8 mm |

*FIGURE 7. CFD-simulation results for the total pressure (Pa) of the coolant during conventional and Ultrasonic Assisted Grinding.*

Apparent becomes a highly dynamic fluctuation of the simulated total pressure accompanied by a temporary increase in local pressure especially in the grinding gap which supports the assumption of an improved flushing of the active zone as mentioned above.

## SUMMARY

Ultrasonic Assisted Grinding of brittle-hard materials like advanced ceramics proved in many applications its superior performance in comparison to conventional processes. Due to the new kinematical system and increased number of setting parameters to take into account the developed simulation is a valuable tool for the deepening of the process

understanding. A 3-dimensional representation of the surface generation and chip characteristics within the limits of the modeled system can be obtained. An additional CFD-simulation in its present version provides another opportunity for qualitative analyses of flow conditions in the otherwise inaccessible contact zone.

## REFERENCES


[1] Daus, Nikolai-Alexander: Ultraschall-unterstütztes Quer-Seiten-Schleifen. Ph.D. thesis TU Berlin, 2004.

[2] Pei, Zhijian: Rotary Ultrasonic Machining of Ceramics: Characterisation and Extensions. Ph.D. thesis University of Illinois at Urbana-Champaign, 1995.

[3] Uhlmann, Eckart; Daus, Nikolai-Alexander: Ultraschallunterstütztes Schleifen – Einsatzvorteile durch ein innovatives Schleifverfahren. BMBF – Final Report, 2000.

[4] Zitt, Udo Rudi: Modellierung und Simulation von Hochleistungsschleif-prozessen. Ph.D. thesis Universität Kaiserslautern, 1999.

[5] Kempa, Bernd: Zahnflankenprofilschleifen mit galvanisch-gebundenem CBN. Ph.D. thesis WZL der RWTH Aachen, 1999.

[6] Hou, Zengxuan: Beitrag zur voxelbasierten Simulation des fünfachsigen NC-Fräsens. Ph.D. thesis TU Berlin, 2003.

# New systematic and time-saving procedure to design complex shaped tools for the application of ultrasonic assisted grinding

**Christian Brecher[1]; Ralf Schug[1]; Andreas Weber[2], Christian Wenzel[1]**
**[1] Department Machine Tools**
**[2] Department Process Technology**
**Fraunhofer Institute for Production Technology IPT**
**Aachen, Germany**

## INTRODUCTION

The advantages of the process of ultrasonic assisted grinding are well-known for about 50 years. One main advantage is the reduction of infeed forces while grinding hard and brittle materials such as glass and ceramics. Contrary, the force reduction can be used to increase the removal rates of the grinding processes. FIGURE 1 shows the reduction of the infeed forces during glass grinding with cup grinding wheels depending on the ultrasonic amplitude $x_a$. On the right side the same figure shows the possible increase of removal rates up to 230% using ultrasonic waves

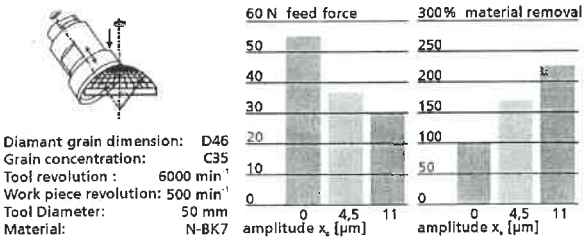


*FIGURE 1. In feed force reduction and increase of removal rates using ultrasonic waves*

To realize these advantages, the grinding tool is stimulated with ultrasonic waves. Therefore, a piezoelectric ultrasonic-transducers and a booster element are integrated in a grinding spindle. Before entering the tool the mechanical amplitudes of the waves are increased by the booster element (FIGURE 2).

The main task in designing tools for the process of ultrasonic assisted grinding is to define their geometry in such a way that their mode of vibration is longitudinal and without any transversal losses (FIGURE 3). Due to a lot of investigation nowadays, there is a good knowledge and many data bases which enable the prediction of the vibration within cylindrical booster elements in a very accurate way. In the same manner the numerical assisted designs of noncomplex shaped grinding tools are often very realistic.

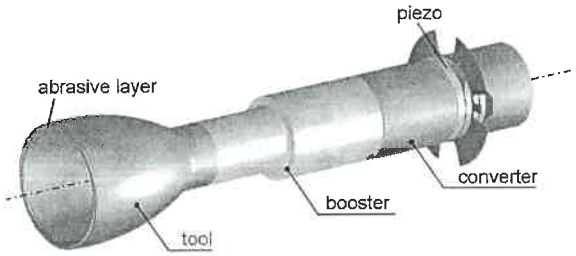


*FIGURE 2. Principle assembly of an ultrasonic transducer with tool*

In contrast to this, the prediction of the dynamic behavior of complex tools as they are used for cup wheel grinding is not yet accurate. A good vibration behavior of the tool decisively depends on the experience of the design engineer. Until now design and tuning is a strong iterative procedure without the possibility to determine the behavior of complex shaped tools or a type series of cup grinding wheels. Therefore, the authors have generated a very quick and accurate procedure to define the necessary design of a type series of cup wheels for the process of ultrasonic assisted grinding.

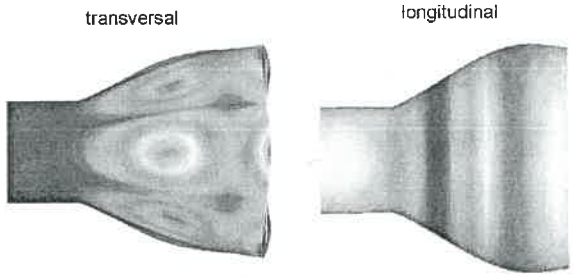


*FIGURE 3. Example for a transversal and a longitudinal eigenmode of a grinding tool*

## PROCEDURE FOR THE AUTOMATED DESIGN OF GRINDING TOOLS USING FEA

The main disadvantages of the FEA calculations are the time consuming manual evaluation of the outcome, the missing of eligible information and the high amount of iterations to find a sufficient design of the tool.

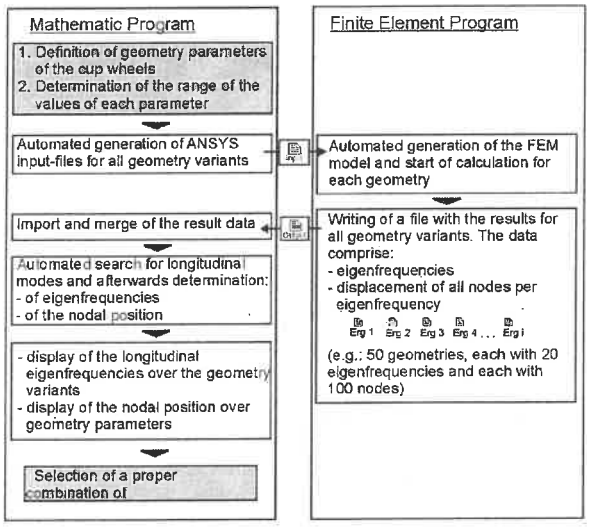
Mathematic Program
1. Definition of geometry parameters of the cup wheels
2. Determination of the range of the values of each parameter
Automated generation of ANSYS input-files for all geometry variants
Import and merge of the result data
Automated search for longitudinal modes and afterwards determination:
- of eigenfrequencies
- of the nodal position
- display of the longitudinal eigenfrequencies over the geometry variants
- display of the nodal position over geometry parameters
Selection of a proper combination of
Finite Element Program
Automated generation of the FEM model and start of calculation for each geometry
Writing of a file with the results for all geometry variants. The data comprise:
- eigenfrequencies
- displacement of all nodes per eigenfrequency
Erg 1 Erg 2 Erg 3 Erg 4 ... Erg i
(e.g.: 50 geometries, each with 20 eigenfrequencies and each with 100 nodes)

*FIGURE 4. Procedure to automatically design complex shaped grinding tools*

To abolish these disadvantages a procedure has been developed which automatically varies geometry parameters of the tool within the FEA and furthermore automatically evaluates the results of the calculation. For that he brought together a FEA software with the mathematical software Matlab. FIGUR 4 shows in detail the single steps of the procedure.

Starting from a basic geometry (Figure 5) a first step of the procedure is the automated generation of a variety of input-files with all necessary information for the FEA program while changing selected geometry parameters. For a tool geometry the changeable parameters are e.g.:

- tool length
- tool diameter
- tool contour (e.g. form of spline)
- thickness

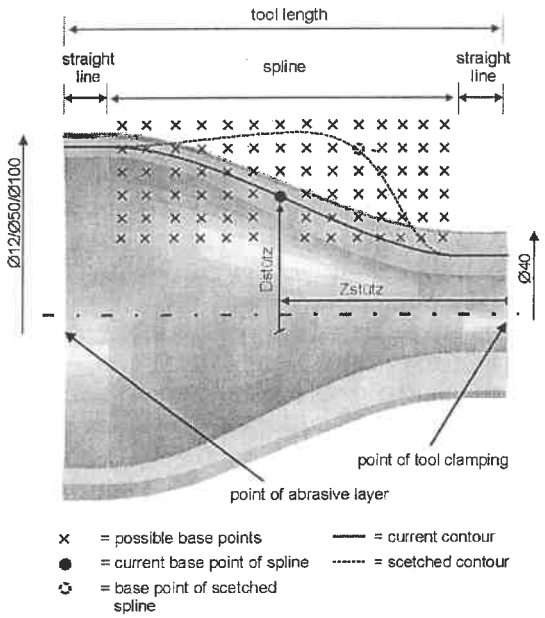


*FIGURE 5. Basic tool geometry for the FEA analysis.*

The input files automatically start the FEA to calculate the modal parameters (eigenfrequency and eigenmodes) for each tool geometry. After the calculation the results are available as an ASCII-File with the information about all eigenfrequencies up to 22 kHz and for all eigenfrequencies the displacement of each FEA node is stored (Figure 6). For further analysis these information are automatically transfered into Matlab

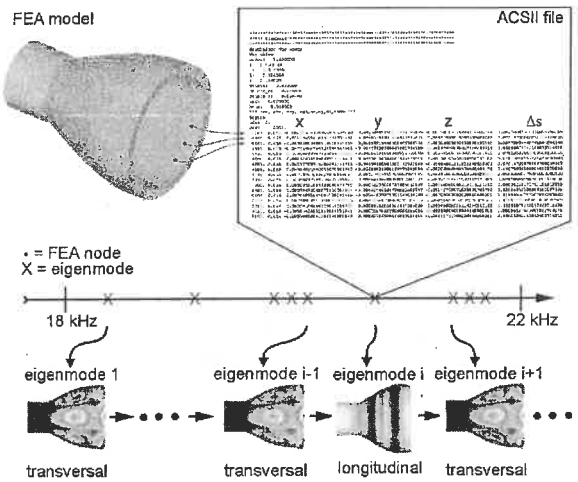


*FIGURE 6. FEA outcome and selection of longitudinal eigenmodes*

Furthermore, for a systematic analysis the author has developed a filter to determine the longitudinal eigenmode in-between all transversal eigenmodes. This enables for the first time the possibility to determine:

- all possible geometries to realize the user defined eigenfrequency (white lines in FIGURE 5)
- the amplitude transmission for all tool geometries
- the distances between the focused and the neighbouring frequencies
- the position of the node plane for all tool geometries

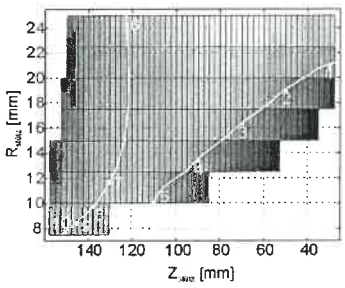


| Nr. | Node position [mm] | | Amplification [µm/µm] |
|---|---|---|---|
| | axial | radial | |
| 1 | 63,95 | 17,37 | 4,79 |
| 2 | 64,34 | 17,42 | 4,74 |
| 3 | 63,97 | 17,02 | 4,69 |
| 4 | 63,83 | 17,03 | 4,79 |
| 5 | 63,66 | 16,62 | 5,53 |
| 6 | 72,89 | 23,75 | 0,79 |
| 7 | 66,39 | 17,95 | 2,25 |
| 8 | 65,88 | 17,96 | 2,57 |
| 9 | 65,57 | 17,08 | 2,74 |
| 10 | 65,43 | 17,12 | 2,81 |

*FIGURE 7. Tool geometries which lead to longitudinal eigenmode at 20 kHz*

The knowledge of the position of the last mentioned node enables to realize an additional point of connection. With this additional connection between the vibration elements and the spindle rotor, spindle systems can be designed much stiffer than usual systems.
The procedure has been developed for the application of ultrasonic assisted grinding but can also be applied for all other complex tools

## VALIDATION OF SIMULATION RESULTS

Several test geometries were manufactured for the intensive validation of the simulation results.

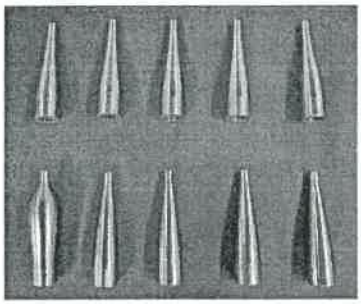

*FIGURE 8. Example of manufactured tool geometries with a cup wheel diameter of 14 mm.*

Figure 8 for example shows tool geometries with a wheel diameter of 14 mm. In a further step these different geometries were exposed with ultrasonic waves of 20 kHz at a test bench (FIGURE 9) while measuring the amplitude of vibration at the outer surface. The test results have shown that the predicted eigenfrequencies correspond very well with the measured frequencies. Similarly, the correspondents of the node positions was very good. The variations were in the range of 100 Hz respectively 2 mm.

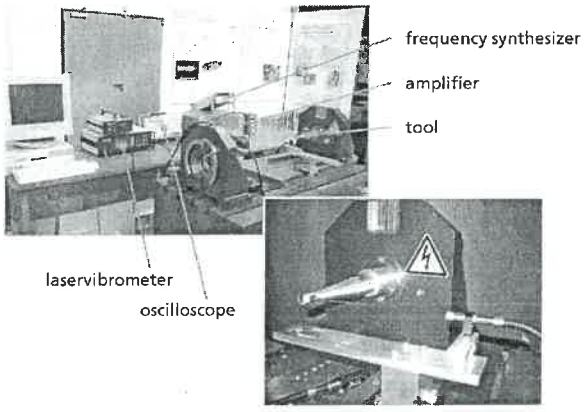


*FIGURE 9. Example of manufactured tool geometries with a cup wheel diameter of 14 mm.*

## SUMMARY AND CONCLUSION

Ultrasonic grinding leads to a reduction of process forces while grinding brittle or hard materials. This effect on the other hand can be used to increase the material removal by increasing the in feed respectively. To assist good process conditions all components influencing the wave propagation have to be designed in a way that they have a longitudinal eigenfrequency at 20 kHz.

To design those components very accurate a systematic and time saving procedure was generated that allows the selection of an optimized geometry out of a multitude of geometries after calculating their dynamic behavior. Therefore, the two software tools Ansys and Matlab were connected with each other to reduce the time-consuming steps while iteratively simulating the eigenparameters.

The procedure was validated within multitude investigation at a piezo actor driven test set up.

REFERENCES
[1] Markov, A. I.: Ultrasonic Machining of Intractable Materials, London ilife books LTD, 1966
[2] Brecher, C.; Klocke, F.; Schug, R.; Weber, A.: Ultraschalleinsatz – Produktionssteigerung bei der Zerspanung von Glas und Keramik, Industrielle ielle Diamanten Rundschau IDR, 39. Jahrgang, III/2005, Seite 244-250, ISSN 0935, 2005
[3] Kuttruff, H.: Physik und Technik des Ultraschalls, ; Hirtzel, Stuttgart, 1988
[4] Wahl, M.: Angewandte Strukturanalyse; Vorlesungsumdruck der Fachhochschule Aachen, ISBN 3-89653-567-6, Verlag Mainz, 1999

# EXPERIMENTAL STUDY ON ROTARY ULTRASONIC MACHINING OF GRAPHITE/EPOXY PANEL

**Z.C. Li[1], Z.J. Pei[1], T. Sisco[2], A. C. Micale[2], and C. Treadwell[3]**
**[1]Department of Industrial and Manufacturing Systems Engineering**
**Kansas State University**
**Manhattan, KS, USA**
**[2]The Boeing Company**
**Everett, WA, USA**
**[3]Sonic-Mill**
**Albuquerque, NM, USA**

## ABSTRACT
Rotary ultrasonic machining (RUM) is introduced into drilling holes on graphite/epoxy (GREP) panels for the first time. The feasibility to machine GREP using RUM is investigated. Effects of RUM process parameters (ultrasonic vibration, federate, and spindle speed) on cutting force, MRR, and hole entrance/exit edge quality are also presented.

## INTRODUCTION
Graphite/epoxy (GREP) composites are utilized in aerospace and automotive industries due to their high strength and lightweight [1-4]. For example, GREP composites have been used increasingly in aircraft components like rudders, vertical tail fin skins, and horizontal stabilizer skins, etc. [1-2]. One of the challenging technical issues for GREP is the damage problems (such as delamination and fiber pull-out etc.) resulted from machining [3-4].

Several papers have reported studies on machining of GREP. Ramulu and Arola [4] and Colligan et al. [5] investigated the surface integrity in water jet and abrasive water jet cutting of GREP. Wang et al. [6] and Kohkoner et al. [7] studied cutting and milling of GREP respectively using tungsten carbide and polycrytalline inserts. Ludin [8] investigated trimming of GREP using Nd:YAG laser. Shanmugam et al. [9] conducted a comparative study of water abrasive jet machining over laser machining for GREP. Lau et al. [10] proposed machining of GREP by electrical discharge machining (EDM). Sadat [11] employed finite element method (FEM) to investigate the delamination during drilling of GREP. However, water-jet machining at high cutting speeds produces delamination, laser machining produces thermal stress and a heat-affected zone, and EDM requires conductive properties of the workpiece and produces surface damage and higher tool wear [3]. Therefore, there is a need to develop more cost-effective machining methods for GREP.

Among non-traditional machining processes, rotary ultrasonic machining (RUM) is a relatively low-cost, environment-benign process. In RUM, a rotating core drill with metal-bonded diamond abrasives is ultrasonically vibrated in the axial direction and fed towards the workpiece. Coolant pumped through the core of the drill washes away the swarf, prevents jamming of the drill, and keeps it cool. This process is illustrated in FIGURE 1.

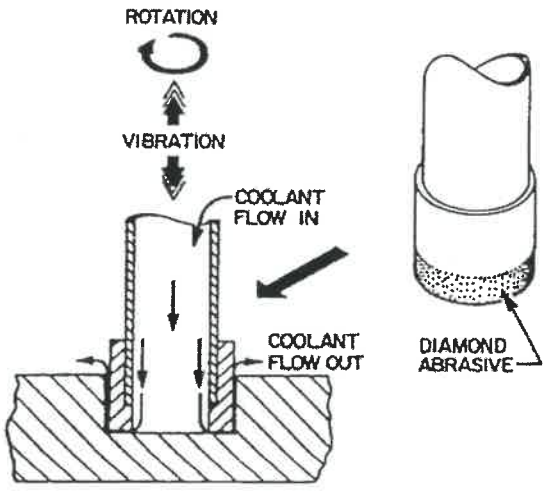


*FIGURE 1. Illustration of RUM process.*

RUM has been employed to machine many types of materials [12-20]. However, no reports have been published on RUM of GREP. In this paper, the viability of RUM on GREP is studied for the first time. Effects of RUM process parameters (ultrasonic vibration, feedrate, and

spindle speed) on cutting force, MRR, and hole entrance/exit quality are also investigated.

## EXPERIMENTAL DETAILS

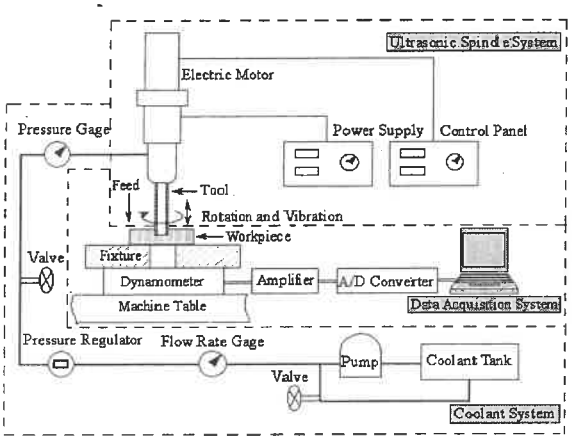


*FIGURE 2. Illustration of of experimental setup.*

The experimental setup is schematically illustrated in FIGURE 2. It mainly consists of an ultrasonic spindle system, a data acquisition system, and a coolant system. RUM tests are performed on an ultrasonic machine of Sonic Mill Series 10 (Sonic-mill®, Albuquerque, NM, USA). Diamond core drills (N.B.R. Diamond Tool Corp., LaGrangeville, NY, USA) are used to drill the GREP panel (Provided by The Boeing Com., Everett, WA, USA). The drills have outer and inner diameters of 9.54 mm and 7.82 mm respectively, and consist of metal-bonded diamond grains of mesh size from 80 to 100. Mobilemet® S122 water-soluble cutting oil (MSC Industrial Supply Co., Melville, NY, USA) diluted by water with the ratio of 1 to 20 is used as coolant.

Output variables are cutting force, material removal rate (MRR), and hole entrance/exit edge quality. The cutting force along the feedrate direction is measured by a KISTLER 9257 dynamometer (Kistler Instrument Corp, Amherst, NY, US). The dynamometer is mounted atop the machine table and beneath the workpiece to measure the cutting force, as shown in Fig. 2. MRR in the experiments is calculated using the following equation:

$$MRR = \frac{\pi \cdot \left[ (D_{out}/2)^2 - (D_{in}/2)^2 \right] \cdot d}{T}$$

where, $D_{out}$ is the diameter of drilled hole, $D_{in}$ the diameter of drilled rod, $d$ workpiece thickness, and $T$ the time it takes to drill the hole. The drilled hole entrance/exit edge quality is observed under a digital video microscope of Olympus DVM-1 (Olympus America Inc., Melville, NY, US). The process parameters are listed in Table 1.

*TABLE 1. RUM process parameters.*

| Parameter | Value |
|---|---|
| Spindle speed (rpm) | 3000; 4000; 5000; 6000 |
| Feedrate ($mm \cdot s^{-1}$) | 0.032; 0.04; 0.048; 0.056 |
| Ultrasonic vibration frequency (KHz) | 20 |
| Ultrasonic vibration power* (%) | 0; 35 |

*Ultrasonic vibration power controls the amplitude of ultrasonic vibration.

## RESULTS AND DISCUSSION

### Effects of Ultrasonic Vibration

#### *Cutting Force*

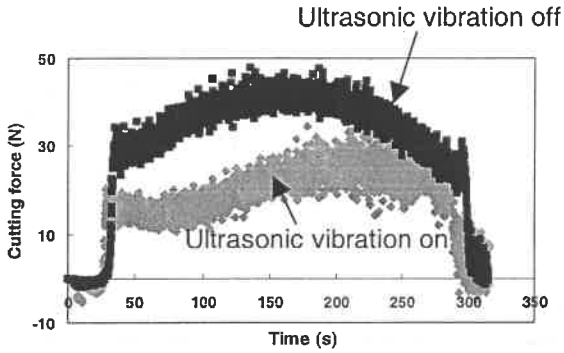


*FIGURE 3. Effects of ultrasonic vibration on cutting force.*

FIGURE 3 shows the effects of ultrasonic vibration on cutting force. Note that the RUM process becomes a core drilling process with the vibration off. It can be seen that the cutting force decreases significantly when the ultrasonic vibration is on. FIGURE 4 shows the comparisons of the maximum/average cutting force when the ultrasonic vibration is on and off. With the help of ultrasonic vibration, the maximum cutting force decreases about 23% while the average cutting force decreases about 43%.

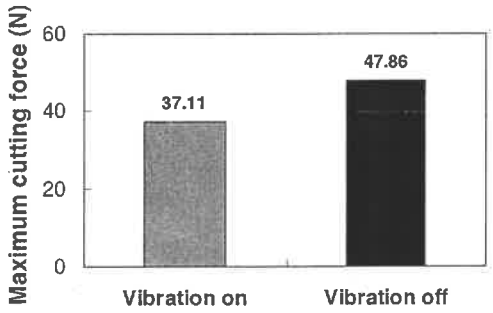


(a) Maximum cutting force

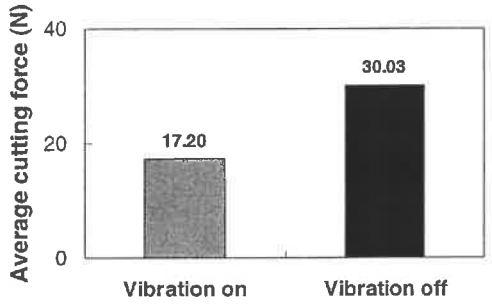


(b) Average cutting force

*FIGURE 4. Effects of ultrasonic vibration on cutting force.*

***Hole Entrance/Exit Edge Quality***

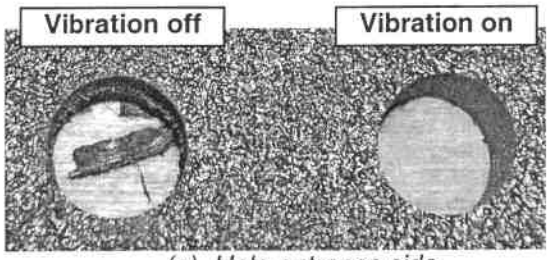


(a) Hole entrance side

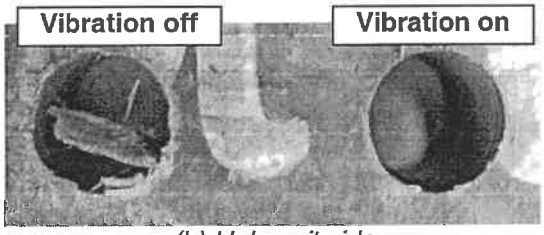


(b) Hole exit side

*FIGURE 5. Effects of ultrasonic vibration on hole entrance/exit edge quality.*

FIGURE 5 shows the effects of ultrasonic vibration on hole entrance/exit edge quality. There are no delaminations around the hole entrance edges in either case, as shown in FIGURE 5(a). For the hole exit side, the edge quality of the hole drilled when the vibration is off is much worse than the hole drilled when the vibration is on. There exist significant GREP delaminations and fiber pull-out around the exit edge for the hole drilled when ultrasonic vibration is off, as shown in FIGURE 5(b). It can be concluded that the hole exit edge quality can be improved significantly when the ultrasonic vibration is on.

***Process Stability***

It is also found that ultrasonic vibration has a great effect on the process stability during RUM of GREP. Fig. 6 shows the comparison of "wastes" drilled off from the GREP panel when the vibration is on or off. When the ultrasonic vibration is off, the tool is easy to be jammed by the GREP scraps, as shown in FIGURE 6. The jammed tool has to be taken apart from the machine. The drilling process is much more stable when the ultrasonic vibration is on. A whole GREP rod (or plug) can be achieved, as shown in FIGURE 6, and there is no tool jamming.

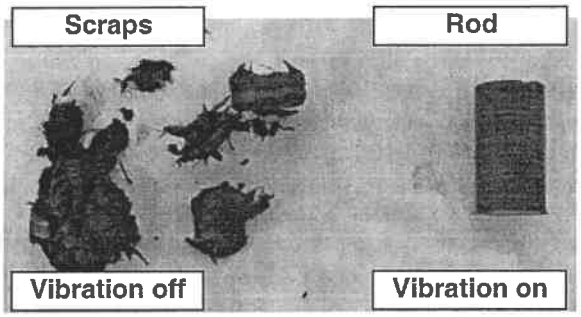


*FIGURE. 6. Effects of ultrasonic vibration on rod/scrap formation.*

**Effects of Feedrate**

***Cutting Force***

FIGURE 7 shows the effects of feedrate on cutting force. As the feedrate increases from 0.032 mm/s to 0.056 mm/s, the maximum cutting force increases from 30 N to 55 N as shown in FIGURE 7(a) while the average cutting force increases from 13 N to 25 N.

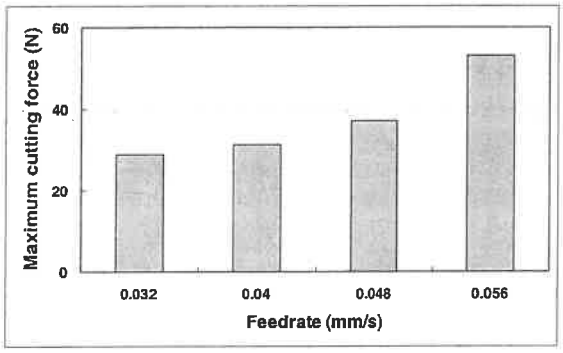


*(a) Maximum cutting force*

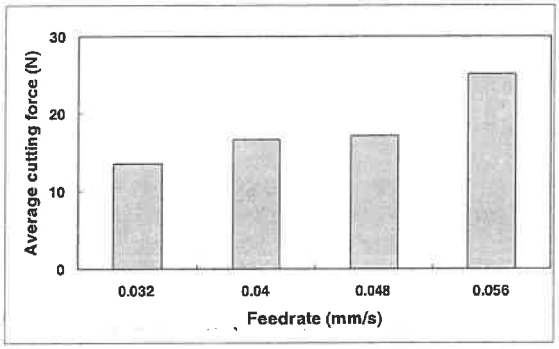


*(b) Average cutting force*

*FIGURE 7. Effects of feedrate on cutting force.*

***MRR***

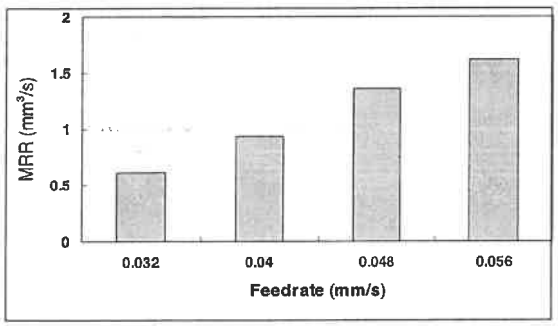


*(a) MRR*

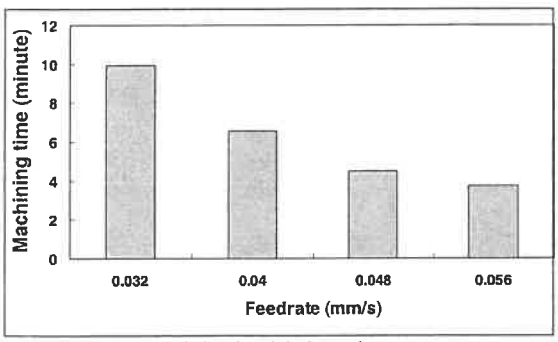


*(b) Machining time*

*FIGURE 8. Effects of feedrate on MRR and machining time.*

FIGURE 8 shows the effects of feedrate on MRR. As the feedrate increases from 0.032 mm/s to 0.056 mm/s, the MRR increases from 0.61 $mm^3/s$ to 1.62 $mm^3/s$ as shown in FIGURE 8(a) while the time it takes to drill through the GREP panel (the thickness of the panel is 14.11 mm) is reduced from ~10 mins to ~3.5 mins as shown in FIGURE 8(b).

***Hole entrance/exit edge quality***

There are no significant delaminations and fiber pull-out around the hole entrances and exits as the feedrate increases.

**Effects of Spindle Speed**

As the spindle speed increases from 3000 rpm to 6000 rpm, the maximum cutting shows a slight decrease as the spindle speed increases, as shown in FIGURE. 9(a). There are no significant changes in the average cutting force, as shown in FIGURE. 9(b). There are no observable delaminations and fibre pull-out around the hole entrances and exits.

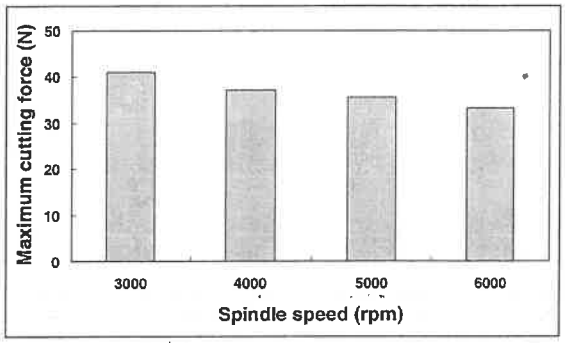


(a) Maximum cutting force

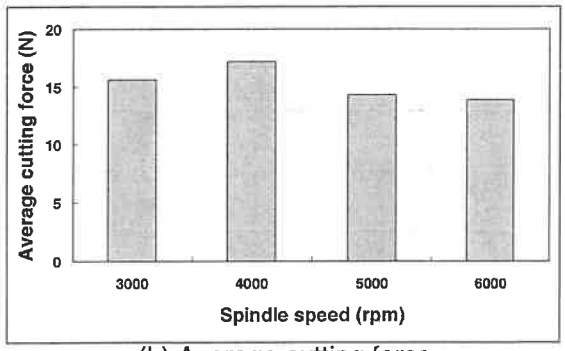


(b) Average cutting force

*FIGURE 9. Effects of spindle speed on cutting force.*

## CONCLUSIONS

In the present paper, rotary ultrasonic machining (RUM) is introduced into drilling GREP panels for the first time. The effects of RUM process parameters (ultrasonic vibration, feedrate, and spindle speed) on the RUM performances are also studied. The following conclusions can be drawn from the study:

1) The drilled hole exit edge quality can be improved significantly with the help of ultrasonic vibration. There are nearly no delamiations and fibre pull-out around the hole exit.
2) The drilling process when ultrasonic vibration is on is much more stable than that when ultrasonic vibration is off.
3) The cutting force decreases significantly when the ultrasonic vibration is on.
4) As the feedrate increases from 0.032 mm/s to 0.056 mm/s, the maximum/average cutting force increases significantly; the MRR increases from 0.61.mm$^3$/s to 1.62 mm$^3$/s while the time it takes to drill through the panel can be reduced from ~10 mins to ~3.5 mins.
5) The maximum cutting force decrease slightly as the spindle speed increases. The spindle speed does not affect the average cutting force and hole entrance/exit edge quality significantly.

## REFERENCES


[1] Peters S.D. Handbook of Composites (2nd edition). Chapman & Hall, London, UK, 1998.

[2] Anonymous. Composite Materials – A Bright Future in Aerospace Application. Metallurgia. 1985; 53 (8): 366-368.

[3] Wang D. Machining Characteristics of Graphite Epoxy Composite. Ph.D. Dissertation, University of Washington: 1993.

[4] Ramulu M, Arola D. Water Jet and Abrasive Water Jet Cutting of Unidirectional Graphite/epoxy Composite. Composites. 1991; 24(4): 299-308.

[5] Colligan K, Ramulu M, Arola D. Investigation of Edge Quality and Ply Delamination in Abrasive Waterjet Machining of Graphite/epoxy. American Society of Mechanical Engineers, Material Division (MD), Machining of Advanced Composites. 1993; 45: 167-185.

[6] Wang D, Wern C.W, Ramulu M, Rogers E. Cutting Edge Wear of Tungsten Carbide Tool in Continuous and Interrupted Cutting of a Polymer Composite. Materials and Manufacturing Processes. 1995; 10(3): 493-508.

[7] Kohkoner K.E, Anderson S, Strong A.B. Machining Graphite Composites with Polycrystalline Diamond End Mills. Proceedings of 23rd International SAMPE Conference, Kiamesha Lake, NY, USA. 1991; 23: 1036-1046.

[8] Ludin D. Laser Trimming of Graphite/epoxy Laminates. Proceedings of 55th Annual Forum of the American Helicopter Society, Montreal, Que., Can. 1999; 1766-1773.

[9] Shanmugam D.K, Chen F, Siores E, Brandt M. Comparative Study of Jetting Machining Technologies over Laser Machining Technology for Cutting Composite Materials. Composite Structures. 2002; 57(1): 289-296.

[10] Lau W, Wang M, Lee W. Electrical Discharge Machining of Carbon Fiber Composite Materials. International Journal of Machine Tools and Manufacture. 1990; 30(2): 297-308.

[11] Sadat A.B, Chan W, Wang B. Delamination of Graphite/epoxy Laminate during Drilling Operation. ASME Transactions, Journal of Energy Resources Technology. 1992; 114(2): 139-141.

[12] Cleave D.V. Ultrasonics Gets Bigger Jobs in Machining and Welding. Iron Age. 1976; 218(11): 69-72.

[13] Graff K.F. Ultrasonic Machining. Ultrasonics. 1975; May: 103-109.

[14] Petrukha P.G. Ultrasonic Diamond Drilling of Deep Holes in Brittle Materials. Journal of Russian Engineering. 1970; 50(10): 70-74.

[15] Hu P, Zhang J, Jiao Y, Pei Z.J, Treadwell C. Experimental Investigation on Coolant Effects in Rotary Ultrasonic Machining. Proceedings of the NSF Workshop on Research Needs in Thermal Aspects of Material Removal Processes, Stillwater, OK, USA. 2003; 340-345.

[16] Li Z.C, Jiao Y, Deines T.W, Pei, Z.J, Treadwell C. Development of an Innovative Coolant System for Rotary Ultrasonic Machining. International Journal of Manufacturing Technology and Management. 2005; 7(2-4):318-328.

[17] Pei Z.J, Prabhakar D, Ferreira P.M, Haselkorn M.M. Rotary Ultrasonic Drilling and Milling of Ceramics. Ceramic Transactions. 1995; 49(10): 185-188.

[18] Pei Z.J, Ferreira P.M. Modeling of Ductile-mode Material Removal in Rotary Ultrasonic Machining. International Journal of Machine Tools and Manufacture. 1998; 38(10-11): 1399-1418.

[19] Zhang Q.H, Zhang J.H, Jia X, Ai X. Fracture at the Exit of the Hole during the Ultrasonic Drilling of Engineering Ceramics. Journal of Materials Processing Technology. 1998; 84(1-3): 20-24.

[20] Dam H, Quist P, Schreiber M.P. Productivity Surface Quality and Tolerance in Ultrasonic Machining of Ceramics. Journal of Materials Processing Technology. 1995; 51(1-4): 358-368.

[21] Treadwell C, Pei Z.J. Machining Ceramics with Rotary Ultrasonic Machining. Ceramic Industry. 2003; June: 39-42.

[22] Pei Z.J, Ferreira P.M. An Experimental Investigation of Rotary Ultrasonic Face Milling. International Journal of Machine Tools and Manufacture. 1999; 39(8): 1327-1344.

[23] Khanna N, Pei Z.J, Ferreira P.M. Experimental Investigation of Rotary Ultrasonic Grinding of Ceramic Disks. Transactions of the North American Manufacturing Research Institution of SME. 1995; 23: 67-72.

[24] Li Z.C, Jiao Y, Deines T.W, Pei Z.J, Treadwell C. Experimental Study on Rotary Ultrasonic Machining (RUM) of Poly Crystalline Diamond Compacts (PDC). CD-ROM Proceedings of the 13th Annual Industrial Engineering Research Conference (IERC-2004), Houston, TX, USA. 2004.

[25] Li Z.C, Pei Z.J, Zeng, W.M, Kwon P, Treadwell C. Preliminary Experimental Study of Rotary Ultrasonic Machining of Zirconia Toughened Alumina. Transactions of the North American Manufacturing Research Institution of SME. 2005; 33: 89-96.

# NUMERICAL SIMULATION OF VIBRATION ASSISTED ELECTRON BEAM MACHINING PROCESS

**Z.G. Wang[1], Yoshiaki Daichi[2], Kazuo Yamazaki[1], Sadao Sano[2], and Yoshiyuki Uno[3]**
**[1]Department & Aeronautical Engineering**
**University of California, Davis**
**Davis, CA 95616**
**[2]Sodick Co. Ltd, Japan**
**Yokohama, Japan**
**[3]Department of Mechanical Engineering**
**Okayama University, Okayama 700-8530, Japan**

## INTRODUCTION

Recently, energy beam processing has been widely used in industries to machine difficult to cut materials and produce miniaturized components. The material removal is achieved by increasing the internal energy of atoms in the workpiece, consequently the work material with high internal energy is removed atom by atom, or atom cluster by atom cluster. Thus, this method is able to achieve high machining accuracy [1]. Another significant advantage of the energy beam processing is that there is no limitation imposed by workpiece hardness and ductility. Therefore this technique has a potential to be a new way to machine hard die steels and aeronautical alloys. Among all energy beam processing techniques, the electron beam (EB) process gains more and more attentions nowadays, because the electron beams can be controlled easily and accurately, and their power is generated at a very considerately high-efficiency. Moreover, in most cases, this EB process happens in a vacuum or near vacuum condition, thus the oxidation of the hot workpiece with oxygen is eliminated. Therefore, the EB process has been successfully used for welding, brazing, alloying, and other types of surface treatment [1-4].

Different from the traditional focused EB with a diameter of 0.5mm, the large area plasma-based EB (PBEB) with an effective diameter of 60 mm has been used in this paper. Using this proposed method, it is possible to smooth the workpiece surface of a certain area without beam scanning. The irradiation shot duration is 2-4 μs, so the workpiece can be machined within a very short time. In reference [4], Yu et al found that the machined surface roughness was reduced, and its corrosion resistance and glossiness were greatly improved after PBEB irradiation. However, some craters still exist on the machined surface after PBEB irradiation, which remain a problem for the roughness improvement and quality control of the machined surfaces.

One possible solution is to apply external forces to reduce and eliminate the craters during the melting and solidification process. In mass and fluid transfer community, the external forces are often generated by rotating or oscillating the solid body. The oscillation of the solid body is widely used to introduce an additional relative motion between the fluid and the solid body, thus it leads to an enhancement in the heat and mass transfer during the solidification process [5]. Besides, the oscillation could be an alternative method for removing the liquid condensate. In this study, a new method is proposed to improve the machined surface roughness and reduce the number of cavities by vibrating the worktable during solidification of melted surfaces in PBEB irradiation as shown in Fig. 1. Then, a simulation system using FEM package ABAQUS is developed to verify the proposed solution.

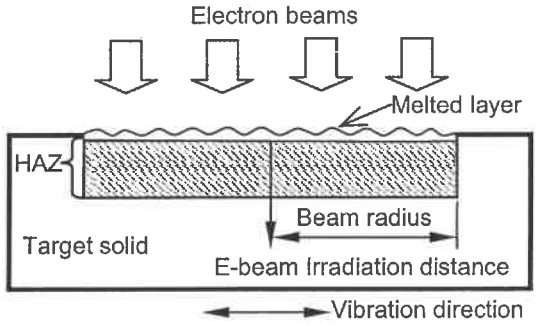


FIGURE 1. *Illustration of solidification of melted surface under vibration.*

## SIMULATION METHODOLOGY

Due to the extremely short EB duration, many difficulties exist in experimental investigation of

electrons and work materials interaction, such as measuring the transient surface temperature, and the moving speed of the solid-liquid interface. The interactions between electrons and work materials are so complicated that it is almost impossible to obtain a realistic analytical solution for them [6]. In addition, the coupled, nonlinear and non-equilibrium processes involved in electrons and material interactions induce an extremely high heating rate and a high temperature gradient. Under these extreme situations, molecular dynamics (MD) simulation, which analyzes the movement of atoms directly, is suitable to investigate evaporation of the melted surface layer in the EBM process [6]. However, due to its prohibitively large computational requirements both in terms of CPU time and memory, it is almost impossible to simulate the solidification process at a micron scale using MD. Thus, the continuum approach will be used to solve the solidification problem after evaporation. When the vibration is applied in the EBM process, thermal/fluid dynamics and mechanical displacement are involved in the solidification, which makes the problem very complicated. Finite element method is used to simulate the solidification process during the vibration assisted PBEB irradiation.

In mass and fluid transfer community, the external forces are often generated by rotating or oscillating the solid body. The oscillation of the solid body is widely used to introduce an additional relative motion between the fluid and the solid body, thus it leads to an enhancement in the heat and mass transfer during the solidification process. Besides, the oscillation could be an alternative method for removing the liquid condensate [5]. In this study, a new approach is proposed to smooth the workpiece surface by vibrating the worktable during solidification.

There are three objectives to use FEM methods to study the vibration assisted solidification during the EBM process. First, with a FEM method, a better understanding will be acquired of the physical phenomena of solidification at a micron-scale. Second, the important solidification processes involving scales that are extremely time consuming to be resolved using MD simulation can be analyzed with continuum-based methods within a reasonable time. More importantly, FEM simulation can verify whether vibration helps to smooth workpiece surfaces in the EBM process.

## SIMULATION OF COUPLED THERMAL-DISPLACEMENT INTERACTION

As mentioned, thermal/fluid dynamics and mechanical displacement are involved in the solidification, which makes the problem very complicated. In the last meeting report, it has been verified that it is possible to investigate structural and thermal response resulting from the coupling between the melted metal and tank, rather than a detailed solution in the fluid. In this meeting report, the simulation model has been revised to make it more similar to the practical case.

### Problem Description

From previous experiments, it was found that there were some small cavities observed on the machined surfaces after the EBM process, as shown in Fig. 2. In order to save the computation time, a 2-D coupled thermal-displacement interaction is firstly considered. According to Fig. 2, it can be assumed that the geometry of melted surface is shown in Fig. 3. The model consists of a tank filled with melted metal. The tank measures 2.0 × 0.2 mm, which is filled with 0.15 mm of melted metal. Pure master-slave contact is defined between the tank (master) and the melted metal (slave). The melted metal is subjected to gravity loading. Consequently, an initial geostatic stress field is defined to equilibrate the stresses caused by the self-weight of the melted metal. The tank is modeled as a rigid body and is meshed with R2D2 elements, and a graded mesh of CPE4RT elements is used for the melted metal.

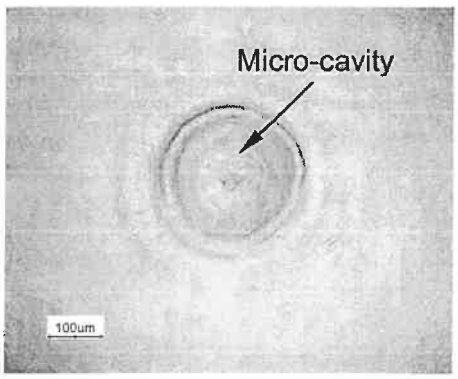


Figure 2. *Microscopic view of the machined surface after EBM process.*

In this study, the melted metal is considered as an incompressible and viscid fluid material. An effective method for modeling fluid in

ABAQUS/Explicit is to use a simple Newtonian viscous shear model. The shear viscosity also acts as a penalty parameter to suppress shear modes that could tangle the mesh, but a high shear viscosity will result in an overly stiff response. In this paper, the shear viscosity is chosen from the published data.

Figure 3. *Diagram of the coupled thermal-displacement interaction problem.*

In this paper, the carbon steel is used as the work material, and its mechanical and thermal properties are listed in Table 1. In order to simulate solidification, the latent heat effect was approximated by a sharp increase in heat capacity with a narrow temperature range where phase change takes place. Owing to the difficulties of numerical integration in the phase-change region where the heat capacity has a sharp peak, the enthalpy, which is the integral of the heat capacity with respect to temperature, is used instead in the solution procedure [7, 8]. The shear viscosity of melted metal depends on its temperature, and it is critical to choose an appropriate viscosity-temperature curve for a phase change analysis. The viscosity-temperature curve used in this study is shown in Fig. 4.

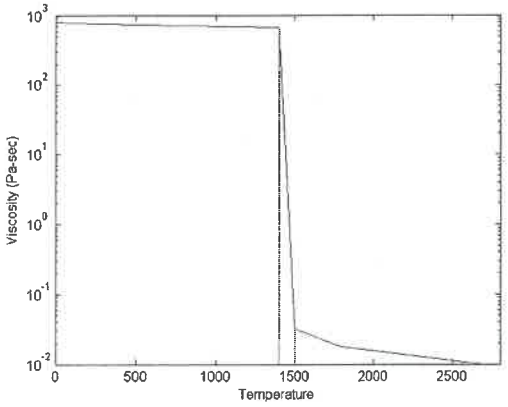


Figure 4. *Temperature dependent viscosity used in this study.*

## Adaptive Meshing

For problems when large deformations occur, it needs to maintain a high-quality mesh throughout an analysis. Adaptive meshing is such a tool that makes it possible by allowing the mesh to move independently of the material [7, 8]. Adaptive meshing in ABAQUS does not alter the topology (elements and connectivity) of the mesh. Because the fluid flow phenomenon modeled in this example results in large mesh motions, it is necessary to increase the intensity and frequency of adaptive meshing. The frequency value is reduced to 5 increments from a default value of 10, and the number of mesh sweeps used to smooth the mesh is increased to 3 from a default value of 1. In the simulation, sliding boundary regions are used for all contact surface definitions on the melted metal, and the default values are used for all other parameters and controls in ABAQUS for this coupled thermal-displacement interaction problem.

*TABLE 1. Mechanical and thermal properties of the carbon steel.*

| Parameters | Values |
|---|---|
| Density (kg/m$^3$) | 7893.2 |
| Thermal capacity (J/Kg-C) | 456.0 |
| Latent heat of fusion (KJ/Kg) | 247 |
| Thermal conductivity (W/m-C) | 55.0 |

## Surface Tension

The surface tension of liquid metals plays an important role in the rapid solidification at a micron scale. Under normal gravity conditions, surface tension forces contribute significantly to fluid flow (Marangoni or thermo-capillary flows) in solidification processes [9]. However, there is no built-in feature in ABAQUS specifically for surface tension. But it is possible add the surface tension to the melted surface. In a 2-D simulation problem, an edge traction could be used for this function, while a skin with standard membrane element could be added to the free surface in a 3-D simulation domain [7, 8]. Initially, edge tractions are used to handle surface tension in the simulation.

In this study, at first, the edge traction is treated as distributed pressure, which is applied by using the *DSLOAD options. ABAQUS/Explicit also provides a user subroutine *VDLOAD to define the variation of the distributed load magnitude as a function of position for a group of points. In this paper, the non-uniform pressure is defined in the user subroutine VDLOAD. When a pressure load needs to be applied, this subroutine will be called for load integration points associated with each non-uniform load definition.

## RESULTS AND DISCUSSION

With the decrease of problem size, the simulation model contains a few very small elements, which will force ABAQUS/Explicit to use a small time increment to integrate the entire model in time. This makes the simulation process very time consuming. By scaling the masses of these controlling elements at the beginning of the step, the stable time increment can be increased significantly, yet the effect on the overall dynamic behavior of the model may be negligible. Unfortunately, when the viscosity is incorporated into the simulation model, the mass scaling technique is not applicable because the shear viscosity is mass dependent. Therefore, it is not possible to use mass scaling method to speed up the simulation process. The only way to improve the computation efficiency is to use high-performance computers. In this paper, a dual core Dell Precision 380 workstation is used for the FEM simulation of the solidification process.

A velocity pulse in the form of a sine wave is prescribed for the tank along the horizontal direction. The vibration conditions used in the simulation are listed in Table 2. From the point of view of fluid dynamics, the assisted vibration generates the shearing forces in the melted area. Assume that the solid target is very large, with a moving speed $v$, and that the melted surface is free to move. If this solid target is moving with certain speed, it causes the melted metal to undergo shear flow. The shear stress is proportional to the velocity gradient of the melted metals. The layer near to the solid target has maximum velocity gradient, so larger shear stress exists in this layer, which takes it to move together with the solid target.

*TABLE 2. Vibration conditions used in the FEM simulation.*

| Test | Vibration frequency | Vibration amplitude |
|---|---|---|
| 1 | 8000 Hz | 5 μm |
| 2 | 4000 Hz | 10 μm |
| 3 | 4000 Hz | 5 μm |

The simulation analysis mainly focused on the effect of dragging forces and surface tension on smoothing melted surface. In the EBM process, the initial temperature distribution of the heat affected area is firstly estimated as shown in Fig. 5. The melting temperature of the target material is in the range of 1450~1500°C. Target material with a temperature in this range is at a liquid/solid coexistence state, which is also called mushy state, as shown in Fig. 5. When the temperature of target material is greater than 1500°C, its viscosity is quite small. After the temperature decreases to a value lower than 1500°C, its viscosity significantly increases. In the EBM process, the temperature of the melted metal gradually decreases after EB irradiation. Figure 6 (a) shows the temperature distribution after 0.0003 seconds. With the decrease of temperature, the viscosity of the melted surface increases greatly. This increased viscosity results in higher shear stress inside this layer and causes its movement along with the solid target, as shown in Fig. 6 (b). This also causes an increase of moving speed for the lower layer of the heat affected area. While the viscosity of the top layer is still very low because of its high temperature, so limited shear forces are applied to it. Initially the surface tension is the dominant source to smooth the craters on the workpiece surface.

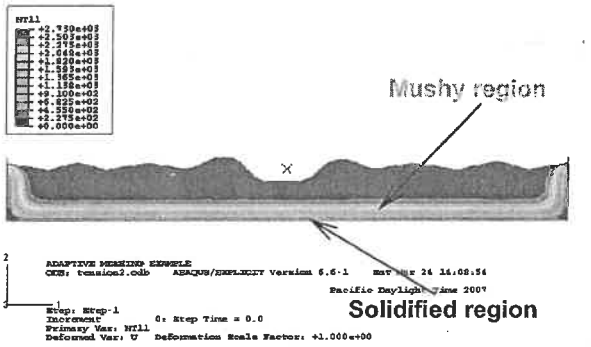


*FIGURE 5. Initial temperature distribution and surface profile of the studied problem.*

As the solidification process continues, larger shear forces are transferred to top surface. At this time, the dragging forces applied on the top surface together with the surface tension helps to smooth the workpiece surface. As the simulation time reaches 0.0075 seconds, the surface profile and temperature distribution of the melted surface for Test 1 and 2 are presented in Fig. 7. After the same simulation time, the temperature in the heated affected zone for Test 1 is less than that for Test 2. It indicates that the vibration at high frequency is able to improve the heat transfer further during the solidification process. Figure 7 also indicates that the final surface roughness for Test 1 is more uniform than that for Test 2. Therefore, high frequency vibration is a more optimal condition.

Figure 8 shows the average von Mises stress in the target material for two test cases. At high frequency, larger Mises stress is found inside the target material. This is attributed to larger acceleration speed applied on the heat affected area at high frequency. In the vibration assisted solidification process, it is these internal forces that help smooth the craters at the top surface. On the contrary, at low frequency, the lower shear forces are applied on the melted metal in the heat affected area.

In the vibration assisted solidification, the left and right sides of the solid target also oscillate, which pushes the nearby melted metal to move and produces a wave in the melted metal. This may be another reason why the width of the central crater becomes smaller.

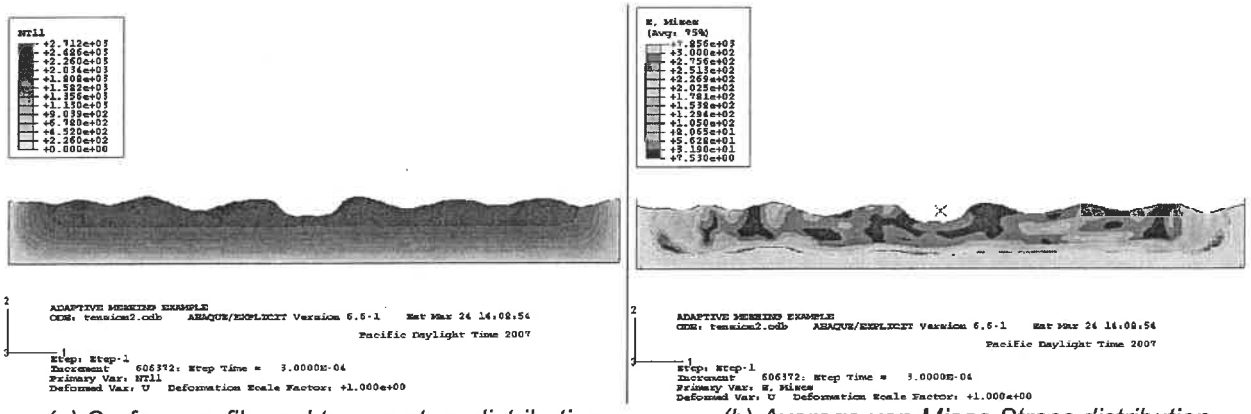

*(a) Surface profile and temperature distribution* *(b) Average von Mises Stress distribution*

*FIGURE 6. Deformed surface profile and temperature distribution for Test 1.*

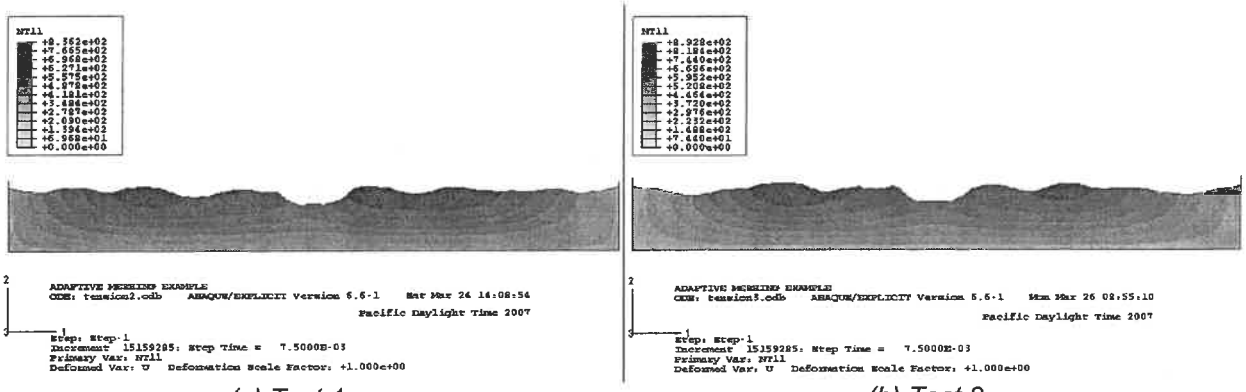

*(a) Test 1* *(b) Test 2*

*FIGURE 7. Deformed surface profiles for Test 1 and Test 2.*

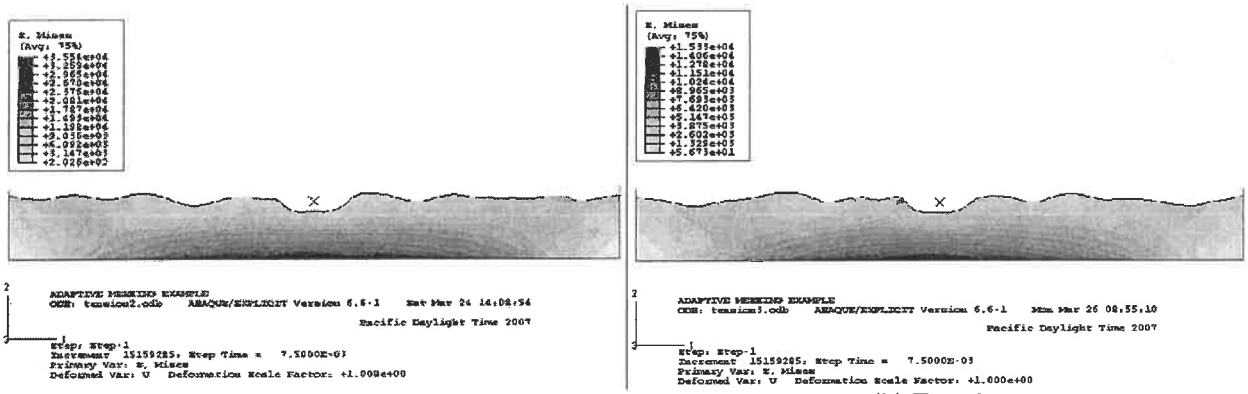

*(a) Test 1* *(b) Test 2*

FIGURE 8. *The average von Mises stress in the target material for Test 1 and Test 2.*

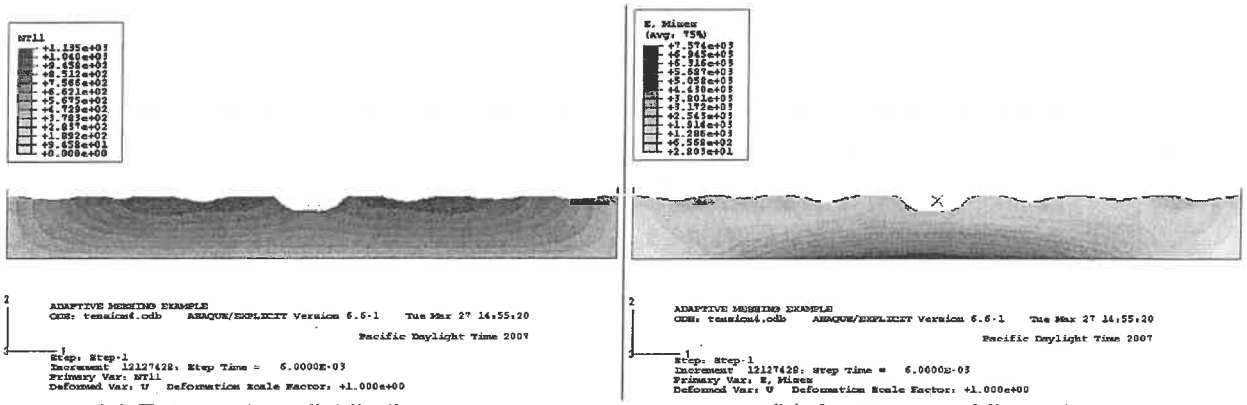

(a) *Temperature distribution* (b) *Average von Mises stress*

FIGURE 9. *Simulation results for Test 3.*

In order to investigate the effect of vibration amplitude on the vibration assisted solidification process, one more test is carried out and the simulation results are shown in Fig. 9. From Fig. 7(b) and Fig. 9(a), it can be seen that the final machined surface at low vibration amplitude is more uniform than that at high vibration amplitude. Therefore, high vibration frequency and medium value of vibration amplitude is an optimal vibration condition.

From the simulation result, it is also found that the material at the top surface is solidified when the temperature reduces below its melting point. At this time, the effect of surface tension becomes less and less. Even though, the applied vibration still can transfer some shear forces to the material at the top surface, it is not enough to smooth the top surface any more. Therefore, in order to fully take advantage of the assisted vibration, it is necessary to use the surface tension effect together with the assisted vibration to generate external forces to smooth the top surface when the top surface is still at its liquid state.

## CONCLUSIONS

In this paper, a finite element method is used to simulate the vibration assisted EBM process. The simulation result shows that good quality surfaces are achieved when vibration is applied to the worktable. This is attributed to the surface tension and the additional forces applied to the melted metals via vibrating the worktable, which can smooth the workpiece surface. The optimal vibration conditions are found at a medium vibration amplitude and high vibration frequency. Therefore, vibrating the worktable during the EBM process would be a potential solution to eliminate the micro-craters, which are inevitable in the conventional EBM process.

## REFERENCES


[1] Taniguchi N. Introduction, in: Energy-beam processing of materials: Advanced manufacturing using various energy sources. Oxford University Press: 1989.

[2] Günzel R, Rogozin AI, Astrelin VT. Fast, uniform, and large-scale heat treatment by plasma-based electrons. Vacuum; 2002; 65: 59-65.

[3] Schiller S, Heisig U, Panzer S. Electron beam technology. Wiley, New York: 1982.

[4] Yu Z, Wang ZG, Yamazaki K, Sano S. Surface finishing of die and tool steels via plasma-based electron beam irradiation. Journal of Materials Processing Technology. 2006; 180: 246-252.

[5] Cheng, CH, Shiu CC. Oscillation effects on frost formation and liquid droplet solidification on a cold plate in atmospheric air flow. International Journal of Refrigeration. 2003; 26 (1): 69-78.

[6] Wang ZG, Yamazaki K, Daichi Y, Sano S. Numerical Simulation of High Productive Surface Finishing by Electron Beam Irradiation with Vibration Assistance, Transactions of the North American Manufacturing Research Institution of SME. 2007; 35: (Accepted for publication)

[7] ABAQUS. Version 6.6 ABAQUS Users' Manual, ABAQUS Inc. 2006.

[8] ABAQUS. Version 6.6 Theory Manual, ABAQUS Inc. 2006.

[9] Man KF. Surface Tension Measurements of Liquid Metals by the Quasi-Containerless Pendant Drop Method, International Journal of Thermophysics. 2000; 21(3): 793-804.

# Simulation of Elliptical Vibration Cutting Process with Thin Shear Plane Model

**Eiji Shamoto[1], Norikazu Suzuki[1] and Rei Hino[1]**
[1]Department of Mechanical Science and Engineering
Nagoya University
Nagoya, Aichi, Japan

## INTRODUCTION

The elliptical vibration cutting was first proposed in 1993 [4-7]. Since then, some ultrasonic elliptical vibration tools have been developed, and their machining performance has been investigated for some difficult-to-cut materials [8, 9,13]. Recently, this technology has been tested in industries mainly for ultraprecision diamond cutting of dies, molds, and optical parts.

On the other hand, there have been less investigations on basic mechanics of the elliptical vibration cutting. An analytical model of the orthogonal elliptical vibration cutting process, in which all velocities, forces and vibrations are perpendicular to the cutting edge, was developed and verified experimentally to predict theoretical roughness, critical relief angle, shear angle, etc., and to clarify effects of speed ratio, i.e. maximum vibration speed in the nominal cutting direction / the nominal cutting speed, vertical vibration amplitude and phase difference between the two directional vibrations [7]. However, the practically applied processes are not generally the orthogonal type. The elliptical vibration locus is usually inclined around the cutting direction in most of the industrial applications.

Therefore, simple analytical models of the three dimensional (3D) elliptical vibration cutting processes are proposed in the present research in order to simulate the process quickly and to understand the basic mechanics. The results simulated with the present models are compared with experimental data published in the previous papers [7,12].

## ELLIPTICAL VIBRATION CUTTING PROCESS WITH UNIQUE PHENOMENON OF FRICTION

Figure 1 shows a schematic illustration of the elliptical vibration cutting process. The cutting starts at the time $t_1$, and the small part left in the previous cycle is cut at small depth until the time $t_2$, when the rake face contacts with the chip formed in the previous cycle. In the actual process, this small part may be burnished and pushed into the workpiece and the chip because of cutting edge roundness. After the time $t_2$, the workpiece material is sheared and removed as the chip at large depth of cut. As the tangent of cutting path exceeds the shear direction at the time $t_6$, the frictional direction is reversed. In the actual process, the tool moves together with the chip in the shear direction near $t_6$ without the sudden reversal of friction because of elasticity. Then, the tool is separated from the chip at the time $t_5$, when the tangent is parallel to the rake face. The reduced or reversed friction leads to significant reduction of cutting force, energy and heat generation [4-6].

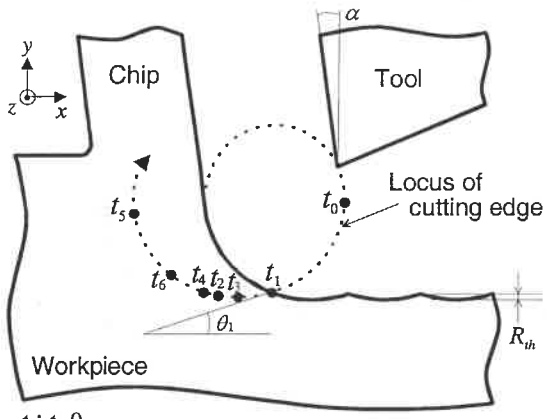


$t_0$: $t$=0
$t_1$: Beginning of cutting
$t_2$: Contact betweeen rake face and chip
$t_3$: Bottom of locus
$t_4$: End of finished surface generation
$t_5$: End of cutting
$t_6$: Reversal of friction
$\theta_1$: Critical relief angle
$R_{th}$: Theoretical rougthness

*FIGURE 1. Elliptical vibration cutting process.*

Figure 2 shows the chip formation processes of orthogonal ordinary cutting and elliptical vibration cutting. It shows that the chip thickness is much smaller in the elliptical vibration cutting though the cutting conditions are the same. Figure 3 shows the cutting forces measured in the both processes. The negative thrust force shown in Fig. 3(b) indicates the reversal of friction, and this leads to the significant increase of shear angle, see Fig. 2, and the significant

reduction of cutting force, see Fig. 3 [4-6].
Figure 4 shows typical chips observed in practical ultraprecision elliptical vibration cutting with single crystal diamond tools. The chips are usually continuous and the chip thickness is almost constant as shown in the figures, although the instantaneous cutting direction is varied. This suggests that the shear deformation may be caused by average or total force applied to the workpiece material in one cycle of the elliptical vibration.

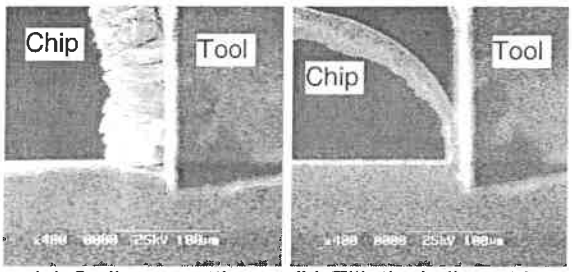


*(a) Ordinary cutting* *(b) Elliptical vib. cutting*

[Conditions] Workpiece: Copper, rake: 0 deg, cutting speed: 0.26 mm/min, depth of cut: 10 μm, elliptical vibration: circular, amp.: 10 $\mu m_{p\text{-}p}$, freq.:1.2 Hz

*FIGURE 2. Direct observation of chip formation processes.*

As mentioned above, the elliptical cutting process can be divided into the two processes, i.e. the micro cutting or burnishing process from $t_1$ to $t_2$ and the cutting process with the reduced or reversed friction from $t_2$ to $t_5$. When the depth of cut is large enough relatively to the vertical amplitude of vibration, the former micro machining period is negligible. On the other hand, when the depth is extremely small and the cutting edge is sharp enough, the latter cutting period vanishes, and the process may be similar to micro milling except that the rake face is not inclined during cutting and that the tool path is elliptical.
Judging from the observations of process and chips, it is considered that the constant continuous chip formation with the unique frictional phenomenon is the main process in many of the practical elliptical vibration cutting. Whereas the mechanism of the former micro machining can be understood as the ordinary micro machining process, the latter chip formation process with the reversed or reduced friction is unique and academically interesting. Therefore, the former process is not considered and the latter process is modeled and discussed in the present research.

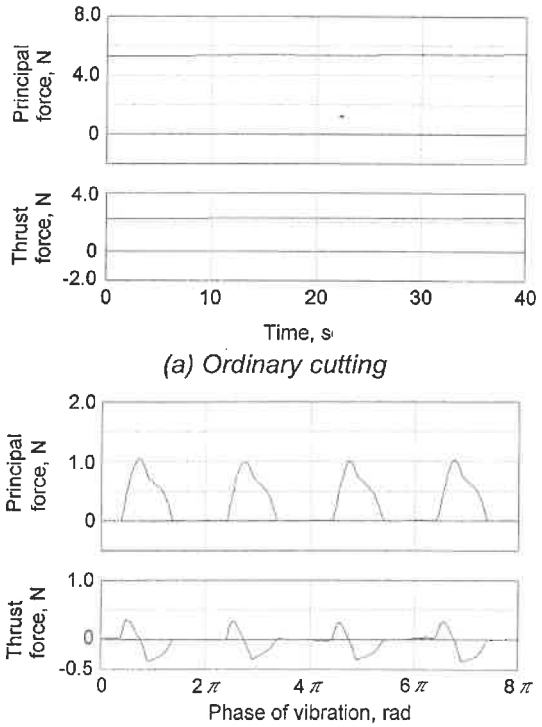


*(a) Ordinary cutting*

*(b) Elliptical vibration cutting*

[Conditions] Same as Fig. 2

*FIGURE 3. Transient cutting forces measured in ordinary cutting and elliptical vibration cutting.*

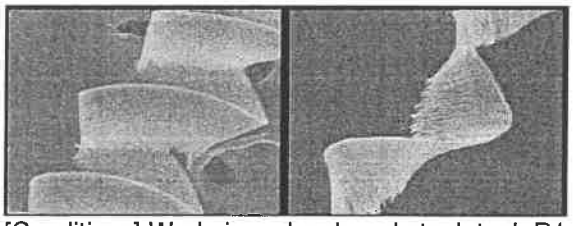

[Conditions] Workpiece: hardened steel, tool: R1 mm, rake: 0 deg, cutting speed: 2.5 m/min, depth of cut: 10 μm, feed rate: 10 μm/rev, vibration: circular, amp.: 10 $\mu m_{p\text{-}p}$, freq.:20 kHz

*FIGURE 4. Chips formed by ultraprecision elliptical vibration cutting.*

For simplicity, the cutting edge is assumed sharp enough, and the elastic deformation is neglected. The instantaneous depth of cut is decreased gradually during the latter cutting period, but this effect is also neglected, i.e. the depth is assumed constant. The simple thin shear plane model is employed, and the maximum shear stress and minimum energy principles are separately applied for simple simulations and better comprehension of the continuous chip formation process. The above issues neglected here may be considered in the

future for more precise analysis and comprehension.

## GEOMETRY OF 3D ELLITPTICAL VIBRATION CUTTING PROCESS

Figure 5 shows various types of elliptical vibration cutting. Figure 5(a) is the orthogonal type. Figure 5(b) is the oblique type which is intermittent cutting with sidewise motion of the cutting edge or a rotary tool on average, which is equivalent to oblique cutting with reduced width of cut [10-12]. In this case, the friction is not reduced, but the cutting force is reduced by the reduction of actual width of cut [11]. This is why knives are pulled in the cutting edge direction to reduce the force.

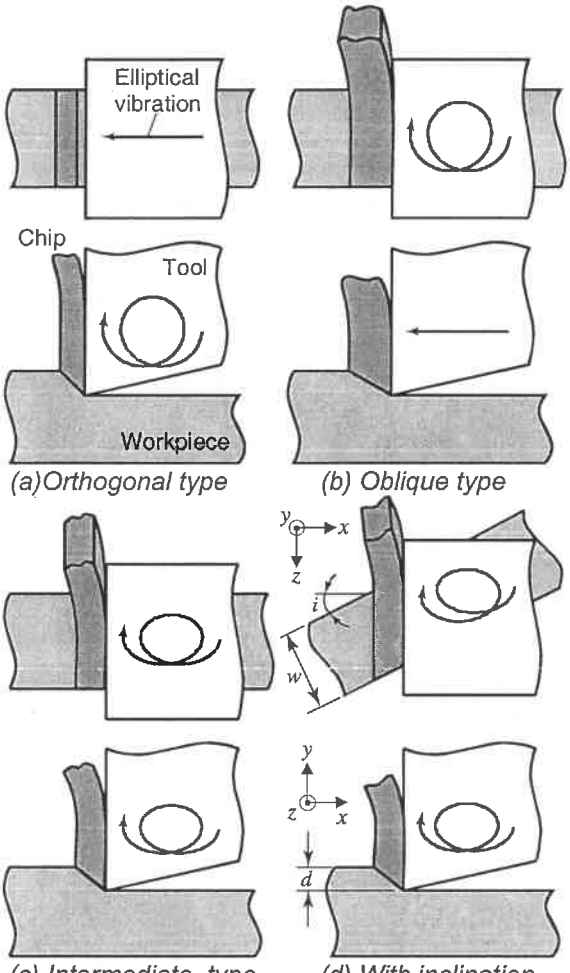


(a)Orthogonal type (b) Oblique type

(c) Intermediate type (d) With inclination

*FIGURE 5. Various types of elliptical vibration cutting processes.*

Figure 5(c) shows intermediate type between the above two types, which has both effects, i.e. the thrust force is reduced or reversed and the actual width of cut is reduced. This intermediate type is utilized widely in practice. Furthermore, the cutting edge is not always perpendicular to the cutting direction, as shown in Fig. 5(d), where the obliquity of cutting direction is denoted by an inclination angle $i$. In this case, the inclination of cutting direction enhances obliquity of the inclined elliptical vibration.

The tool is vibrated at an angular frequency $\omega$ and fed at a nominal cutting speed $V_c$, and the workpiece is stationary here. Then, the tool path with the vibration can be expressed as follows.

$$\begin{aligned} x(t) &= a\cos(\omega t) - V_c t\cos i \\ y(t) &= b\cos(\omega t + \varphi_y) \\ z(t) &= c\cos(\omega t + \varphi_z) + V_c t\sin i \end{aligned} \tag{1}$$

where $x$, $y$ and $z$ are Cartesian coordinates of the relative position between the tool and the workpiece in the direction normal to the cutting edge, the thrust direction and the cutting edge direction respectively, see Fig. 1 and Fig. 5(d). The nominal cutting direction lies on the $x$-$z$ plane, i.e. finished surface. $a$, $b$ and $c$ are vibration amplitudes in the $x$, $y$ and $z$ directions respectively. $t$ is time and $\varphi_y$ and $\varphi_z$ are phase shifts of the vibrations in the $y$ and $z$ directions respectively.

When the minimum relative speed in the direction normal to the rake face is negative, the cutting process becomes intermittent.

$$V_c\cos i\cos\alpha - \omega\sqrt{(a\cos\alpha - b\sin\alpha\cos\varphi_y)^2 + (b\sin\alpha\sin\varphi_y)^2} < 0 \tag{2}$$

where $\alpha$ is the normal rake angle which is the rake angle in the plane normal to the cutting edge.

Under this intermittent condition, the time $t_5$ (see Fig. 1) is obtained by solving Eq. (3), since the relative speed in the direction normal to the rake face becomes zero at $t_5$.

$$\begin{aligned} &\{a\omega\sin(\omega t_5) + V_c\cos i\}\cos\alpha \\ &\quad - b\omega\sin(\omega t_5 + \varphi_{xy})\sin\alpha = 0 \end{aligned} \tag{3}$$

The rake face is separated from the chip at $t_5$, and then it comes back to the same plane at $t_2+T$, where $T$ is a vibration period. Thus, $t_2$ can be solved numerically by the following equation.

$$\{x(t_2+T)-x(t_5)\}\cos\alpha+\{y(t_5)-y(t_2+T)\}\sin\alpha=0$$
$$\therefore\ a\{\cos(\omega t_2)-\cos(\omega t_5)\}\cos\alpha$$
$$+b\{\cos(\omega t_5+\varphi_y)-\cos(\omega t_2+\varphi_y)\}\sin\alpha \quad (4)$$
$$=V_c(T-t_5+t_2)\cos\alpha\cos i$$

The other parameters $t_1$, $t_3$, $t_4$, $\theta_1$ and $R_{th}$ can also be solved in a similar way to the orthogonal elliptical vibration cutting [4].

## PREDICTION OF SHEAR DIRECTION IN 3D ELLITPTICAL VIBRATION CUTTING PROCESS

The shear direction in the 3D vibration cutting process is assumed to be constant, judging from the direct observation of the process and the chips obtained in the practical cutting operations as mentioned above. The shear direction is predicted by extending the 3D thin shear plane model [10,11] as follows.

As the shear direction $\vec{v}_s$ (unit vector) is constant, the chip also moves in the same direction independently of the instantaneous tool velocity $\vec{V}_T$, i.e. instantaneous cutting velocity. Thus, the instantaneous velocity of the chip material $\vec{V}_M$ is derived by:

$$\vec{V}_M=\left|\vec{V}_M\right|\vec{v}_s=\frac{\vec{V}_T\cdot\vec{n}}{\vec{v}_s\cdot\vec{n}}\vec{v}_s \quad (5)$$

where $\vec{n}$ is a unit vector normal to the rake face and given by $(-\cos\alpha,\sin\alpha,0)$, and $\vec{V}_T$ is given by the time-derivative of tool position:

$$\vec{V}_T=\big(-a\omega\sin(\omega t)-V_c\cos i,-b\omega\sin(\omega t+\varphi_y),\\ -c\omega\sin(\omega t+\varphi_z)+V_c\sin i\big) \quad (6)$$

The friction $\vec{f}$ (unit vector) acts in the opposite direction of the relative motion between the tool and the chip.

$$\vec{f}=\frac{\vec{V}_T-\vec{V}_M}{\left|\vec{V}_T-\vec{V}_M\right|} \quad (7)$$

Then, the direction of resultant cutting force $\vec{r}$ (unit vector) can be obtained as follows, assuming a constant frictional angle $\beta$.

$$\vec{r}=\vec{n}\cos\beta+\vec{f}\sin\beta \quad (8)$$

The resultant force $\vec{R}$ needs to produce the shear force $F_s$ in the shear plane, and hence it can be calculated by:

$$\vec{R}=\frac{F_s}{\vec{r}\cdot\vec{v}_s}\vec{r}=\frac{\tau wd\sqrt{(\vec{v}_s\cdot\vec{e}_y)^2+(\vec{v}_s\cdot\vec{e}_x)^2}}{(\vec{v}_s\cdot\vec{e}_y)(\vec{r}\cdot\vec{v}_s)\cos i}\vec{r} \quad (9)$$

where $\tau$ is shear stress in the shear plane, $w$ and $d$ are the width and depth of cut, see Fig. 5(d), and $\vec{e}_x$ and $\vec{e}_y$ are unit vectors in the $x$ and $y$ directions respectively. This force is varied with the varying cutting velocity $\vec{V}_T$, and thus the instantaneous cutting power $U$ is given by:

$$U=\vec{R}\cdot\vec{V}_T \quad (10)$$

The shear direction is predicted with the two fundamental principles separately. One is the maximum shear stress principle. It is assumed that the shear occurs in the maximum shear stress direction, where the resultant force makes 45 degrees with the shear direction and also the shear plane [10,11]. In the present 3D vibration cutting process, the resultant force is varied. Therefore, it is assumed that the shear direction is determined by summation of the instantaneous resultant force $\vec{R}_{sum}$ during the cutting period from $t_2$ to $t_5$.

$$\vec{R}_{sum}=\sum\left|\vec{V}_M\right|\vec{R} \quad (11)$$

where $\left|\vec{V}_M\right|$ is multiplied in the present paper as a weight function, because the influence on the shear deformation may be increased as the removed material is increased. As a result, the shear direction $\vec{v}_s$ and the summed force $\vec{R}_{sum}$ need to satisfy the following equation.

$$\frac{\vec{R}_{sum}}{\left|\vec{R}_{sum}\right|}=\vec{v}_s\cos45°+\vec{n}_s\sin45° \quad (12)$$

where $\vec{n}_s$ is a unit vector normal to the shear plane and given by:

$$\vec{n}_s=\frac{\vec{v}_s\times\vec{e}_y}{\left|\vec{v}_s\times\vec{e}_y\right|} \quad (13)$$

Therefore, the correct shear direction $\vec{v}_s$ can be searched as follows. First, $\vec{R}_{sum}$ is calculated by Eqs. (5-11), and then $\vec{v}_s$ is checked by Eqs. (12, 13). If the error between the left and right sides of Eq. (12) is not small enough, the shear direction $\vec{v}_s$ is updated. The correct vector is searched numerically by the iteration.

The other fundamental shear angle prediction is based on the minimum energy principle. The shear direction is determined here so that the total cutting energy $E$ becomes minimum, where $E$ is given by integrating instantaneous cutting power numerically from $t_2$ to $t_5$ as follows.

$$E = \sum U \Delta t \tag{14}$$

Thus, solution of the shear direction $\vec{v}_s$ can be found by searching $\vec{v}_s$ iteratively so that the energy becomes the minimum.

The above analytical models are applied to simulation of the 3D elliptical vibration cutting process here. However, the models are also valid for other cutting processes including the 3D linear vibration cutting where constant continuous chips are formed. The present models give the same solutions as the oblique cutting models [10,11] when $i \neq 0$ and $a=b=c=0$, and they yield to Merchant's [2] and Krystof's [1] (or Lee-Shaffer's [3]) models when $i$ is also zero.

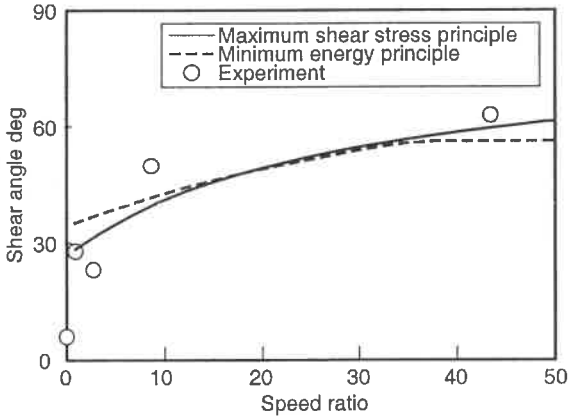


[Conditions] Same as Fig. 2

*FIGURE 6. Shear angles at various speed ratios in orthogonal type of elliptical vibration cutting.*

## SIMULATION RESULTS AND DISCUSSIONS

The developed analytical models are applied to the orthogonal and oblique types of elliptical vibration cutting, and simulated results are compared here with some published data.

Figure 6 shows the shear angles predicted and measured [7] at various speed ratios in the orthogonal type. The friction angle $\beta$ utilized in the simulation is identified 23.5 deg by the forces measured in the ordinary cutting, see Fig. 3(a). Figure 7 shows the chip flow angles predicted and measured [12] at various speed ratios in the oblique type of elliptical vibration cutting. $\beta$ is 41.3 deg [12] in the simulation.

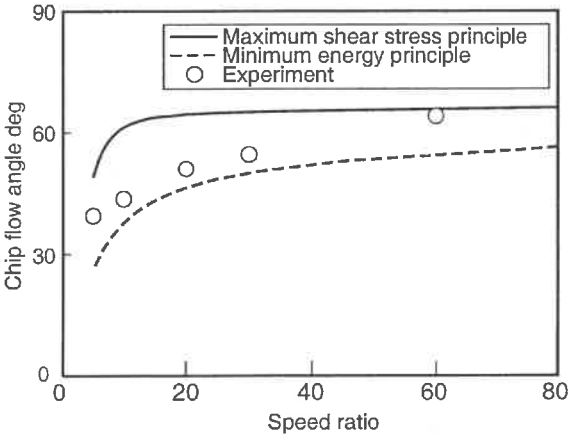


[Conditions] Workpiece: aluminum, rake: 0 deg, depth of cut: 50 μm, vibration: circular, amp.: 1 $mm_{p\text{-}p}$, freq.:10 Hz

*FIGURE 7. Chip flow angles at various speed ratios in oblique type of elliptical vibration cutting.*

Considering the simplicity of analytical models, the characteristic angles predicted with either principle agree roughly with the experimental data, as shown in the figures. It shows that the two types of elliptical vibration cutting process can be predicted quickly and roughly with the models developed here. The rough agreements suggest that the orthogonal and oblique types of elliptical vibration cutting can be understood as the unique chip formation process with reversal of friction and the oblique cutting with the reduced width of cut respectively.

Transient cutting forces in the intermediate type are also predicted and compared with experimental data [12] in Fig. 8. $\beta$ is 41.3 deg and $\tau$ is 94.3 MPa [12]. The results are in a good agreement during the cutting period, as shown in the figure. The disagreement is considered to be caused mainly by the elastic deformation, which is neglected here. The thrust force is reversed in the cutting period by the orthogonal component of the elliptical vibration. The force in the cutting edge direction, which is shown by "normal" in the figure, corresponds to the

obliquity of cutting process. This is caused by the oblique component of the elliptical vibration, and it also reduces the cutting force by reducing the actual width of cut [11]. The measured peak principal force was 140 N as shown in the figure, while average principal force measured in the ordinary cutting was 480 N [12]. It is considered that this significant reduction is caused by combination of the above two effects.

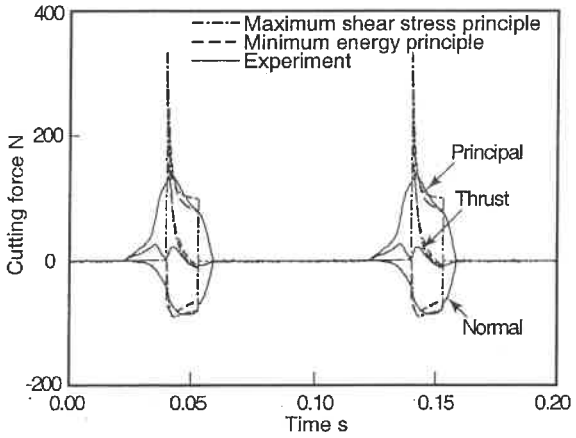


[Conditions] Workpiece: aluminum, rake: 0 deg, depth of cut: 0.3 mm, width of cut: 2mm, cutting speed: 94.3 mm/min, vibration: circular, amp.: 1 $mm_{p-p}$, freq.:10 Hz, inclination of elliptical vibration: 80 deg from orthogonal type, i.e. 10 deg from finished surface

*FIGURE 8. Transient cutting forces in intermediate type of elliptical vibration cutting.*

## CONCLUSION

The simple analytical models of the 3D elliptical vibration cutting are developed by employing the thin shear plane model and either the maximum shear stress principle or the minimum energy principle. The simulated results agree roughly with the experimental data published previously. The models represent the unique cutting mechanics of two types of elliptical vibration cutting. The simplified models and the simulated and experimental data are helpful to understand the processes. They suggest that the continuous chip formation process in the oblique type of elliptical vibration cutting is the unique cutting process with the reversal phenomenon of friction, and the oblique type of elliptical vibration cutting is equivalent on average to the cutting process with the sidewise motion of tool. The practical elliptical vibration cutting can be understood as the intermediate process between the two types.

## REFERENCES


[1] Krystof J. Berichte uber Betriebswissenschaftliche Arbeiten, Bd., 12, VDI Verlag.: 1939

[2] Merchant M.E. Mechanics of the Metal Cutting Process. II. Plasticity Conditions in Orthogonal Cutting. J. Applied Physics: 1945; 16: 318-324

[3] Lee, E.H., Shaffer B.W. The Theory of Plasticity Applied to a Problem of Machining. J. Applied Mechanics: 1951; 18; 405-413

[4] Shamoto E., Moriwaki T. Fundamental Study on Elliptical Vibration Cutting. Proc. 8th Annual Meeting, ASPE: 1993; 162-165

[5] Shamoto E., Moriwaki T. Study on Elliptical Vibration Cutting. Ann. CIRP: 1994; 43/1: 35-38

[6] Shamoto E., Morimoto Y., Moriwaki T. Elliptical Vibration Cutting (1st Report, Cutting Principle and Basic Performance) (in Japanese). J. JSPE: 1996; 62/8: 1127-1131

[7] Shamoto E., Morimoto Y., Moriwaki T. Elliptical Vibration Cutting (2nd report, Study on Effects of Vibration Conditions) (in Japanese). J. JSPE: 1999; 65/3: 411-417

[8] Shamoto E., Moriwaki T. Ultraprecision Diamond Cutting of Hardened Steel by Applying Elliptical Vibration Cutting. Ann. CIRP: 1999; 48/1: 441-444

[9] Shamoto E., Ma C.X., Moriwaki T. Ultraprecision Ductile Cutting of Glass by Applying Ultrasonic Elliptical Vibration Cutting. Proc. of 1st Int. Conf. and general meeting of EUSPEN: 1999; 408-411

[10] Shamoto E., Altintas Y. Prediction of Shear Angle in Oblique Cutting with Maximum Shear Stress and Minimum Energy Principles. Trans. ASME J. Manuf. Sci. Eng.: 1999; 121: 399-407

[11] Shamoto E. Study on Three Dimensional Cutting Mechanics (1st Report, Comprehension and Vector Formulation of Oblique Cutting Process) (in Japanese). J. JSPE: 2002; 68/3: 408-414

[12] Shamoto E., Song Y.C., Sassa K., Yoshida H., Hino R., Moriwaki T. Proposal of Oblique Type of Elliptical Vibration Cutting and Its Basic Performance. J. JSPE: 2003; 69/7: 970-975

[13] Suzuki N, Haritani M, Yang J., Hino R., Shamoto E. Elliptical Vibration Cutting of Tungsten Alloy Molds for Optical Glass Parts. Ann. CIRP: 2007; 56/1: to be published

# MATERIAL PROPERTIES FOR MODELING VIBRATION ASSISTED MACHINING

**Richard L. Rhorer**
**National Institute of Standards and Technology**
**Manufacturing Metrology Division**
**Gaithersburg, Maryland**

The vibration-assisted machining adds high frequency motion and additional forces to an already very complex machining process. To incorporate vibration assisted machining into modern manufacturing processes it will be necessary to simulate the process with models and to help demonstrate the advantages and disadvantages of these added complexities. To model any machining process in a predictive environment it is necessary to have an understanding of the effect of material properties on the process parameters. The material property traditionally needed for machining models is the shear flow stress of the material appropriate for the particular process. Because machining is a very high strain-rate process, and machining usually involves elevated temperatures, the flow stress as a function of strain-rate and temperature becomes important. The material test method most commonly used for obtaining high strain rate properties of metals is the split Hopkinson pressure bar, or also called a Kolsky Bar.

The Kolsky Bar approach of determining appropriate dynamic material properties is presented in this paper with an emphasis on the strain rate effects on flow stress. If the strain rate of a machining process is affected by a vibrating tool, can a change in flow stress due to strain rate effects explain the machining performance enhancement of vibration-assisted machining? This paper provides some examples of strain rate effects on the flow stress of steel and aluminum that will be useful in modeling vibration assisted machining. The strain-rate effect has been investigated using the NIST Pulse Heated Kolsky Bar, and the method with some representative results will be presented in this paper.

As an interesting historical note: some of the earliest use of the finite element method for modeling machining processes—now becoming widely used industry—was from the precision engineering community (John Strenskowski's work at NCSU in the 1970s).

# MACHINING FORCES FOR ELLIPTICAL VIBRATION-ASSISTED MACHINING[1]

**D. E. Brehl, M.A. Cerniway, T.A. Dow,and N. Negishi**
**Precision Engineering Center**
**North Carolina State University**
**Raleigh, North Carolina, USA**

## INTRODUCTION

In "elliptical vibration-assisted machining" (EVAM), a single-point diamond tool is driven in a tiny ellipse at high frequency. This tool tip motion is superimposed on the principal upfeed motion of the workpiece. An important benefit of EVAM is that machining forces are significantly reduced compared to conventional diamond machining. Most reports of EVAM tool forces are average values for an entire vibration cycle since systems typically operate at ultrasonic frequencies and sampling rates of several hundred KHz are thus required to measure force variation within an individual cycle. A reduction in average tool forces can be expected for EVAM simply because the tool separates from the workpiece for a portion of each elliptical cycle. To measure forces within a vibration cycle, Moriwaki and Shamoto [1] used a research unit that operated at 0-10 Hz. This system was run without lubricant inside the vacuum chamber of a scanning electron microscope (SEM), so that secondary causes of tool force reduction—such as improved lubricant penetration to the rake face—were eliminated. As illustrated in Figure 1, the instantaneous as well as the average cutting (principal) and thrust forces in EVAM were shown to be smaller than the conventional machining forces.

Observing that the thrust force in Figure 1 is negative during part of each cutting cycle, Moriwaki and Shamoto argued that in EVAM the upward motion of the tool helps to pull the chip out of the workpiece. Thrust force reversal acts to change the effective shear angle for chip formation, leading to reduced cutting force.

The authors contend that tool force reduction in EVAM derives from the geometry of overlapping successive elliptical toolpaths. In EVAM the chip thickness is established by the overlap between tool passes, and the maximum chip thickness is less than or equal to the depth of

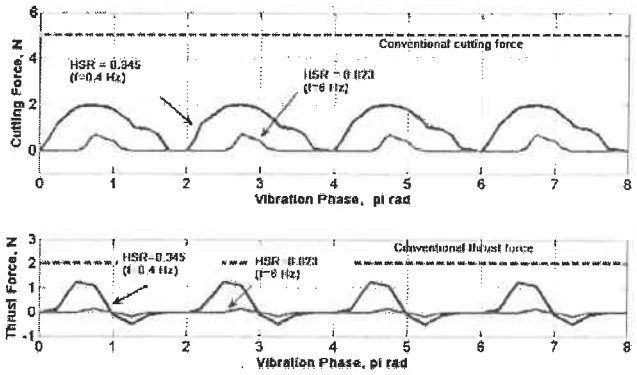


*FIGURE 1. Comparison between cutting (top) and thrust forces (bottom) for EVAM and conventional precision machining. Note force reduction grows more marked with increasing horizontal speed ration HSR. Redrawn from [1].*

cut, which determines the uncut chip thickness for conventional machining. In EVAM the tool makes many small chips, and executes many passes at lower tool force in a specified time interval. In conventional machining the tool travels a much shorter distance with higher force. For the same volumetric material removal, the work performed by EVAM is therefore consistent with that of conventional machining.

In the current research, a tool force model originally developed for steady-state conventional diamond machining is modified to consider the transient in EVAM. Included are the effect of varying chip thickness, variation in tool contact surface area and of progressively increasing negative rake angle during the machining cycle. Theoretical tool force predictions are verified against experimental data obtained using the Ultramill, an EVAM tool developed by at North Carolina State University. Figure 2 shows the Ultramill concept. Sinuosidal voltage signals, with a phase difference between them, are applied to parallel piezoelectric actuator stacks. A toolholder is driven by the

[1] This paper was written as part of work supported by NSF grant DMI-0423315, monitored by G. Hazelrigg.

stacks, acting a linkage to convert their reciprocating motion into elliptical tool tip motion.

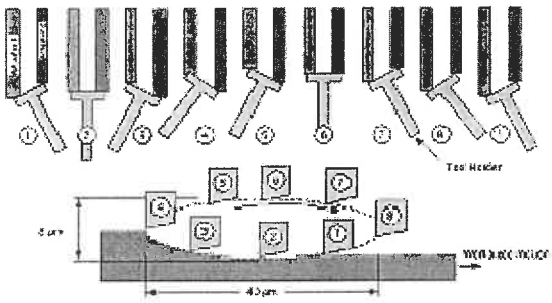

*FIGURE 2. Ultramill EVAM concept*

## EVAM DESCRIPTION

In EVAM the position at time *t* of the tool tip can be described by

$$X(t) = A * \cos(2\pi * f * t) + V * t \quad (1)$$

$$Z(t) = B * \sin(2\pi * f * t) \quad (2)$$

where *X(t)* and *Z(t)* are the instantaneous tool tip positions in the upfeed and depth of cut directions, *V* is the upfeed velocity of the work material, *f* is the tool vibration frequency, and *A* and *B* are respectively the semi-major axis (X-direction amplitude) and semi-minor axis (Z-direction amplitude) for the machining ellipse.

An EVAM cycle can be characterized by three parameters. The "upfeed index" $F_{UP}$ (Eq. 3) is the distance traveled by the tool relative to the work in one cycle. The "horizontal speed ratio" *HSR* (Eq. 4) relates the peak cutting speed of the tool to the upfeed velocity.

$$F_{UP} = \frac{V}{f} \quad (3) \qquad HSR = \frac{V}{2\pi f * A} \quad (4)$$

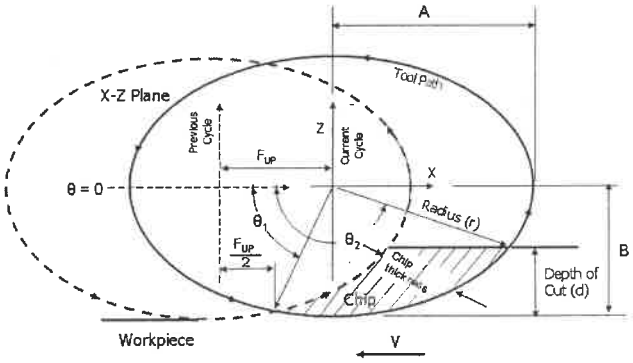


*FIGURE 3. EVAM cycle. Two successive cutting passes are approximated by overlapping ellipses. Maximum chip thickness is less than or equal to depth of cut, contributing to reduced tool forces (Z-axis scale is exaggerated compared to X).*

Small values of $F_{UP}$ and *HSR* lead to low theoretical surface roughness. The third characterizing parameter, "duty cycle", is the fraction of each cycle the tool is cutting. Duty cycle becomes larger with increasing *HSR* and also with increasing ratio of depth of cut, *d*, to the ellipse vertical amplitude *B*.

The workpiece upfeed motion means that relative to the workpiece, the toolpath is distorted from a true elliptical shape. When the horizontal speed ratio is small (*HSR* < 0.1), the toolpath can be accurately approximated by overlapping ellipses spaced at intervals of $F_{UP}$ as shown in Figure 3

Chip geometry is affected by the ratio of depth of cut, *d*, to the ellipse vertical amplitude *B*. When $d/B \leq 1$, the tool exits the workpiece before completing its elliptical pass and small discontinuous chips are produced. Figure 4a. When $d/B > 1$ the chip remains attached to the workpiece and a long discontinuous chip is produced with small attached segments regularly spaced at intervals of $F_{UP}$.

## TOOL FORCE MODEL

For small crossfeed rates, operations such as turning, facing and raster machining approximate orthogonal cutting. In this situation there are two tool forces, the cutting (or principal) force and the thrust force. These tool forces each can be considered as having two components. The first consists of the forces associated with plastic deformation required to form the chip. The second component consists of friction forces between the tool and workpiece. In both traditional and precision diamond machining, friction arising from contact between the chip and engaged portion of the tool rake face is a major portion of the thrust force. In precision diamond machining, the depth of cut is small relative to the dimensions of tool features such as the cutting edge radius and flank wear land, so that the friction forces associated with these features are significant additions to the thrust and cutting forces

Arcona [4] developed a model for single-point diamond turning which gives machining forces in terms of material properties, chip geometry, tool contact area, and material shear angle:

$$F_C(t) = \frac{H * a_C(t)}{3} * \left[\frac{\cot(\varphi(t))}{\sqrt{3}} + 1\right] + \mu_F * \sigma_F * a_F(t) \quad (5)$$

$$F_T(t) = \mu * \left[\frac{H * a_C(t)}{3} * \left(\frac{\cot(\varphi(t))}{\sqrt{3}} + 1\right)\right] + \sigma_F * a_F(t) \quad (6)$$

$$\sigma_F = 0.62\,H * \sqrt{\frac{0.43\,H}{E}} \quad (7)$$

where $F_C(t)$ and $F_T(t)$ are respectively the instantaneous cutting and thrust forces, $a_C(t)$ is the instantaneous cross-section area of the uncut chip, $H$ is the material surface hardness, $E$ is the material elastic modulus, $\mu$ is the friction coefficient between the tool rake face and chip, and $\varphi(t)$ the instantaneous shear angle of the chip. The "friction area" between the tool and the work, $a_F(t)$, consists of the contact area of the cutting edge radius between the rake face and flank face, the area of the wear land behind the edge radius, and the region where elastic springback causes material to contact the flank face after being passed over by the tool. These regions are shown in Figure 4. It is readily seen that for a worn tool the friction area $a_F(t)$ will be larger than for a sharp tool, since cutting edge radius and/or the flank wear land length will be greater. The variables $\mu_F$ and $\sigma_F$ are, respectively, the coefficient of friction for the friction area and the average normal stress in the material arising from elastic behavior.

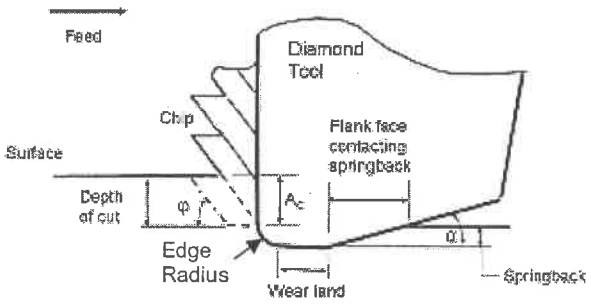


*FIGURE 4. Friction contact regions of diamond tool used in tool force model, including components of* $a_F(t)$*: edge radius, wear land, and springback contact area.*

For conventional diamond turning, the machining forces $F_C(t)$ and $F_T(t)$, the shear angle $\varphi(t)$, the uncut chip cross-section $a(t)$, and the friction area $a(t)$ are all constant. In the EVAM force model, these variables become functions of the tool position on the elliptical machining path, which in turn can be derived from the time-based kinematic functions (Equations 1,2).

Figure 5 shows conceptually the determination of the instantaneous uncut chip area $a_C(t)$ for the situation when $d/B < 1$ with discontinuous chips being produced. A round-nosed tool cutting a single groove is considered, but the method can be extended to other tool cross sections and to overlapping successive tool passes in the crossfeed direction. The sectional view in Figure 5 shows two consecutive tool passes and the change in the chip thickness along the centerline of the groove. On the preceding pass, a transient surface is created. The current pass makes a chip by cutting into the transient surface. The instantaneous chip thickness is the vertical separation between the two toolpaths at the same upfeed (horizontal) position for the region where the consecutive toolpaths overlap (Position 1). Otherwise the instantaneous chip thickness is the vertical distance between the workpiece surface and the toolpath (Positions 2, 3). In conventional machining the chip thickness is equal to the depth of cut, but it in EVAM the maximum chip thickness is less than or equal to the depth of cut. The oblique pictures of the tool rake face in Figure 5 show the instantaneous chip cross section area $a_C(t)$ for a round nosed tool at Positions 1, 2, and 3 indicated on the sectional side view.

Figure 6 shows a side view of the tool at the three positions on the toolpath from Figure 5. At Position 1 the tool is at the bottom of the elliptical tool path and frictional contact area $a_F(t)$ is at a maximum. It consists of the contact area associated with the cutting edge radius, the flank wear land behind the cutting edge, and the portion of the flank that contacts the just-cut work surface due to elastic springback. At Position 2 the tool is part way through the cutting pass, and $a_F(t)$ consists of the cutting edge radius and the flank wear land. At Position 3 the tool is about to exit the work material and $a_F(t)$ is only due to the edge radius.

Cerniway [2] provides mathematical details for calculating $a_C(t)$ and $a_F(t)$.

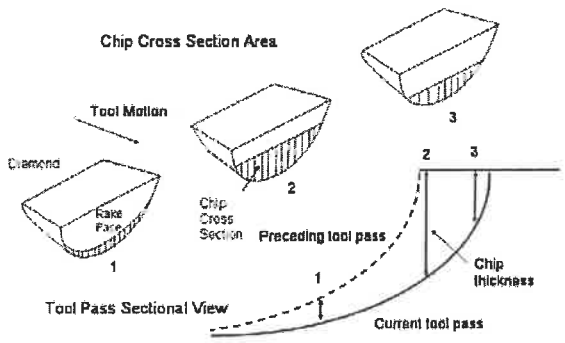


*FIGURE 5. Chip formation at 3 points of tool pass. Chip thickness is established by the overlap between two successive elliptical tool passes.*

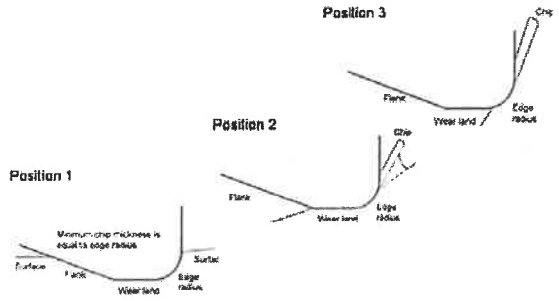


*FIGURE 6. Reduction in friction contact area* $a_F(t)$ *as tool progresses through 3 different positions in elliptical ycle as shown in Figure 5.*

It is apparent from Figure 6 that the instantaneous tool rake angle becomes increasingly negative as the tool proceeds along the elliptical path. Nakayama [5] and Dautzenburg [6] investigated shear angle formation due to rake angle geometry and material hardness. They determined that shear angle decreased with increasing negative rake angle, although comprehensive predictive models were not obtained. For EVAM force prediction, the instantaneous shear angle $\varphi(t)$ is assumed to be the bisector of the angle formed between the instantaneous rake angle, $\gamma(t)$ and the tool rake face. For a tool of zero nominal rake, this leads to $\varphi(t)$ = 45 degrees when the direction of machining is horizontal, which is consistent with the shear angle for copper and aluminum under these conditions.

Work hardening of the material will take place when the depth of cut (or chip thickness in EVAM) is of the same order of magnitude as the tool edge radius [7]. If the instantaneous chip thickness falls within this work-hardened region the hardness $H$ used in Equations 5-7 must be adjusted. The EVAM tool force model used correction curves developed by Evans that varied the hardness according to the depth of cut and tool edge radius.

To estimate EVAM tool forces using the model, the basic procedure is: for time $t$, find the tool positions for the current and preceding passes. From this uncut chip thickness and cross section area $a_C(t)$, and the friction contact area $a_F(t)$ can be determined. Next the instantaneous tool rake angle is found, and from it the shear angle $\varphi(t)$. Finally the instantaneous material hardness H is found. These instantaneous values are inserted into Equations 5, 6, and 7 to estimate the cutting force and thrust forces at time $t$. The machining forces can be calculated at multiple points to construct curves showing the variation throughout an elliptical vibration cycle. The average forces can be estimated by numerically integrating forces throughout a complete cycle and dividing by the cycle period.

## PREDICTED AND MEASURED EVAM TOOL FORCES

Cerniway [2] and Negishi [3] investigated EVAM tool forces for a range materials, vibration frequencies, tool conditions, and depths of cut. The EVAM model described in the preceding section was used to predict thrust and cutting forces. Cerniway used a prototype low-frequency version of the Ultramill ($f$ < 400 Hz), while Negishi used a next-generation model at frequencies of 1 to 4 KHz. In both cases machining forces were measured by a 3-axis load cell installed between the vacuum chuck of the diamond turning machine and the workpiece. This sensor location gave a natural frequency for the measurement loop of 12.5 KHz, considerably greater than if the load cell were installed between the Ultramill and the tool post. If the EVAM frequency is near the measurement loop's natural frequency then the force values will be distorted by resonance effects, while if it is significantly larger than the measurement loop natural frequency the force measurement will be attenuated and artificially low values obtained. Negishi found that when machining with a frequency of 4 KHz there was significant distortion in the force signal from the measurement loop vibrations being unable to die out between EVAM cycles, but at 1 KHz distortion was minimal.

Cerniway conducted groove-cutting experiments at 10 Hz in C1100 copper to compare measured and predicted EVAM machining forces. The

vibration ellipse amplitudes were 47.5 µm x 7.3 µm ($A$ x $B$) and the depth of cut was 6 µm ($d/B$ = 0.82). The tool had zero rake and a nose radius of 3 mm. Representative results are shown in Figures 7, 8, and 9. These figures plot the predicted and measured EVAM machining forces for the portion of the cycle during which the tool is cutting. Figure 7 and 8 show the effect of changing duty cycle. In these plots the tool is considered to be "worn" with an estimated edge radius of 300 nm. In Figure 7 the duty cycle is 25%, which gives a maximum chip thickness equal to the depth of cut. In this case peak EVAM cutting force is 46% of the predicted conventional cutting force, while peak EVAM thrust force is 73% of the predicted conventional thrust force. In Figure 8, the duty cycle is 23%. The peak EVAM cutting force is only 30% of the the conventional cutting force, and the peak EVAM thrust force is 64% of the conventional thrust force. This reduction in peak EVAM force as duty cycle grows smaller is mainly due to the reduction in maximum chip thickness and chip cross section $a_C(t)$ caused by the closer spacing of overlapping elliptical tools passes at the smaller duty cycle. Since the tool is worn, the friction contact area $a_F(t)$ is large relative to $a_C(t)$, and is the reason why the EVAM thrust force decreases less rapidly than the EVAM cutting force.

Figures 8 and 9 show the effect of tool wear condition, for the same machining parameters and a 23% duty cycle. In Figure 9 the tool is "sharp" with an estimated edge radius of 40 nm, while the tool in Figure 8 is "worn" (300 nm edge radius). The peak EVAM cutting force for the sharp tool is 33% of the peak worn tool EVAM cutting force (and 21% of the predicted conventional sharp tool cutting force). The peak EVAM sharp tool thrust force is 21% of the peak EVAM thrust force with a worn tool (37% of the conventional sharp tool thrust force). With the sharp tool the friction contact area $a_F(t)$ in Equations 5 and 6 becomes very small, and tool forces are essentially established by the chip thickness and cross section area $a_C(t)$.

In Figures 7 thru 9 the measured EVAM machining forces are seen to be in good agreement with forces predicted by the model. Cerniway also conducted EVAM groove cutting tests in 6061-T6 aluminum and 1018 steel. Frequency, machining ellipse, and depth of cut were the same as for the copper tests described above. A "worn" tool was used in these tests.

Table 1 shows peak measured EVAM tool forces when machining these materials, along with associated C1100 copper results. For all

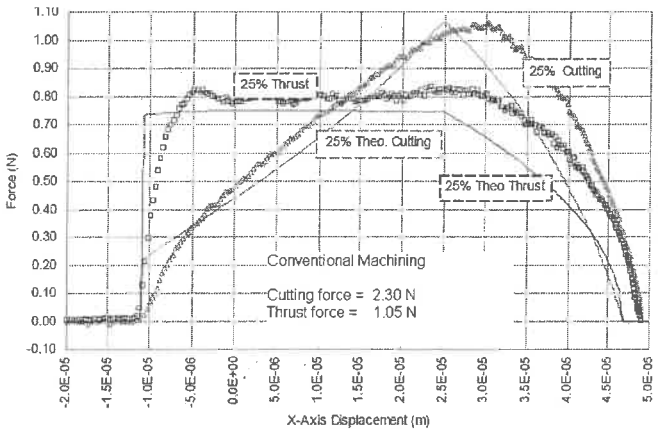


*FIGURE 7. Predicted and measured EVAM tool forces at 25% duty cycle. C1100 copper, f = 10 Hz, depth of cut = 6 µm. Worn tool.*

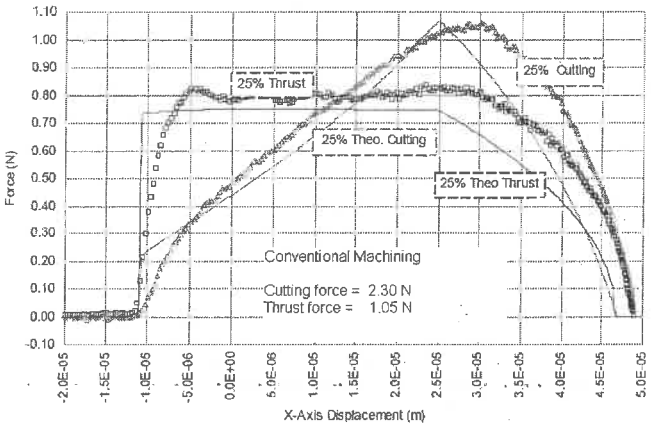


*FIGURE 8. Predicted and measured EVAM tool forces at 23% duty cycle. C1100 copper,. f = 10 Hz, depth of cut = 6 µm. Worn tool.*

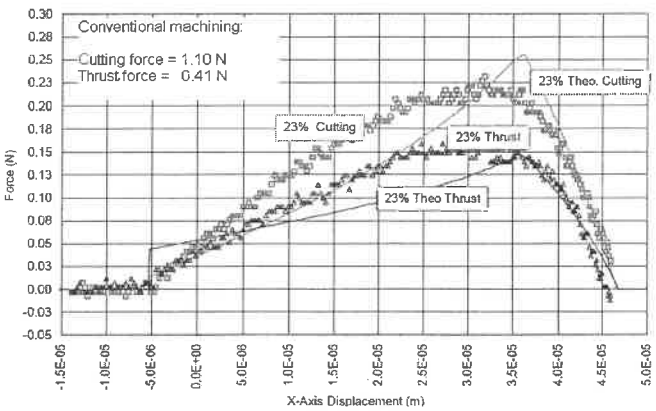


*FIGURE 9. Predicted and measured EVAM tool forces at 23% duty cycle. C1100 copper,. f = 10 Hz, depth of cut = 6 µm. Sharp tool.*

*TABLE 1: Measured EVAM Machining Forces*

| Duty Cycle | C1100 Copper<br>*E* 123 GPa<br>*H* 0.84 GPa | | 6061-T6 Aluminum<br>*E* 69 GPa<br>*H* 0.88 Gpa | | 1018 Steel<br>*E* 205 GPa<br>*H* 1.57 GPa | |
|---|---|---|---|---|---|---|
| | C [N] | T [N] | C [N] | T [N] | C [N] | T [N] |
| | | | | | | |
| 22 % | 0.40 | 0.67 | 0.48 | 0.88 | 0.70 | 1.21 |
| 23 % | 0.70 | 0.71 | 0.83 | 0.93 | 1.23 | 1.28 |
| 25 % | 1.05 | 0.83 | 1.26 | 1.09 | 1.85 | 1.49 |
| Conv cutting | 2.44 | 1.29 | 2.51 | 1.52 | 3.82 | 2.00 |
| Machining conditions: *f* = 10 Hz<br>Ellipse = 47.5 µm x 7.3 µm (*A x B*)<br>Depth of Cut, *d* = 6 µm *d/B* = 0.82 | | | | | | |
| Tool: Nose radius = 3mm<br>Edge radius ~ 300 nm (worn) | | | | | | |

Notes: "C" = cutting force "T" = thrust force
*H* is Vickers hardness

materials EVAM cutting forces are reduced to 20-50% of the conventional cutting force, and EVAM thrust forces to 60-75% of the conventional thrust force, depending on the duty cycle.

Negishi performed single-groove cutting experiments in 6061 aluminum at 1 KHz. The vibration ellipse amplitudes were 20 µm x 4 µm (*A x B*). The tool had zero rake angle and a nose radius of 500 µm. Predicted and measured EVAM machining forces were compared for 4 different depths of cut and were within 5%. Figure 10 shows tool forces in the cutting portion of the machining cycle for when depth of cut was 8.9 µm (*d/B* = 2.2). In this case a continuous chip was produced due to the depth of cut being greater than the ellipse vertical amplitude.

These results do not show the thrust force reversal reported by Moriwaki and Shamoto (see Figure 1). Cerniway attributed this to their machining at *d/B* ≈ 3, creating a continuous chip that remains attached to the workpiece. The thrust reversal is explained as being caused by the tool interacting with the overhanging chip during the portion of the cycle that the rake is out of contact with the uncut material. This argmument appears to be invalidated by Negishi's result for a similar value of *d/B* (Figure 10). One difference between the processes is that the Moriwaki-Shamoto tool vibrates in a nearly-circular path while the Ultramill uses a highly-eccentric ellipse with the face

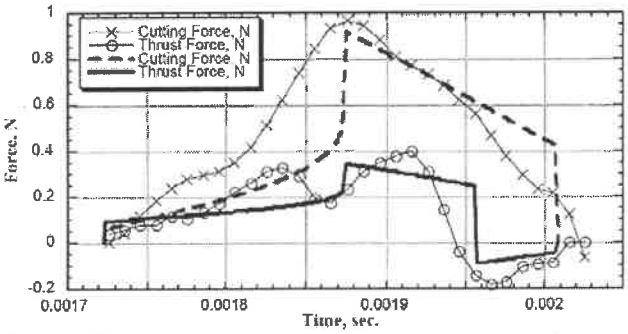


*FIGURE 10. Predicted and measured EVAM tool forces at 1000 Hz when cutting 6061 aluminum. Depth of cut = 8.9 µm, (d/B=2.2), 25% duty cycle.*

parallel to the upfeed direction. The conflict remains unresolved.

## CONCLUSIONS

1. A tool force model was developed for EVAM, derived from an existing model for conventional diamond turning. Instantaneous chip cross-section, and contact area behind the rake face are determined as a function of the tool position in the elliptical machining path. Material shear angle is varied to reflect the changing tool rake angle. Work hardening effects are included.

2. Machining tests were conducted in copper, aluminum, and steel. Depending on machining conditions, peak EVAM cutting forces were 20-50%, and peak EVAM thrust forces were 60-75% of the values for conventional machining. Good agreement was obtained between experimental results and predictions by the force model.

## REFERENCES

1] Shamoto, E., Moriwaki, T., "Study on Elliptical Vibration Cutting", 1994, *CIRP Annals* , v43:1

[2] Cerniway, M., "Elliptical Diamond Milling: Kinematics, Force, and Tool Wear", MS thesis, NCSU, 2001

[3] Negishi, N., "Elliptical Vibration-Assisted Machining with Single Crystal Diamond Tools", MS thesis, NCSU, 2003

[4] Arcona, C., "Tool Force, Chip Formation and Surface Finish in Diamond Turning", PhD dissertation , NCSU, 1996

[5] Dautzenberg, J., Hijink, J., Van der Wolf, A., "The Minimum Energy Principal Applied to the Cutting Process of Various Workpiece Materials and Tool Rake Angles", *CIRP Annals*, v31:1m 1982

[6] Nakayam, K., Minoru, A., Torahiko, K., "Machining Characteristics of Hard Materials", *CIRP Annals*, v37:1, 1988

[7] Dresher, J., "Tool Force, Tool Edge, and Surface Finish Relationships in Diamond Turning", PhD dissertation, NCSU, 1991

# Wheel Loading Reduction with Vibration Assisted Grinding

**Ping Zhang and Michele H. Miller**
**Department of Mechanical Engineering-Engineering Mechanics**
**Michigan Technological University**
**Houghton, Michigan**

## ABSTRACT

Chip accumulation (loading) on a grinding wheel causes a number of deleterious effects, particularly when grinding with fine grain wheels. Methods for reducing wheel loading include frequent dressing, in-process dressing, self-dressing, application of cryo-cooling, and optimum position of coolant. As an alternative to these techniques, we present vibration assisted grinding. Experiments show that wheel loading decreases with increased vibration frequency and amplitude. Under some circumstances, loading reduces almost 80%. In examining the underlying mechanisms of this loading reduction we focus on the role of grinding temperature and chip geometry. With artificial heating, wheel loading could be made to increase almost 200%. The temperature reduction observed in vibration assisted grinding is, therefore, considered the primary reason for loading reduction in this process. The role of chip size was also investigated through experimentation. Vibration assistance produces a higher percentage of small chips. The change in chip size distribution in vibration assisted grinding is postulated as a secondary reason for loading reduction.

## INTRODUCTION

Grinding is an effective machining process in the manufacture of hard materials due to its multiple abrasive cutting particles. While a single point may dull and require re-sharpening, a grinding wheel distributes wear over many cutters and is capable of replenishing itself. However, the condition of the grinding wheel constantly changes as grits wear and chips accumulate in the spaces between grits. Chip accumulation (or loading) is particularly problematic with fine grit wheels. It occurs when workpiece chips either adhere to the grits or embed in the spaces between them. Wheel loading can result in deterioration in the surface finish, as well as an increase in grinding forces and temperature. As a consequence of higher temperature, the rate of abrasive wear increases. Thus the overall performance of the grinding operation is directly affected by the amount of wheel loading.

Wheel loading occurs when chips adhere to active wheel grains. Mechanical interlocking of chips with the surface asperities of the grinding wheel is a common mechanism for wheel loading, and is influenced by the space between grains and chip size [1]. Chemical affinity and diffusion affect adhesion between wheel and workpiece [2]. In addition, temperature is a possible major contributor in adhesion [3].

Methods for reducing wheel loading include frequent dressing, in-process dressing, more aggressive grinding conditions and self-dressing, application of cryo-cooling, and optimum position of coolant [4-8]. Our research investigates vibration assisted grinding as a way of reducing wheel loading. In early studies of the vibration assisted grinding process, differences in the extent of wheel loading were observed but not quantified [9]. This paper looks more closely at the effects of vibration parameters on loading as well as the role of chip size/shape and temperature in the loading process.

## MEASUREMENT OF WHEEL LOADING

Methods for measuring wheel loading include chemical detection, calorimetry, spectroscopy, eddy current sensing, magnetization, radio-tracing, and x-ray fluorescence [10-14]. We adopted a simple approach employing microscope images and image analysis software. A portable, long-range microscope (Scionscope) and camera would capture images of the full width of the wheel surface. Then image analysis software would determine the percentage of chip loading. Figure 1 shows a typical image first as acquired and then after conversion to black-and-white. The black area represents the chip area, and the software can calculate its percentage. In our testing, we took seven images around the wheel, analyzed each image, and recorded the average percentage value as the chip loading condition for each situation.

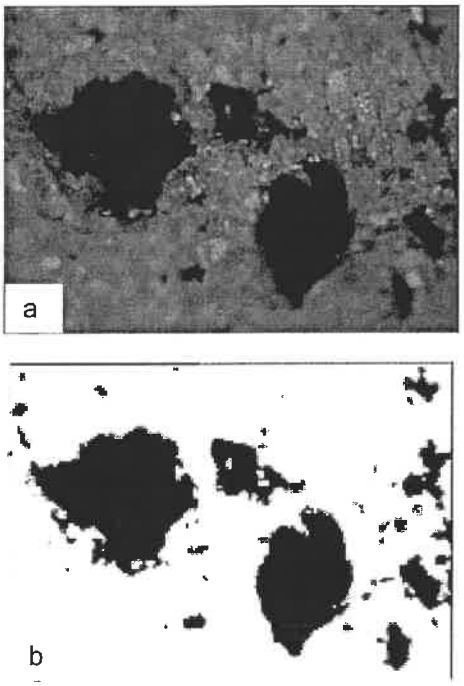


*FIGURE 1. (a) Raw image of wheel surface; (b) black and white image*

**EXPERIMENTAL PROCEDURE**

The effects of vibration assistance on loading were measured in a series of experiments. Amplitude and frequency of vibration were varied, and loading of the grinding wheels was measured. Figure 2 shows the experimental setup. A magnetostrictive actuator vibrates the workpiece. The vibration amplitude is measured using a capacitance gauge connected to a digital oscilloscope. A signal generator modulates the actuator and the workpiece in the radial direction with respect to the wheel.

Before each grinding test the wheel is trued with a diamond nib for five passes with a depth of cut of 10 μm. (In one truing pass, the diamond nib moves back and forth one time across the width of the wheel surface). Next, the workpiece is ground flat. Again, the wheel is trued. The actuator then begins modulating the workpiece, and vibration parameters are set with the signal generator. The workpiece feeds past the rotating grinding wheel with a desired depth of cut. After each back and forth grinding pass the depth of cut is indexed. At regular intervals, the grinding process is stopped, and images of the wheel are collected.

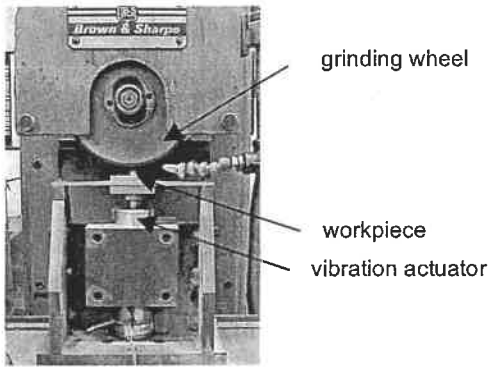


*FIGURE 2. Experimental setup for wheel loading tests*

**FREQUENCY AND AMPLITUDE EFFECT**

To determine the effects of vibration frequency and amplitude on loading, tests were conducted with aluminum oxide wheels grinding 1018 steel workpieces. Table 1 describes the conditions common to all the tests. Starting with freshly trued wheels, loading was measured at regular time intervals. Figure 3 shows a representative result for the effect of frequency on the evolution of loading whereby the rate of wheel loading tends to decrease with increased vibration frequency.

*TABLE 1. Conditions for wheel loading tests*

| | |
|---|---|
| Workpiece | 12.7x12.7x50.8 mm 1018 steel |
| Wheel | 38A80-IVBE |
| Wheel rpm | 2900 rpm |
| Depth of cut | 0.020 mm |
| Coolant | None |

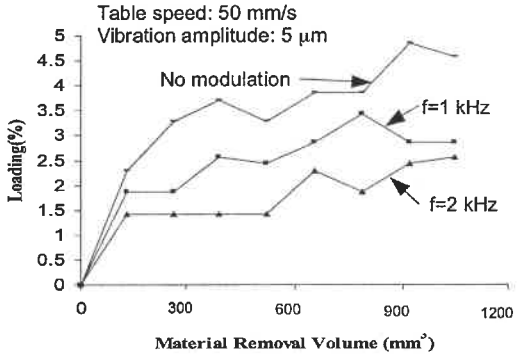


*FIGURE 3. Effect of vibration frequency on loading*

To investigate the effect of amplitude, four tests were performed at three different amplitude conditions, with the loading percentage measured only at the end of each test (after 100

grinding passes). Figure 4 shows the results for amplitudes of 1.25, 2.5, and 5 μm. The middle point of each bar is the average loading value; the upper and lower points are the average ± one standard deviation. Wheel loading clearly decreases with increased vibration amplitude.

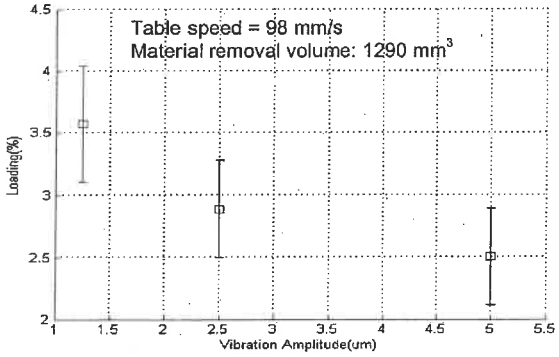


*FIGURE 4. Effect of vibration amplitude on loading*

## GRINDING TEMPERATURE

In an attempt to explain the reduced loading with modulation, two factors–temperature and chip dimensions–were investigated further. A primary advantage of vibration assisted machining processes is reduced machining temperature (and thus tool wear). In surface grinding experiments workpiece temperatures were measured approximately 1 mm below the surface [17]. Surface temperatures were then estimated using a band moving heat source model [18]. Figure 5 plots surface temperature as a function of vibration frequency and amplitude. Higher frequencies and amplitudes correspond with lower temperatures.

The relationship between temperature and loading was subsequently explored in a set of grinding tests in which the workpiece was artificially heated. A disk shaped heater (10 mm OD with a 2 mm ID center hole) was placed under the workpiece. The workpiece was heated to four different initial temperature, and 50 passes of grinding were done. The temperatures immediately before and after grinding were recorded. Experiments at each condition were conducted four times. Figure 6 shows the average loading percentage at each condition (identified by its final temperature). The error bars indicate ± 3 standard deviations. The figure shows that wheel loading increases substantially with increased external heat.

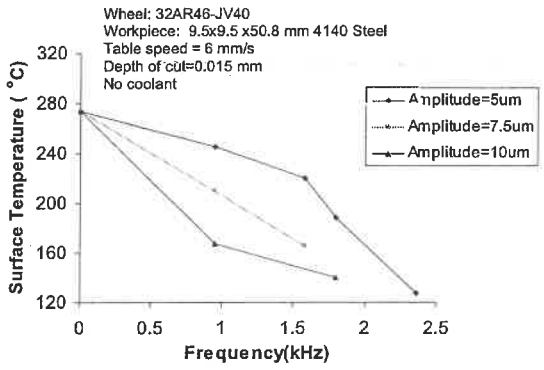


*FIGURE 5. Effect of vibration assistance on workpiece surface temperature*

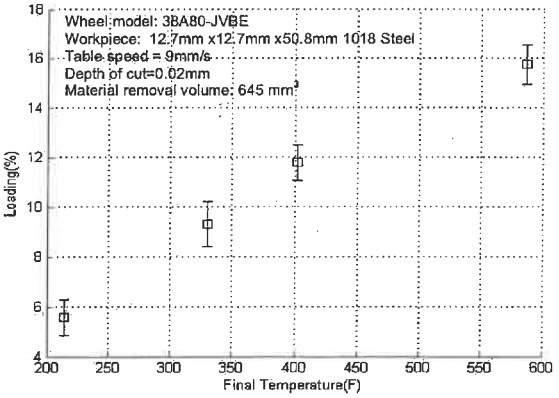


*FIGURE 6. Effect of workpiece temperature on loading*

One reason for the strong temperature effect may be that, at elevated temperatures, chips are more inclined to deform to the shape of the grinding wheel and to embed in the space between grits. Also, high temperature allows more diffusion between wheel material and workpiece material, thus promoting adhesion. Because temperature is a very important factor affecting wheel loading, it needs to be considered when searching for ways to reduce loading. Vibration assistance offers a means for reducing temperature and, consequently, loading.

## CHIP SIZE AND SHAPE

We postulated that a second cause for reduced loading in vibration assisted grinding is modification of chip size and shape. To test this hypothesis we collected and analyzed approximately 500 hundred chips. Figures 7 and

8 are typical SEM images of 1018 steel chips from both conventional and vibration assisted grinding processes. No obvious differences are evident; they are both long, curled and have machining marks. The analysis was made quantitative by using SEM images and image analysis software to calculate aspect ratios and areas of chips. The aspect ratio is defined as the ratio of the major to minor axis a/b of the best fitting ellipse (see Figure 9).

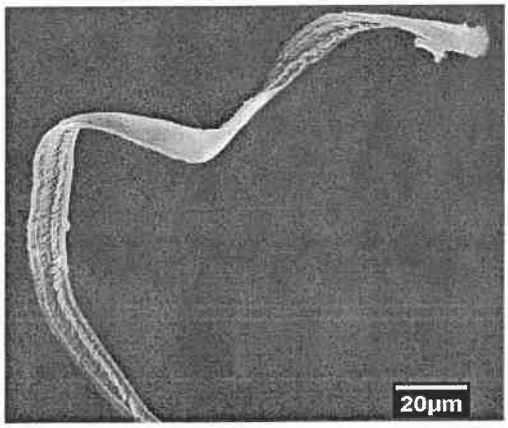


*FIGURE 7. Chip from conventional grinding*

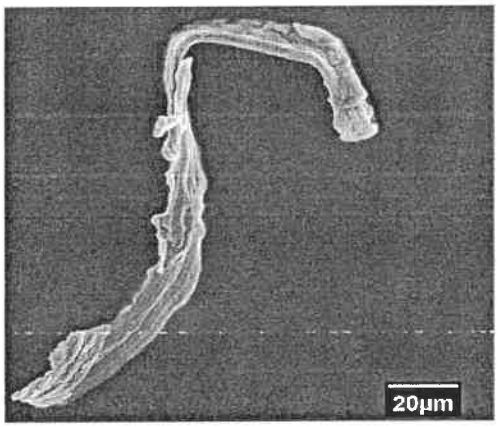


*FIGURE 8. Chip from vibration assisted grinding (f=2 kHz, A=5 μm)*

Figure 10 compares the distribution of aspect ratios. It shows little difference between conventional and vibration assisted grinding.

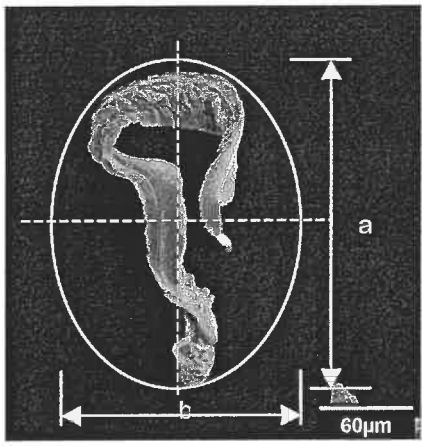


*FIGURE 9. Calculation of chip aspect ratio*

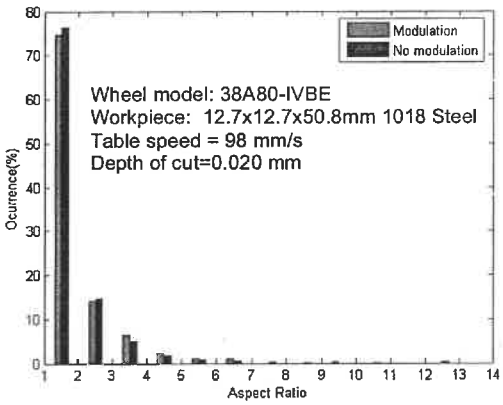


*FIGURE 10. Comparison of chip aspect ratios*

Figure 11 compares chip size distributions. Chip sizes range from 50 $\mu m^2$ to 10,000 $\mu m^2$, but most are less than 2,000 $\mu m^2$. The vibration assisted grinding process produces more small chips than the conventional grinding process. The correlation between smaller chips and reduced loading rates allows for the possibility that smaller chips is the reason for reduced loading in vibration assisted grinding. Perhaps smaller chips get cleared out of the contact zone more easily and are less likely to become lodged between grits by mechanical interlocking.

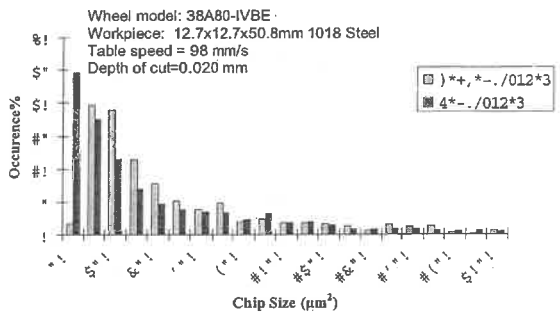


*FIGURE 11. Comparison of chip sizes*

## CONCLUSIONS

By introducing high frequency vibratory motion to the workpiece, a reduction in grinding wheel loading was realized. Wheel loading decreases with increased vibration frequency and amplitude. Under some circumstances, loading reduces almost 80% in our testing. Temperature is identified as a primary reason for loading reduction in the vibration assisted grinding process. In our testing, wheel loading was made to nearly triple with an artificial increase in temperature. By analyzing chip shape and size, a correlation between chip size and wheel loading was found. Smaller chip sizes in vibration assisted grinding may be another cause of reduction in wheel loading.

## REFERENCES


[1] A. P. Nagaraj, A. K. Chattopadhyay, On some aspects of wheel loading, Wear 135 (1998) 41-52.

[2] T. A. Konig, D. H. Lauer Schmaltz, Loading of the grinding wheel phenomenon and measurement, Annals of CIRP 27 (1978) 217-220.

[3] S. Yossifon, C. Rubenstein, The grinding of workpieces exhibiting high adhesion, Transactions of the ASME 103 (1981) 144-155

[4] L. Pilbin, Truing and dressing devices for precision grinding, Society of Manufacturing Engineers - Technical Paper MR88-625 (1988) 1-18.

[5] T.M.A. Maksoud, L.M.J. Wong, In-process automatic dressing system for grinding wheels, Proc Instn Mech Engrs 214 (Part B) (2000) 799-803.

[6] H. K. Tonshoff, T. Friemuth, In-process dressing of fine diamond wheels for tool grinding, Precision Engineering 24 (2000) 58-61.

[7] M. Hirao, T. Yasui, Waterjet in-process dressing, Proceeding of 1999 ASPE Annual Meeting (1999) 95-98.

[8] S. Paul, P. P. Bandyopadhyay, A. B. Chattopadhyay, Effects of cryo-cooling in grinding steels, Journal of Materials Processing Technology 37 (1993) 791-800.

[9] W. Qu, The effects of high frequency vibration on the grinding process, Michigan Technological University PhD Dissertations (1999).

[10] A. K. Srivastava, K. Sriram, G. K. Lal, A New Technique for Evaluating Wheel Loading, Int. J. Mach. Tool Des. Res. 25 (1) (1985) 33-38.

[11] D. Dornfeld, H. Cai, An investigation of grinding and wheel loading using acoustic emission, Transactions of the ASME 106 (1984) 28-33.

[12] T. Suto, H. Inoue, Loading on wheel surface in precision traverse grinding-study on high precision traverse grinding (2nd report), Kikai Gijutsu Kenkyusho Shoho/Journal of Mechanical Engineering Laboratory 37 (6) (1983) 250-261.

[13] J. Williams, H. Yazdzik, In-process dressing characteristics of vitrified bonded CBN grinding wheels, American Society of Mechanical Engineers, International Gas Turbine Institute (Publication) IGTI 6 (1991) 243-250.

[14] W. Koenig, H. Lauer-Schmaltz, Loading of the grinding wheel phenomenon and measurement, Gen Assem of CIRP 28th, Manuf Technol (1978) 217-220.

[15] W. Qu, K. Wang, M.H. Miller, Y. Huang, A. Chandra, Using vibration-assisted grinding to reduce subsurface damage, Precision Engineering 24 (4) (2000) 329-337.

[16] J. Yang, L. Hao, Ultrasonic vibration grinding - a new approach in the precision processing of deep holes in ceramics, Binggong Xuebao/Acta Armamentarii 19 (3) (1998) 287-288.

[17] P.M. Mahaddalkar, Force and temperature reduction in vibration assisted grinding, Michigan Technological University MS Thesis (2002).

[18] N. R. DesRuisseaux, Thermal analysis of the grinding processes, Transactions of the ASME (May, 1970) 428-434.

# 3D shape mirror surface grinding of die steel with ultrasonically oscillated electroplated diamond tools

**Keisuke Hara[1], Hiromi Isobe[2], Akira Kyusojin[3], Manabu Okada[3] and Hideo Yoshihara[4]**
**[1]Graduate School of Nagaoka University of Technology**
**Nagaoka, Niigata, Japan**
**[2]Nagano National College of Technology**
**Nagano, Japan**
**[3]Nagaoka University of Technology**
**Nagaoka, Niigata, Japan**
**[4]Niigata Industrial Creation Organization**
**Niigata, Japan**

## INTRODUCTION

This paper describes to finish 3D shape surface such as curved and inclined surfaces in plastic mold steel (NAK80) using a new mirror surface grinding technique with electroplated diamond tools oscillated by ultrasonic field.

Dies for injection molding parts such as dials of a cellular phone and etc. require a high quality surface finish in terms of both appearance and integrity. In order to finish the dies, manual polishings by a skilled worker has required after machining processes. However, manual polishing causes poor geometrical form accuracies of die and consumes several days (shown in Figure 1). So it is required to establish a machining process to finish dies without manual polishings and to improve surface roughness and form accuracy. Authors noticed ultrasonically assisted grinding is applicable to finish dies. In this study, a milling machine equipped with an ultrasonic spindle carried out grinding experiments. Electroplated diamond tool was used in the experiments. And authors obtained mirror surfaces by face grinding [1] [2]. A final object of this study is to realize mirror surface grinding for injection molding die without manual polishing. Electroplated diamond tool that has high form accuracy and low run-out is necessary for mirror surface grinding of 3D shape. To realize above demands, authors proposed tool-truing method for forming spherical shape of electroplated diamond tool. Electroplated diamond tool was trued by proposed method and used for 3D form mirror surface grinding experiments. Experiments results show that the proposed method can perform mirror surface grinding on 3D surfaces such as convex, concave and inclined. Ground surfaces have 0.2μm*Rz*. And the surfaces can reflect characters clearly. It was confirmed that mirror surfaces of die steel are obtained successfully by the proposed method.

## PRINCIPLES

Generally, diamond tools cannot cut ferrous material because of excessive wear as a result of carbon atoms diffusing into bulk and chips [3]. However, ultrasonically assisted diamond cutting can perform ferrous material cutting without severe diamond wear [4] [5]. This reason is considered that temperature of diamond keeps room temperature due to tool separate from workpiece by the periodically vibration (shown in Figure 2). As result, diffusion of carbon atoms of diamond into the bulk and the chips is prevented above phenomenon. Then diamond tool can cut ferrous material without severe wear and realize high-precision machining.

## TOOL MAKING

Electroplated diamond tool was used in the experiments. In this study, ball shape electroplated diamond tool was fabricated and the spherical shape was trued on the machine. Procedure of tool making is written as follows.

### Tool Electroplating

A scheme of electroplating bath is shown in Figure 3. An electroplating liquid was placed in an electroplating bath along with two Ni plates as anodes. The spherical shape carbide substrate (cathode) was placed in the center of an abrasive filter. The abrasive filter was then

inserted into the electroplating bath. The diamond abrasive grain size was #100/120 (the average grain diameter was 150 μm). Area of tip was electroplated onto the carbide substrates in the watt bath; the remaining areas were covered with a mask. The electroplating procedure and conditions are listed in Tables 1 and 2. Figure 4 shows electroplated tool above mentioned. The grinding particle concentration of the tool was 150 to be equivalent to commercial tools.

**Truing method**

Electroplated tools were trued before grinding, as shown in Figure 5. Trued tool was attached on a machine tool spindle and rotated. Truer wheel made of diamond was attached on a high speed spindle which fixed on the machine tool table and rotated 30,000min$^{-1}$. In addition, the machine was moved along arc shape. As a result, envelope shape of the trued tool was become spherical shape under the conditions shown in Table 3.

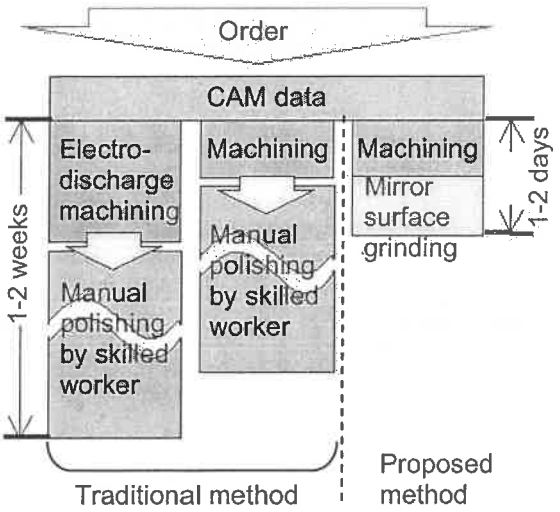


*FIGURE 1. Procedure of making injection molds*

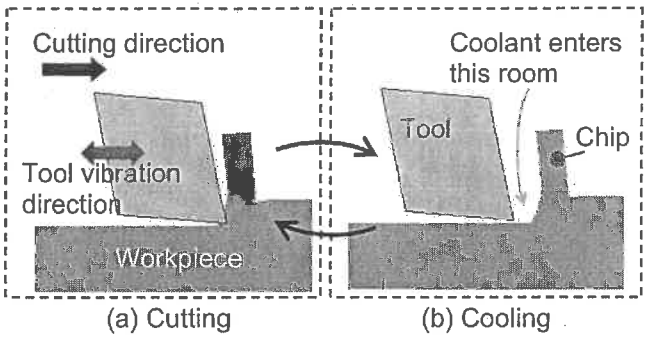


*FIGURE 2. Scheme of ultrasonically assisted cutting*

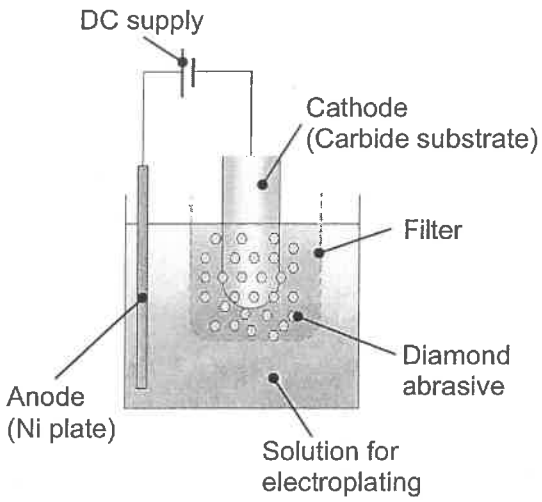


*FIGURE 3. Scheme of tool electroplating*

*TABLE 1. Electroplating procedure and conditions*

| Process | Chemical | Conditions |
|---|---|---|
| Degreasing wash | Surface acting agent solution | 318 K, 5 min |
| Electrolytic degreasing | Surface acting agent solution with sodium nitride | 318 K, 5 A/dm$^2$ 1 min |
| Etching | Solution of ammonium fluoride and hydrochloric acid | Room temp. 1 min |
| Electroplating (base) | Solution of nickel chloride | 318 K, 2 A/dm$^2$ 10 min |
| Electroplating (bonding) | Solution of nickel chloride | 318 K, 2 A/dm$^2$ 20 min |
| Electroplating (fitting) | Solution of nickel chloride | 318 K, 2 A/dm$^2$ 3 hours |

*TABLE 2. Electroplating conditions*

| | |
|---|---|
| Liquid temperature | 318 K |
| Liquid pH | 4.5 ~ 5 |
| Current density | 2 A/dm$^2$ |
| Solution | Solution of nickel chloride |
| Electroplated abrasive | TOMEI diamond #100/120 |

*FIGURE 4. Picture of ball shape electroplated diamond tool*

## GRINDING EXPERIMENT

### Experimental Setup

Figure 6 shows a schematic illustration of the ultrasonically assisted grinding system. The 3D shape grinding experiments were conducted by an NC milling machine (MAKINO V22) with an ultrasonic spindle system (Takesho. Japan). The ultrasonic spindle system was comprised of an ultrasonic spindle, a power supply and a motor speed controller, and could oscillate tools in the axial direction ultrasonically at 60kHz and rotate them up to 10,000 $min^{-1}$.

The grinding tool was the self-electroplated diamond tool described above. The tool radius was 2.7 mm and the grain size was #100/120 with an average diameter of 150 μm.

### Experimental Procedure

Mirror surface grinding experiments were conducted under four kinds of shape, shown in Figure 7, which are (a) incline surface, (b) pyramid shape, (c) convex surface and (d) concave surface. Workpiece was fixed on the machine table. First, the milling machine was used to finish rough shape with carbide ball end mill (NS Tool MSB230). Next, mirror surface was obtained with the electroplated diamond tool. During the mirror surface finishing process, the tool was oscillated in axial direction ultrasonically and rotated 6000$min^{-1}$. Tool paths were made by 2.5D CAM system (Godo, NASUKA). Grinding conditions are listed in Table 4.

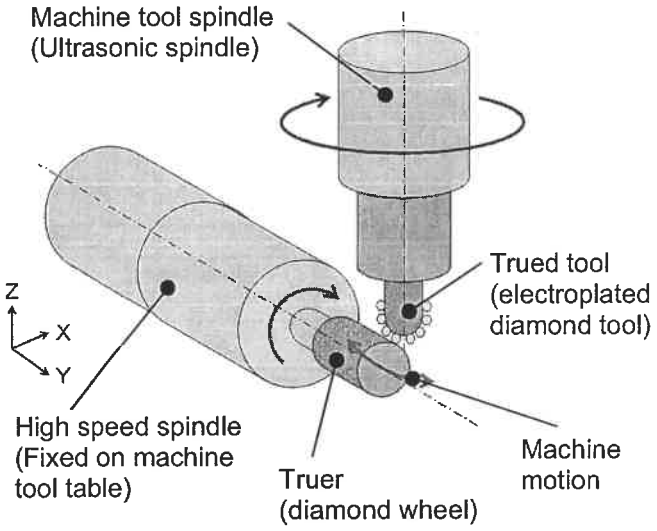


*FIGURE 5. Scheme of spherical shape truing*

*TABLE 3. Truing conditions*

| | |
|---|---|
| Truer | Electroplated diamond wheel (ϕ3.0 SD #325/400) |
| Truer speed | 30,000$min^{-1}$ (280m/min) |
| Trued tool speed | 500$min^{-1}$ |
| Feed rate | 1mm/min |
| Depth of cut | 5μm / path |
| Coolant | JIS N4-7 (oillness type) |
| Ultrasonic vibration | None |

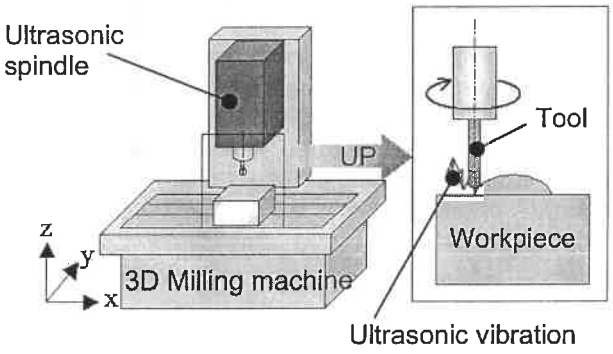


*FIGURE 6. Scheme of experimental setup and method of ultrasonically assisted grinding*

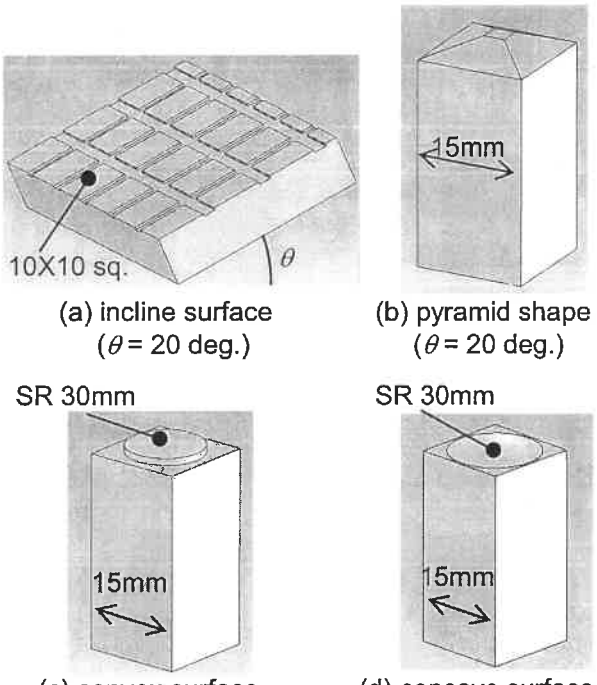


*FIGURE 7. Shapes model for mirror surface finishing experiments*

## RESULTS

Photographs of ground surface, roughness, process times are shown in Figure 8. Results show that ultrasonically assisted diamond grinding can obtain mirror surfaces. In result (a), incline surface was finished roughness 0.34μm*Rz* and surface can reflect background characters clearly. It took about 60 minutes to finish the 100mm$^2$ incline surface. Surface profile of inclined surface and microphotograph were shown in Figure 9. It was seemed that profile had some unevenness these make worse roughness. And wavelength of surface profile was observed which measured pitch was 200μm. The pitch was not equal to sweep length per tool rotation, so reason of generating unevenness was not proved yet. In result (b), pyramid surface was finished that can reflect background characters. It took about 120 minutes to finish the pyramid shape. Result (c) shows a finished convex surface, which was seemed a mirror surface. Surface profile of convex surface is shown in Figure 10, local roughness of the surface outside was 0.35μm*Rz* that observed from the profile (b). In result (d), concave surface was finished that can reflect background characters like concave mirror, which roughness was 0.20μm*Rz* on outside of the surface. And profile of the concave surface was shown in Figure 11. It was confirmed from the experiment results that ultrasonically assisted diamond grinding can produce 3D shape mirror surfaces the ground surfaces reflect background characters clearly.

It is seem that center area of ground surfaces have blur part in results (c) and (d). It reasons were considered as follows; (i) grind speed was low when ground center area of curved surface due to small radius of contact point, (ii) tool envelope shape was not trued accurate spherical form. Introducing of multi axes machine tool is necessary to solve these problems, which can realize high precision tool truing and increase grinding speed.

## CONCLUSIONS

The following conclusions about 3D shape ultrasonically assisted diamond grinding can be drawn.

1. We established the method of manufacture and truing method of spherical shape electroplated diamond tools. Concentration of the tool was 150 result of microscopic observation. The performance of self-electroplated tool was as same as that of commercial tools.

*TABLE 4. Grinding conditions*

| | | |
|---|---|---|
| Workpiece material | | NAK80 (Daido Steel, HRC40, precipitation hardening steel) |
| Tool | Substrate | Cemented carbide |
| | Grain | SD #100/120 electroplated |
| | Shape | Spherical shape / SR2.7mm |
| Spindle speed *S* | | 6000min$^{-1}$ |
| Feed rate *F* | | 200mm/min |
| Radial depth of cut *P* | | 10 μm |
| Axial depth of cut *t* | | 1 μm |
| Ultrasonic vibration | | 60kHz / 0.25 μm |
| Coolant | | JIS N4-7 (oillness type) |

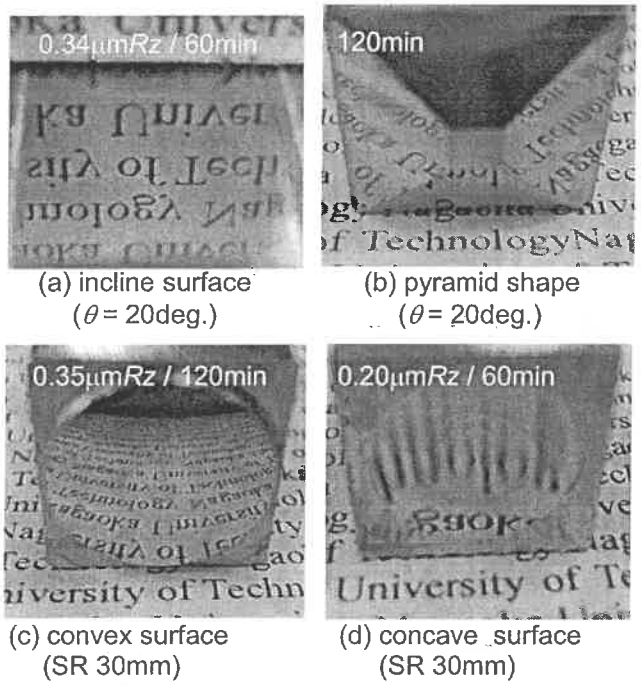


(a) incline surface ($\theta$ = 20deg.)
(b) pyramid shape ($\theta$ = 20deg.)
(c) convex surface (SR 30mm)
(d) concave surface (SR 30mm)

*FIGURE 8. Photographs of ground surfaces*

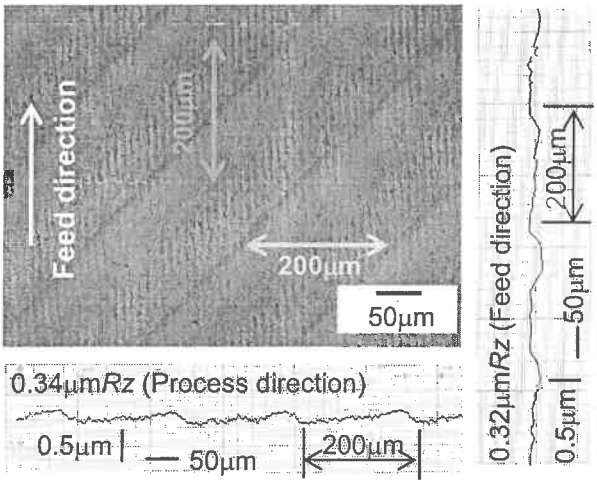


*FIGURE 9. Microphotograph and surface profiles of ground surface*

2. Experiments were conducted to investigate the performances of the 3D shape mirror surface finishing. The results showed that proposed method could fabricate like mirror surfaces which had gloss and could reflect background characters. Measured ground surfaces roughness were 0.35μm*Rz* (inclined surface), 0.34μm*Rz* (convex surface) and 0.20μm*Rz* (concave surface).

Finally, the provided research confirmed that the ultrasonically assisted diamond grinding is a effective method to finish mirror surface of dies.

**ACKNOWLEDGEMENTS**

The support for this research was provided by JST Satellite Niigata of Japan Science and Technology Agency.

**REFERENCES**

[1] K Hara, A Kyusojin, H Isobe, K Yanagi and H Yoshihara. Study on Mirror Surface Grinding of Die Steels by Using Ultrasonically Assisted Diamond Tool. Transaction of International Conference on Leading Edge Manufacturing in 21st Century. 2005; 631-634.

[2] H Isobe, K Hara, A Kyusojin, M Okada and H Yoshihara. Ultrasonically Assisted Grinding for Mirror Surface Finishing of Die With Electroplated Diamond Tools. Transaction of The 2nd International Conference on Positioning Technology. 2006; 219-224.

[3] S. Shimada, H. Tanaka, M. Higuchi, T. Yamaguchi, S. Honda and K. Obata: Thermo-Chemical Mechanism of Diamond Tool in Machining of Ferrous Metals. Annals of CIRP. 2004; 53: 57-60.

[4] J. L. Overcash, J. F. Cuttino. Turnable ultrasonic Vibration-Assisted Diamond Turning of Steel. Proceedings of ASPE 2004. 2004.

[5] T. Moriwaki, E. Shamoto and K. Inoue. Ultra-Precision Diamond Turning of Stainless Steel by Applying Ultrasonic Vibration. Journal of the Japan Society of Precision Engineering. 1991; 57 (11): 1983-88. (In Japanese)

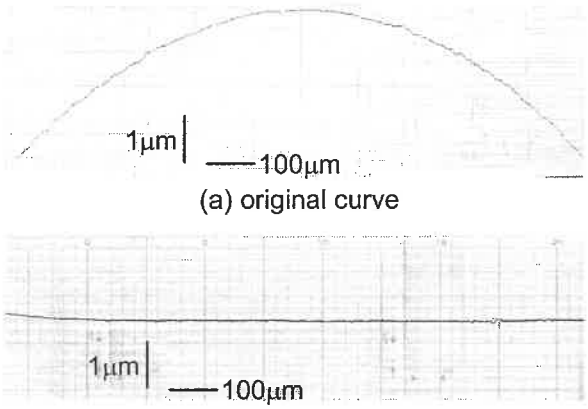


(a) original curve

(b) filtered profile ($\lambda_c$ = 250μm)

*FIGURE 10. Profile of ground convex surface*

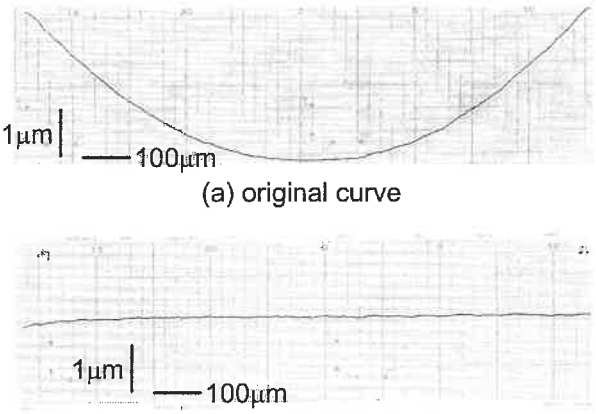


(a) original curve

(b) filtered profile ($\lambda_c$ = 250μm)

*FIGURE 11. Profile of ground concave surface*

# MICROMACHINING OF BRITTLE MATERIALS USING ULTRASONIC ASSISTED LAPPING

**Matthew J. Klopfstein, Oltmann Riemer, and Ekkard Brinksmeier**
**Laboratory for Precision Engineering (LFM)**
**University of Bremen**
**Bremen, Germany**

## INTRODUCTION

Micro-ultrasonic assisted lapping (micro-USAL) also called micro ultrasonic machining [1] or micro ultrasonic abrasive machining [2] shows promise as a manufacturing process for the small batch production of three dimensional microstructures in brittle materials. Micro-USAL was originally employed for the fabrication of holes, however with the addition of X-Y-Z stages three dimensional structures can be created. For example, Sun et al. [1] showed the use of micro-USAL and MEMS fabrication techniques in the production of a silicon air turbine with a rotor diameter of approximately 350 $\mu$m. Yu et al. [3] used micro-USAL to machine silicon with a cavity approximately 220 $\mu$m x 220 $\mu$m x 55 $\mu$m and 1/8 of a sphere in the center. Because brittle fracture often occurs during machining, the obtainable surface roughness is typically greater than 50 nm Sa [4], [5]. This paper presents results on initial attempts to machine two dimensional structures in (100)Si with surface finish less than 50 nm Sa.

## EXPERIMENTAL

Experiments were performed on a custom-built ultrasonic lapping apparatus which is shown schematically in Fig. 1. An ultrasonic generator mounted at the top of the frame operated at a fixed frequency of 20 kHz. The oscillations created by the generator were in the Z-direction and amplified by the horn to create an adjustable oscillation amplitude of 1 – 40 $\mu$m at the tool. The tools used in this work were cylindrical tools made of tungsten carbide with a diameter of 200 $\mu$m. The workpiece was mounted to a holder which was affixed to a computer-controlled X-Y-Z stage. The stage has a positional accuracy of about 0.2 $\mu$m in the Z-direction and about 1 $\mu$m in the X- and Y-directions. The workpiece holder has an acoustic emission sensor mounted to it which was used to establish the location of the workpiece surface without damaging the workpiece. Two water-based slurries which contained monocrystalline diamond with an average particle size of 0.1 $\mu$m and 0.25 $\mu$m were used. Approximately

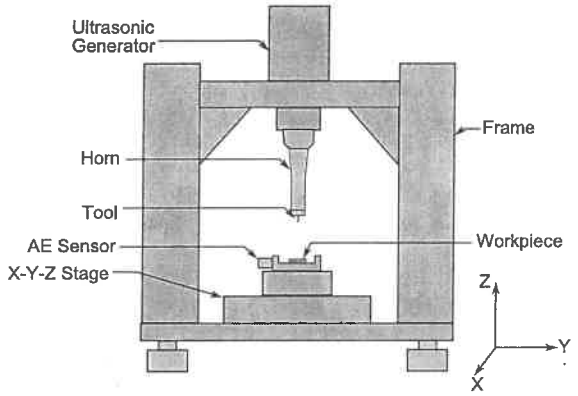


*FIGURE 1. Schematic diagram of the ultrasonic lapping machine.*

three to five milliliters of the slurry was placed on the workpiece prior to machining. The workpieces were cleaved from a 0.5 mm thick, 100 mm diameter wafer of chemo-mechanically polished (100)Si into pieces about 7 mm x 10 mm.

Two different types of structures were machined in the silicon: straight trenches and cylindrical holes. The trenches were made to investigate the achievable surface finish when machining a simple pattern. The cylindrical holes were made as simple two dimensional structures and as a preliminary step toward three dimensional structures. Before machining, the location of the workpiece relative to the tool was determined using the acoustic emission sensor. This was achieved with a computer program which moved the workpiece toward the tool in 50 nm steps and after each step the acoustic emission signal was measured. The difference between the acoustic emission value at this step and the previous step was computed and compared to a threshold value. If the acoustic emission signal exceeded the threshold value, the sample was withdrawn from the tool.

Prior to a "cut" being made, the slope of the workpiece was determined by touching the tool to the surface at the beginning and end of the

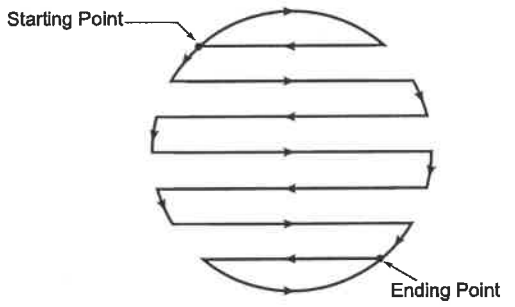


*FIGURE 2. Basic tool path in the X-Y plane for cylindrical holes. The "forward" direction is shown.*

cut for the straight trenches and at three points on the perimeter of a circle for the cylindrical cuts. At each of the points, the surface was touched five times and the average value was taken as the location of the workpiece surface. From the touched points, the slope was calculated in the x-direction for the trenches and in x- and y-directions for the cylindrical holes. The path of the tool was then corrected for the measured slope. For the straight trenches, the cuts were made by plunging the tool into the surface to the desired depth at the start of the cut, moving in a straight line to the end of the cut and then withdrawing the tool. The total length of a cut was 1.4 mm and the cut was in the ⟨110⟩ direction. For the cylindrical cuts a specific tool path was chosen to minimize the effects of wear on the generated surface using the uniform wear method [5]. Based on this method the desired structure was machined in layers where the basic tool path for each layer is shown in Fig. 2. The basic tool path was executed in pairs; first in the forward direction and then the tool was feed into the workpiece and the pattern was repeated in the reverse direction. For the forward direction the deepest portion of the generated cut would be at the top of the figure and tool wear would result in a shallower depth of cut at the bottom. In the reverse direction this would be reversed; the deepest portion would be at the bottom and the shallowest at the top. In this way tool wear can be taken into account. The use of this tool path to generate a cylindrical hole is described more fully below. The velocity during machining was 20 $\mu$m/s for the straight trenches and for the cylinders a velocity from 20 – 50 $\mu$m/s was used. Previous experiments with this micro-USAL equipment found that tool oscillation in the range of 1 – 6 $\mu$m had only a weak influence on the surface roughness [4] so the tool oscillation amplitude was chosen to be 3 $\mu$m for all of the experiments presented here.

The surface roughness of the machined surfaces was measured by white light interferometry (WLI). The form and waviness of the generated surface were removed by performing a Fourier transform of the obtained image and applying an 80 $\mu$m low pass filter. For the straight trenches the area over which the roughness was obtained was 380 $\mu$m x 125 $\mu$m. Some of the surfaces were further examined using atomic force microscopy in the intermittent contact mode.

## RESULTS AND DISCUSSION

Straight trenches were machined using 0.1 $\mu$m and 0.25 $\mu$m diamond abrasive to determine the roughness obtainable for a simple geometry. The commanded depths of cut were 3, 5, 7, and 9 $\mu$m however because of the compliance of the system the final depths were much less than the commanded values. Figure 3(a) shows the average roughness versus the final depth of cut for the case of straight trenches made with the two abrasives. The error bars denote the minimum and maximum values obtained for three cuts with two measurements at different locations for each cut. The error bars for the depth are not shown for clarity; the variation in depth was about ±10% of the measured depth. Figure 3(b) shows an image of part of a cut obtained by WLI with dimensions approximately 300 $\mu$m x 400 $\mu$m x 900 nm height. For cuts with a command depth greater than 3 $\mu$m, the 0.25 $\mu$m diamond abrasive resulted in a higher final depth than the 0.1 $\mu$m abrasive. The roughness of the cut machined with the 0.25 $\mu$m diamond abrasive and a 9 $\mu$m command depth is not shown because it was too rough to measure with the WLI. The roughness of the cuts made with 0.1 $\mu$m abrasive was found to be less than that for the cuts made with the 0.25 $\mu$m abrasive, also the variation in roughness was less. For these reasons the 0.1 $\mu$m diamond abrasive was used for the cylindrical holes. The roughness values obtained, 5 - 15 nm, are less than values previously reported [4] in similar experiments however those values were obtained at a slightly deeper depths of cut. The only other roughness values found in the literature was for the bottom of blind holes machined in silicon and the values were from 160 – 500 nm Sa [6].

Cylindrical holes were machined in silicon with a tool path based on that shown in Fig. 2. To obtain deeper holes, the tool path was composed of

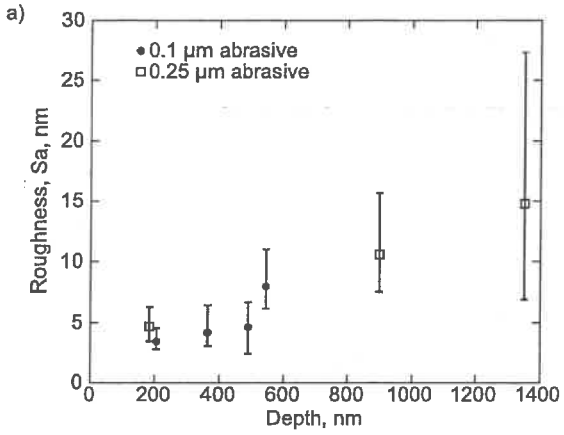


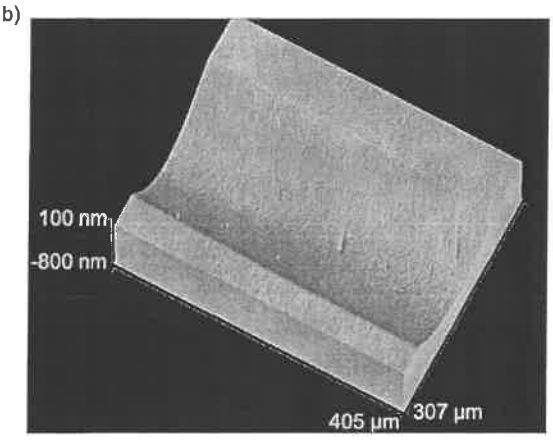


*FIGURE 3. (a) Roughness versus depth of cut for 0.1 μm and 0.25 μm diamond abrasive slurries. (b) White light interferometry image of a portion of a cut made with 0.1 μm diamond abrasive.*

five sets of the basic path where for each set forward and reverse directions were executed. The first set of cuts was performed as shown in Fig. 2 and the successive sets were performed with the basic pattern rotated by 72° which provided approximately 10° of overlap with the preceding cut. The command depth of cut for the five sets were the following: d, 1.5d, 2d, 2.5d, 3d, 3.5d, 4d, 4.5d, 4.75d, and 5d where d was the commanded depth for the first pass. The last two passes with lower depths of cut were finishing passes in an attempt to improve the surface quality.

Figure 4 shows a WLI image of a cylindrical hole approximately 1 mm in diameter with a depth of about 800 nm. This hole was made with a cutting speed of 50 μm/s however there were no significant differences observed in holes produced with a velocity of 20, 30, 40, or 50 μm/s. In Fig. 4 the traces of the last cuts are clearly visible and they have a spacing of about 100 μm with a peak-

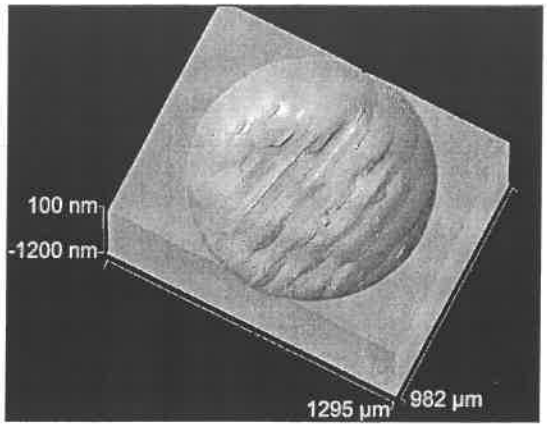


*FIGURE 4. Three dimensional white light interferometry image of a 1 mm diameter cylindrical hole approximately 800 nm deep machined with a speed of 50 μm/s.*

to-valley of about 20 – 30 nm. The depth of the hole ranges from about 700 nm to 950 nm with the deeper portion on the right of the figure. In repeated experiments, it was found that the right portion of the hole was always lower than the left. The cause for this is not currently known but is being investigated.

Although not clearly shown in Fig. 4, the machined surfaces also contained pits which were irregularly shaped with size from 1 μm to 10 μm and a few micrometers deep. These pits typically comprised approximately 3 – 5 % of the surface area of the hole. The surface roughness in the bottom of the hole after the removal of the form and waviness was 3.4 nm Sa over a 742 μm x 596 μm area. For three repeated holes made under the same conditions the roughness ranged from 3 – 17 nm Sa. In Fig. 4 it does not appear that there was severe brittle fracture of the surface however to examine the surface more closely it was measured with atomic force microscopy. Figure 5(a) shows a 1 μm x 1 μm three-dimensional image and Fig. 5(b) shows a cross-section from the three-dimensional image obtained near the center of the hole. The surface is composed of peaks from 1 nm to 5 nm high and a few hundred nanometers wide. Although the sides of the peaks are not all aligned there are portions of the side surfaces that do appear aligned and could be the result of fracture. The surface roughness over the 1 $\mu m^2$ area shown in Fig. 5(a) was approximately 3.7 nm Sa and over a 100 $\mu m^2$ area the roughness was 4.2 nm Sa (figure not shown). Both of these values are consistent with that mea-

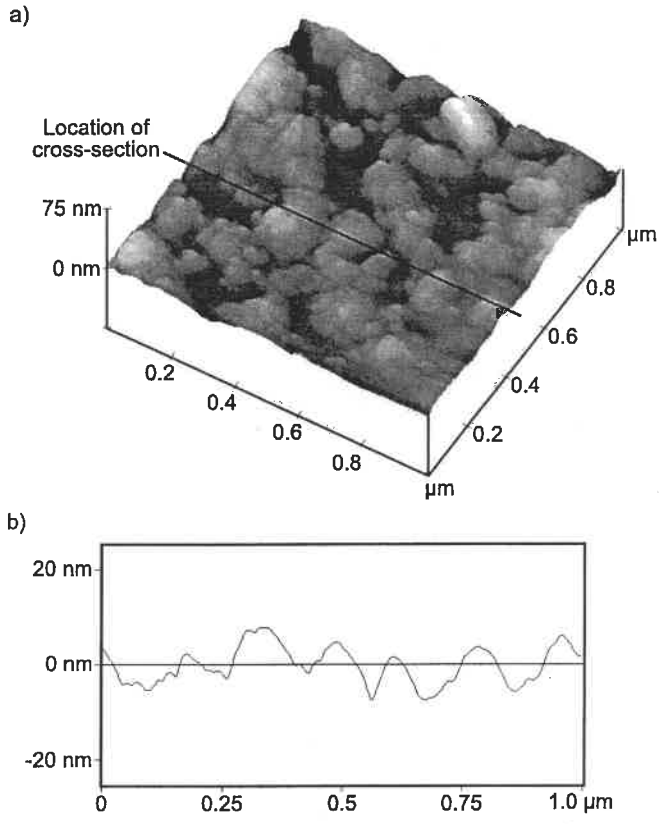


*FIGURE 5. (a) AFM image of the bottom surface of hole with dimensions 1 $\mu$m x 1 $\mu$m x 150 nm total height. (b) Cross-section at location shown in (a).*

sured by white light interferometry.

Figure 6 shows a 400 $\mu$m diameter hole machined with a velocity of 20 $\mu$m/s and the same tool path as for the 1 mm diameter hole. The hole is much more rounded on the bottom with a depth in the center of about 5 $\mu$m which is greater than the depth of the 1 mm diameter hole. Recall that the tool diameter is 200 $\mu$m so the tool is in contact with the center of the hole for a longer time than for the 1 mm diameter hole. Note that the sidewalls of the hole are not vertical as depicted in Fig. 6; they are too steep to be accurately measured with the WLI. The surface roughness of the center portion of the hole was approximately 37 nm Sa over a 240 $\mu$m x 240 $\mu$m area. For three repeated holes, the roughness was 27 - 37 nm Sa in the center portion of the hole.

## SUMMARY

Initial experiments on the machining of single crystal silicon with micro-USAL were presented. The surface roughness of straight trenches was

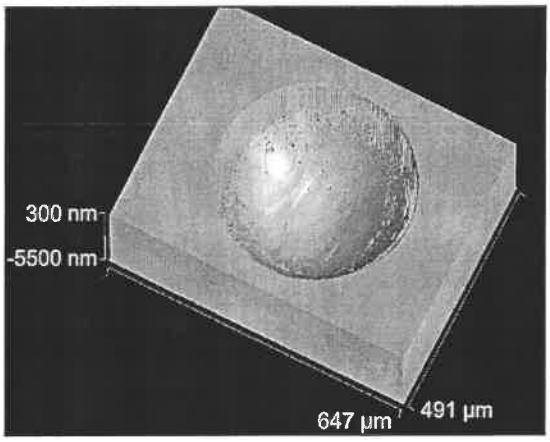


*FIGURE 6. White light interferometry image of a 400 $\mu$m diameter cylindrical hole approximately 5 $\mu$m deep machined with a speed of 20 $\mu$m/s.*

found to be in the range of 5 – 15 nm Sa. It was found that the 0.25 $\mu$m diamond abrasive resulted in higher values of roughness and higher variation in roughness as compared to the 0.1 $\mu$m diamond abrasive. The tool path for cylindrical holes was chosen consistent with the uniform wear method [5]. The surface roughness for the bottom of cylindrical holes ranged from 4 – 40 nm Sa. The velocity of machining in the range of 20 – 50 $\mu$m/s was not found to have an effect on the generated surfaces.

## ACKNOWLEDGMENTS

The authors gratefully acknowledge the support of the Deutsche Forschungsgemeinschaft (DFG) through grant BR825/45-1.

## REFERENCES

[1] Sun XQ, Masuzawa T, Fujino M. Micro Ultrasonic Machining and its Applications in MEMS. Sensors and Actuators A. 1996;57:159–164.

[2] Kuriyagawa T, Shirosawa T, Saito O, Syoji K. Development of Micro Ultrasonic Abrasive Machining System. JSME International Journal. 2002;45:593–600.

[3] Yu ZY, Rajurkar KP, Tandon A. Study of 3D Micro-Ultrasonic Machining. Journal of Manufacturing Science and Engineering. 2004;126:727–732.

[4] Zhang C, Brinksmeier E, Rentsch R. Micro-USAL Technique for the Manufacture of High Quality Microstructures in Brittle Materials. Precision Engineering. 2006;30:362–372.

[5] Yu ZY, Masuzawa T, Fujino M. Micro-EDM for Three-Dimensional Cavities – Development of Uniform Wear Method –. Annals of the CIRP. 1998;47:169–172.

[6] Yu Z, Hu X, Rajurkar KP. Influence of Debris Accumulation on Material Removal and Surface Roughness in Micro Ultrasonic Machining of Silicon. Annals of the CIRP. 2006;55:201–204.

# EFFECT OF ULTRASONIC TORSIONAL MODE VIBRATION CUTTING ON DRILLING IN CFRP LAMINATES

**H.Yagishita**
**Professor-Doctor**
**Dept. of Control and Computer Engineering**
**Vice President of Numazu National College of Technology**
**3600 Ooka, Numazu-city, Shizuoka-pref. 410-8501**
**JAPAN**

## INTRODUCTION

Wide spread applications of composite material have been significantly growing in aerospace, naval, space and automotive industries. Especially, CFRP ( carbon fiber reinforced plastics ) laminates have a higher strength/weight ratio ( about ten times larger tensile strength than advanced aluminum alloy in spite of about one half specific gravity ) and high heat resistance. Therefore, recently most of wing, tail assembly and body of aircraft have been manufactured by assembling several parts made of CFRP laminates. Bolting and riveting are currently the preferred methods for fastening composite skins to the metal or other composite parts in assembly of aerospace and automotive composite structures [1]. Namely, drilling of CFRP laminates is indispensable for manufacturing aircraft and automotive composite structure and the quality of drilled holes strongly affects the fatigue strength of the structure besides the reliability of aircraft.

The particular objective of the present work was to conduct drilling experiments of CFRP laminates in order to investigate the cutting mechanism and the effects of ultrasonic torsional mode vibration cutting. Experimental work was performed to characterize major hole quality parameter and cutting mechanism encountered when drilling CFRP laminates and also to examine specific drilling assisted by ultrasonic torsional mode vibration. Inner surface texture of drilled hole, hole diameter and tool life were investigated and discussed by comparing the results of conventional drilling with those of specific drilling assisted by ultrasonic torsional mode vibration [2].

## EXPERIMENTAL SETUP AND PROCEDURE

### Material Systems

CFRP was made from combining carbon fiber clusters with epoxy-resin matrix, to create a strong, high temperature composite. The CFRP laminates were made of 11 plies of CFRP oriented as follows: ( 0°, 90°, 0°, 90°, 0°, 90°, 0°, 90°, 0°, 90°, 0°), and both the upper and the lower two plies are thinner than mid 7 plies. The workpiece shown in Fig.1 was consolidated from laminates of one oriented carbon fiber prepreg using the autoclave method.

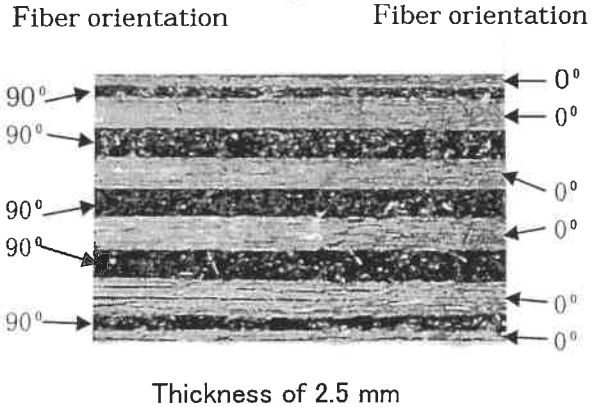


*FIGURE 1. Sectioned view of CFRP laminates.*

## Drilling Experimental Method and Procedure

Drilling experimental setup assisted by ultrasonic torsional mode vibration consists of vibration unit, oscillation unit and display unit as shown in Fig. 2. The taper shank of vibration unit is attached rigidly to the main spindle of CNC milling machine. The electric control signal from oscillation unit oscillates torsionally at 27 kHz the twist drill attached to vibration unit, which are rotating as one body with the main spindle of the milling machine.

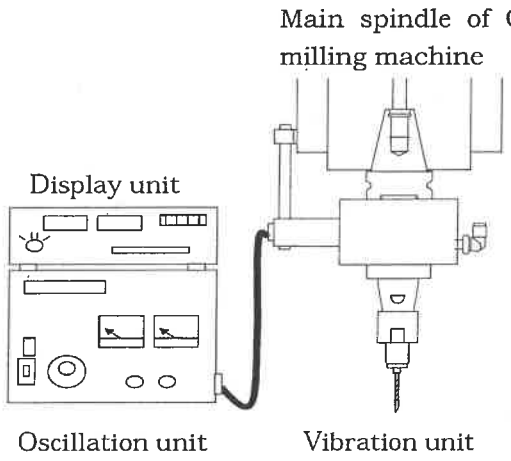


*FIGURE 2. Schematic drilling experimental setup assisted by ultrasonic torsional mode vibration.*

Display unit expresses resonant frequency, tip amplitude of twist drill constantly, and supplied voltage, ampere and electric power selectively during running of the drilling system.

Coated cemented carbide fiber drills of 3 mm diameter, which have a pair of special cutting edge shown in Fig.3, were used for all experiments. As shown in Fig.3, thinning is applied to the chisel edge but margin does not exist being different from a conventional twist drill. The summary of experimental conditions for CFRP laminates is listed in Table 1.

## RESULTS AND DISCUSSION

### Cutting Mechanism

The variation of relative angle between fiber orientation and cutting direction is shown in

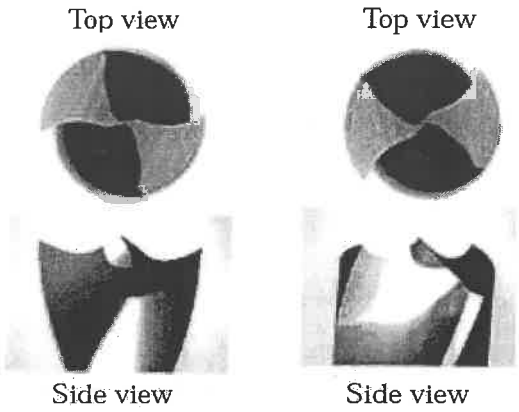


*FIGURE 3. Appearance of coated cemented carbide fiber drill used.*

*TABLE 1. The summary of experimental conditions for CFRP laminates.*

| Drilling of CFRP laminates | |
|---|---|
| Machine tool | Vertical milling machine with CNC control |
| Workpiece material / Shape | CFRP laminates of 11 plies / Plate of 2.5mm thickness |
| Tools / Diameter / Length | Coated cemented carbide fiber drill / 3mm in diameter / 36mm in length |
| Drilling conditions ( Dry cutting ) | Rotational speed 1480rpm (Cutting speed 13.9m/min) |
| | Feed 0.04 mm/rev (Feed rate 59.2 mm/min) |
| Ultrasonic torsional mode vibration cutting | Frequency 27 kHz<br>Amplitude 12.5 $\mu$m<br>Max. vibrational speed 127 m/min<br>Max. power 50 W |

Fig.4(a)(b). (a) and (b) in Fig. 4 show the ply of fiber orientation 0° and 90° respectively. In these figures, the relative angle at A, E in (a) and a, e in (b) is 90°, and the angle at C, G and c, g is 0°, and the angle at B, F and b, f is -45°, and the angle at D, H and d, h is +45° respectively.

Inner surface textures, which are measured

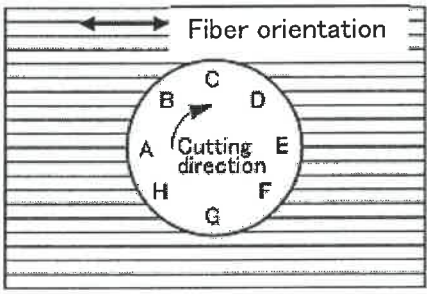


*(a) Ply of fiber orientation 0°*

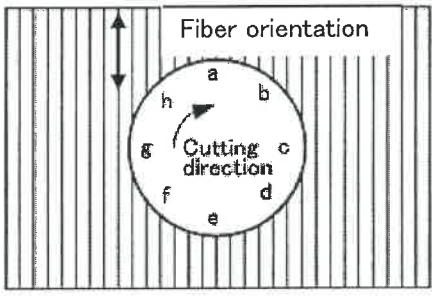


*(b) Ply of fiber orientation 90°*

*FIGURE 4. Relative angle between fiber orientation and cutting direction.*

using a laser beam scanning microscope, at relative angle of 90°, 0° and ±45° are shown in Fig.5(a)(b)(c). (a) at relative angle of 90° shows the almost smooth surface but several dark dots like a circle are found. On the other hand, (b) at relative angle of 0° shows the scratched traces of about 400$\mu$m width, which would be caused by rubbing of cutting edges. In (c) at relative angle of ±45°, two dark areas are seen at D of the angle +45°. From more detailed observations it is confirmed that the dark areas form the craters of 50∽70 $\mu$m depth.

## Hole Quality Assessment

As applicable CFRP laminates, hole quality consists of material integrity, hole diameter and roundness, inner surface texture, and hole exit damage of drilled holes. The present work focuses the subject on inner surface texture, hole diameter and tool life.

### *Effects of Ultrasonic Torsional Mode Vibration Cutting on Inner Surface Texture*

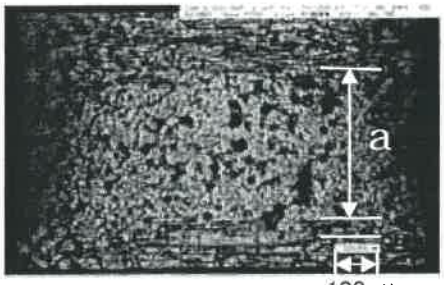


*(a) Relative angle of 90° at position a*

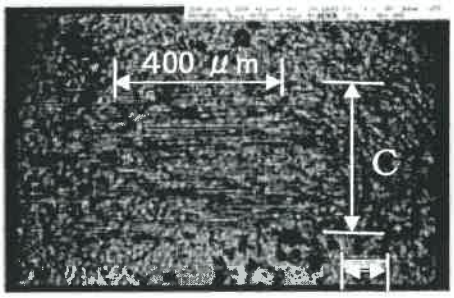


*(b) Relative angle of 0° at position C*

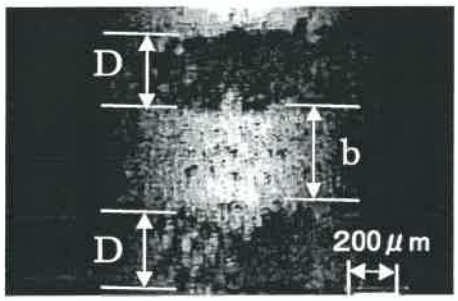


*(c) Relative angle of +45° at position D and -45° at position b.*

*FIGURE 5. Inner surface texture at relative angle of 90°, 0° and ±45°.*

To examine the effect of ultrasonic torsional mode vibration cutting on the inner surface texture of drilled hole, the texture was observed using a laser beam scanning microscope after being cut at the center of hole with an abrasive water jet cutting. Figure 6 (a) and (b) show the inner surface texture of half hole at 19th hole by conventional drilling and that by specific drilling assisted by ultrasonic torsional mode vibration respectively. In Fig. 6 (a), at only position of h and D of the

conventional drilling and (b) is that during specific drilling assisted by ultrasonic torsional mode vibration, respectively. From (a) and (b) in Fig. 7, the crater was generated from first hole during conventional drilling, nevertheless it was found after 30th hole during specific drilling assisted by ultrasonic torsional mode vibration.

### *Effect of Ultrasonic Torsional Mode Vibration Cutting on Hole Diameter*

Figure 8 shows the relationship between deviation of hole diameter from 3 mm and number of machined hole. As shown in Fig. 8, it is seen that scattering of deviation of hole diameter from 3 mm can be reduced from 16 μm to 8 μm by assist of ultrasonic torsional mode vibration. The large scattering of hole diameter during conventional drilling would be induced by the occurrence of crater on the inner surface of hole.

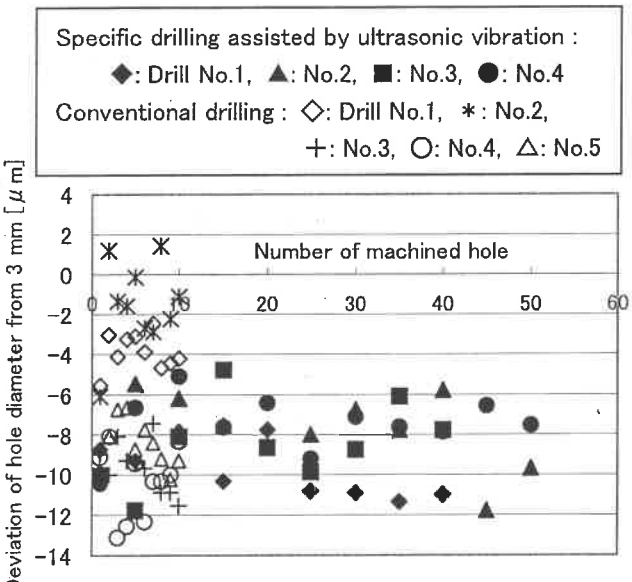


Workpiece material : CFRP laminates of 12.0mm thickness
Length of drill : 46 mm ( Diameter of drill : 3 mm )
Amplitude of vibration : 22.5 μm
( Max. vibrational speed of 229 m/min )
Rotational speed of drill : 2200 rpm ( 20.7 m/min )
Other conditions are the same as those in Table 1.

*FIGURE 8. Relationship between deviation of hole diameter and number of machined hole.*

### Effect of Ultrasonic Torsional Mode Vibration Cutting on Tool Life

Based on the criteria of tool life when the wear width of circumferential cutting edge reaches to 0.07mm, effect of ultrasonic torsional mode vibration cutting on tool life of drill was examined. Since tool life is affected by the occurrence of micro-chipping, drilling tests were executed five times in conventional drilling and also in specific one assisted by ultrasonic torsional mode vibration respectively. As shown in Fig. 9, the assist of

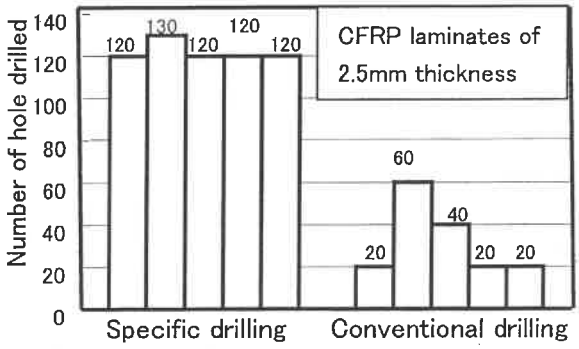


*FIGURE 9. Comparison of tool life between conventional drilling and specific one.*

ultrasonic torsional mode vibration to drilling CFRP laminates is significantly effective to extend the tool life of cemented carbide fiber drill. It can be understood thoroughly that the extension of tool life is caused by temperature increase being restrained at cutting edge due to decrease of rubbing duration between cutting edge and carbon fiber cluster.

### REFERENCES


[1] Waurzyniak , P. Aerospace Manufacturing-Lean FIGHTER. Mechanical Engineering. 2005; Vol.134, No.3: 121-132.

[2] Yagishita H. Cutting Mechanism of Drilling CFRP Laminates and Effect of Ultrasonic Torsional Mode Vibration Cutting. Transactions of the North American Manufacturing Research Institution of SME. 2006; 34: 213-220.

# Author Index


Billa, Sridevi ..... 32
Brecher, Christian ..... 48
Brehl, David E. ..... 21, 71
Bresseler, Bernd ..... 3
Brinksmeier, Ekkard ..... 87
Bulla, Benjamin ..... 3
Bunget, Cristina J. ..... 37
Cerniway, Matthew A. ..... 71
Daichi, Yoshiaki ..... 58
Dambon, Olaf ..... 3
Dow, Thomas A. ..... 21, 71
Hara, Keisuke ..... 82
Heselhaus, Michael ..... 3
Hino, Rei ..... 15, 64
Hübert, Christoph ..... 43
Isobe, Hiromi ..... 82
Klocke, Fritz ..... 3
Klopfstein, Matthew J. ..... 87
Koshimizu, Shigeomi ..... 11
Kyusojin, Akira ..... 82
Li, Zhichao ..... 52
Micale, Antonio C. ..... 52
Miller, Michele H. ..... 77
Negishi, Nobuhiko ..... 71
Ngaile, Gracious E. ..... 37
Okada, Manabu ..... 82
Patten, John A. ..... 27
Pei, Zhi-Jian ..... 52
Rajurkar, Kamlakar P. ..... 32
Riemer, Oltmann ..... 87
Rhorer, Richard L.* ..... 70
Sano, Sadao ..... 58
Schug, Ralf ..... 3, 48
Shamoto, Eiji ..... 15, 64
Sisco, Tanni ..... 52
Sundaram, Murali M. ..... 32
Suzuki, Norikazu ..... 15, 64
Treadwell, Clyde ..... 52
Uhlmann, Eckart ..... 43
Uno, Yoshiuyki ..... 58
Wang, Zhigang ..... 58
Weber, Andreas ..... 3, 48
Wenzel, Christian ..... 48
Williams, Andre D. ..... 27
Yagishita, Hukuzo ..... 92
Yamazaki, Kazuo ..... 58
Yoshihara, Hideo ..... 82
Zhang, Ping ..... 77